INVESTIGATION OF NOVEL GEOMETRICAL DESIGN CONCEPTS FOR DAMPING TREATMENTS

A THESIS SUBMITTED TO
THE GRADUATE SCHOOL OF NATURAL AND APPLIED SCIENCES
OF
MIDDLE EAST TECHNICAL UNIVERSITY

BY

BERTUĞHAN ÇAVUŞ

IN PARTIAL FULFILLMENT OF THE REQUIREMENTS
FOR
THE DEGREE OF MASTER OF SCIENCE
IN
MECHANICAL ENGINEERING

NOVEMBER 2022

Approval of the thesis:

INVESTIGATION OF NOVEL GEOMETRICAL DESIGN CONCEPTS FOR DAMPING TREATMENTS

submitted by **BERTUĞHAN ÇAVUŞ** in partial fulfillment of the requirements for the degree of **Master of Science** i**n Mechanical Engineering, Middle East Technical University** by,

Prof. Dr. Halil Kalıpçılar
Dean, Graduate School of **Natural and Applied Sciences** _____

Prof. Dr. M. A. Sahir Arıkan
Head of the Department, **Mechanical Engineering** _____

Assist. Prof. Dr. Gökhan O. Özgen
Supervisor, **Mechanical Engineering Dept., METU** _____

Examining Committee Members:

Prof. Dr. Ender Ciğeroğlu
Mechanical Engineering, METU _____

Assist. Prof. Dr. Gökhan O. Özgen
Mechanical Engineering, METU _____

Assoc. Prof. Dr. M. Bülent Özer
Mechanical Engineering, METU _____

Assist. Prof. Dr. Orkun Özşahin
Mechanical Engineering, METU _____

Assist. Prof. Dr. M. Selçuk Himmetoğlu
Mechanical Engineering, Hacettepe University _____

Date: 25.11.2022

I hereby declare that all information in this document has been obtained and presented in accordance with academic rules and ethical conduct. I also declare that, as required by these rules and conduct, I have fully cited and referenced all material and results that are not original to this work.

Name, Last name : Bertuğhan Çavuş

Signature :

ABSTRACT

INVESTIGATION OF NOVEL GEOMETRICAL DESIGN CONCEPTS FOR DAMPING TREATMENTS

Çavuş, Bertuğhan
Master of Science, Mechanical Engineering
Supervisor : Assist. Prof. Dr. Gökhan O. Özgen

November 2022, 94 pages

Surface damping treatment concepts are developed utilizing viscoelastic materials as a damping layer where it is applied to the main structure. The main aim for adding these materials is to increase cyclic deformation in the frequency region of interest, which increases dissipated energy from the main structure. Constrained layer damping treatment is the most common, where the viscoelastic layer is constrained by a stiff top layer. Recently, a spacer or standoff layer has been added between the base and constrained damping layer to increase the damping performance of the structure. Adding a standoff layer increases the distance between the damping layer and the base layer, which results in increasing shear strain. Also, the electromagnetic and acoustic metamaterial concepts are extended to reduce vibration levels using the vibration absorber analogy, known as mechanical metamaterial or metastructure concept. It is developed by embedding vibration absorbers to the main structure rather than attaching them in this concept.

In the frame of this thesis study, novel damping treatment designs are developed using surface damping treatment and vibration absorber concepts to optimize dynamic behavior and reduce vibration amplitudes of the main structure. The proposed designs are compared using the performance metric that quantifies the vibration damping performance of the design. Hence, the main aim is to find optimal design geometry that maximizes vibration amplitude reduction with minimum mass.

The modelling of these complex geometries is developed in ANSYS finite element simulation environment. Finally, the proposed optimum designs are manufactured and tested to verify the methodology used and finite element results.

Keywords: Passive Standoff Layer Damping Treatment, Metastructures, Structural Optimization, Vibration Absorbers, Passive Vibration Control Techniques, Standoff Layer

ÖZ

ENERJİ SÖNÜMLEME TASARIMLARI İÇİN ÖZGÜN GEOMETRİK TASARIM KONSEPTLERİNİN İNCELENMESİ

Çavuş, Bertuğhan
Yüksek Lisans, Makina Mühendisliği
Tez Yöneticisi: Dr. Öğr. Üyesi Gökhan O. Özgen

Kasım 2022, 94 sayfa

Yüzey sönümleme işlemi kavramları, ana yapının üzerine uygulanan bir sönümleme katmanı olarak viskoelastik malzemeler kullanılarak geliştirilmiştir. Bu malzemeleri eklemenin ana hedefi, ana yapıdan dağıtılan enerjiyi arttıran ilgili frekans bölgesindeki döngüsel deformasyonu arttırmaktır. Viskoelastik katmanın sert üst tabaka tarafından kısıtlandığı sınırlandırılmış katmanlı sönümleme işlemi en yaygın olanıdır. Son zamanlarda, yapıların sönümleme performanslarını arttırmak için taban ve sınırlandırılmış sönümleme katmanının arasına aralayıcı ya da ara katman eklenmiştir. Sönümleme ve taban katmanı arasındaki mesafe, ara katmanın eklenmesiyle arttırılarak yırtılma geriniminde artış sağlanır. Bunun yanında, elektromanyetik ve akustik metamalzeme kavramları, titreşim seviyelerini azaltmak için titreşim emici anolojisi kullanılarak mekanik meta malzeme veya meta yapı olarak bilinen kavramlara genişletilmiştir. Bu yapılar, bu konseptte titreşim emicilerin ana yapıya takılmak yerine ana yapının içine gömülü halde olacak şekilde geliştirilmiştir.

Bu tez çalışması kapsamında, ana yapının titreşim genliklerini azaltmak ve dinamik davranışlarını en iyilemek için yüzey sönümleme işlemi ve titreşim emici kavramları uygulanarak özgün sönümleme işlemi tasarımları geliştirilmiştir. Önerilen tasarımlar, tasarımların titreşim sönümleme performasını ölçmeye yarayan bir

performans metriği kullanılarak karşılaştırılmıştır. Bu sebeple, en az ağırlıkla titreşim genliği azaltımını sağlayan en uygun tasarım geometrisini bulmak ana hedeftir. Bu kompleks geometrilerin modellenmesi ANSYS sonlu elemanlar simulasyon ortamında tamamlanmıştır. Son olarak, önerilen optimum tasarımlar üretilmiş ve kullanılan yöntemleri ve sonlu elemanlar analiz sonuçlarını doğrulamak için test edilmiştir.

Anahtar Kelimeler: Pasif Ara Katmanlı Sönümleme İşlemi, Metayapılar, Yapısal Optimizasyon, Titreşim Emiciler, Pasif Titreşim Kontrol Yöntemleri, Ara Katman

To My Family

ACKNOWLEDGMENTS

I would like to express my deepest gratitude to my supervisor Assist. Prof. Dr. Gökhan O. Özgen for his advice and patience, brainstorming sessions we had, encouraging, and motivating me to accomplish this study.

I would also thank all the committee members for giving their precious time and advice to improve this study.

I would like to thank my colleagues Hümeyra Beyan and Yiğitcan Ekici for technical support they provided and for sharing this Master of Science path.

I would also appreciate my dearest friends Alper Çelikay and Aykut Çardak for exchanging ideas, keeping my motivation alive, unique, and enjoyable moments we have.

I would also appreciate my dearest parents, Reyhan Çavuş and Ayhan Çavuş, my brother Batuğhan Çavuş, and my sister Berfuğ Çavuş for supporting me whenever necessary not only for this study but throughout life.

Finally, I would express my gratitude to my lovely wife, Burçin Çavuş, for her encouragement, patience, support and for relieving me throughout this study and life.

TABLE OF CONTENTS

LIST OF TABLES

TABLES

LIST OF FIGURES

FIGURES

LIST OF ABBREVIATIONS

ABBREVIATIONS

CLDT	Constrained Layer Damping Treatment
FEA	Finite Element Analysis
FLDT	Free Layer Damping Treatment
PSLDT	Passive Standoff Layer Damping Treatment
VE	Viscoelastic Material
FRF	Frequency Response Function
SCDM	Space Claim Design Modeler
NA	Not Applicable

CHAPTER 1

INTRODUCTION

1.1 Introduction

In many mechanical vibration problems, the main focus is improving system performance to prevent mechanical vibration caused damages such as noise, resonance, and fatigue. Therefore, controlling vibrations is very significant while designing the engineering system to escape such problems. In general, the desired dynamic behavior is achieved by passive and active vibration control techniques. Generally, the actuator eliminates undesired vibrations in active vibration control, whereas viscoelastic materials, vibration isolators, and vibration absorbers are used in passive vibration control. Therefore, the desired vibration levels are achieved by adding extra weight to the structure. Engineering systems must satisfy the best dynamic behavior with the most lightweight solution. Hence, it is a challenging design problem in this field.

Viscoelastic materials maintain specific damping characteristics over various operating temperatures and frequencies. However, it must be added to the structure and chosen considering operating conditions for proper design since its damping characteristics are strongly related to temperature and frequency. Vibration damping can be best explained as the dissipation of vibrational energy from the structure. Therefore, the main aim for adding viscoelastic materials is to increase dissipated energy from the structure. This can be achieved by increasing cyclic deformation in the frequency region of interest. Therefore, understanding deformation shapes is critical. Surface damping treatment concepts are established using these materials as a damping layer. Free layer damping treatment (FLDT) is the simplest one. A viscoelastic material is applied to the structure by coating it in a simple manner. An extensionally deformed damping layer dissipates vibrational energy in this damping

treatment. Constrained layer damping treatment (CLDT) is superior considering the weight point of view since a very thick damping layer is needed for the same amount of damping in FLDT. A viscoelastic material is sandwiched between a stiff base and a constraining layer in CLDT. The damping layer deforms in shear, which increases modeling efforts to explain the deformation pattern in CLDT. Although these treatments are generally sufficient for vibration suppression, they may still not meet the expected dynamic performance characteristics. Therefore, a novel damping treatment needs to be modeled for that specific problem, which generally consists of multiple layers with different damping materials and orientations. For this purpose, a novel spacer layer between the viscoelastic layer and the base structure is applied to enlarge the shear strain on viscoelastic layers by increasing the distance between the viscoelastic layer and the base layer. This concept is known as passive standoff layer damping treatment (PSLDT) in literature.

Electromagnetic and acoustic metamaterial concepts have been studied widely since the 2000s. It is found that no wave propagation occurred at certain frequencies. Later, metastructures or mechanical metamaterial concept is developed, extending no wave propagation logic used in these concepts to damping at certain resonance frequencies. The concept indicates that vibration amplitudes at resonance frequencies can be eliminated with simple spring-mass attachment to the structure. These locally resonant subunits resemble vibration absorbers attached to the structure. The difference is that locally resonant subunits are embedded rather than attached to the main structure from the ground. This results in good damping performance at certain frequencies with less weight added to the structure. However, since it is a resonant vibration problem, these locally embedded vibration absorbers need to be designed appropriately considering the mass, stiffness, and resonant frequencies of the structure. Generally, this can be achieved by tuning geometrical parameters, the total number, and the location of these embedded resonators. Therefore, it can be classified as a passive vibration control method.

1.2 Scope and Objectives of the Thesis

In this thesis study, theory and the concept of surface damping treatment and metastructures are utilized to develop novel standoff layer geometry that possesses the best damping performance with minimum weight. In the literature, various studies can only describe the damping performance of the structure by reducing vibration amplitudes at certain modes. These solutions are generally applicable to particular design problems. Therefore, it is essential to define a suitable performance metric that quantifies the vibration damping performance of the structure more precisely. Hence, the performance metric defined in this study includes the total or added weight of the structure, the total vibration response of the structure, and the average damping values of the first three modes in a specific frequency range. These parameters have an impact on the performance metric. This performance metric and its parameters are used to find the optimum design configuration.

As mentioned before, vibration control of the structure is achieved by adding damping passively and actively. Therefore, increasing the total weight of the structure is inevitable. However, at a certain point, the thickness of the damping layer, standoff layer, and the total number and location of the vibration absorber are optimum. Thus, it is essential to define them correctly. The thickness of the standoff layer is optimized for PSLDT, which defines the best uniform standoff layer thickness for reference CLDT with a uniform standoff layer. Therefore, the reference beam configurations are developed using a certain base, standoff, damping, and constraining layer thickness. Then, the reference CLDT with a uniform standoff layer beam is optimized according to the defined performance metric using structural and parametric optimization. Therefore, the reference baseline configurations are compared with previous scaled versions of PSLDT in literature and developed novel design alternatives in this study.

The mechanical metamaterial concept is a very recent topic in literature. Thus, there are very few studies to investigate the effect of adding damping material to the main structure since the modeling complexity is increasing. Also, metastructure design

looks for weight efficient solutions. So, most proposed designs prevent adding or bonding damping sheets to the main structure. However, it is well known that better damping performance can be achieved by adding viscoelastic materials at specific locations. This study investigates the effects of adding damping material to the main structure for metastructure design.

All in all, defining a suitable performance metric, optimizing the thickness of the standoff layer, optimizing standoff layer geometry to improve damping performance, investigating the effects of adding damping materials to metastructure and verifying the results of novel design alternatives with experiments are the main objectives of the thesis.

1.3 Background

1.3.1 Literature Survey

Metamaterials are developed materials created to have extraordinary properties which are not observed naturally. Metamaterials are first introduced by investigating the propagation of electromagnetic waves in matter. Soviet physicist Veselago shows that it is possible to have negative dielectric constant ϵ and magnetic permeability μ theoretically using the dispersion relation [1]. These unique properties result in no wave propagation at certain frequencies. Acoustic metamaterials are developed considering the similarity between electromagnetic and acoustic waves. Liu et al. fabricated one of the first acoustic metamaterials considering that effective elastic constants can be negative. They used lead balls as a core material coated with silicone rubber in a cubic structure where epoxy is filled as the matrix material. Experimental results show that two apparent dips occurred before a peak in transmission curves. As in electromagnetic waves, this indicates that no wave propagation is occurred at certain frequencies. These regions are called bandgaps. It is found that local resonances of the lead balls (as core materials) reveal effective negative constants [2]. In the light of their pioneering work, acoustic metamaterials are theoretically and

experimentally investigated where locally resonant tiny subunits occurred inside the unit cells. These unit cells are created in a very limited space considering the wavelength of the main structure. Therefore, producing these structures is very expensive, considering the micro and nanomanufacturing methods applied. Acoustic metamaterials have possible applications in acoustic imaging, subwavelength waveguides, and acoustic absorbers [3]. Later, it was found that the actual working mechanism is based on the working mechanism of the conventional vibration absorber, where the applied force is balanced out by the inertia forces of the masses depending on the acoustical or optical mode. The concept of the negative effective mass and wave propagation in metamaterial structure (acoustical or optical mode) is studied in detail. Local resonances of these subunits create frequency bandgaps called stop bands where no wave propagation is occurred between acoustical and optical modes. It shows that these locally resonant subunits do not require as tiny as before; instead, they are simple spring-mass subsystems attached to the structure, significantly reducing challenges on design, modeling, and manufacturing of acoustic metamaterials [3,4]. Therefore, it is possible to reduce vibration levels by properly designing broadband vibration absorbers along with the primary structure. These concepts of the acoustical metamaterials are extended to model mechanical metamaterials, namely metastructures.

Metastructures that consist of the primary structure (or the host structure) and locally resonant subunits are created by embedding these subunits to the primary structure rather than attaching them to reduce vibration levels of the main structure. These internal locally resonant subunits can be spring-mass, mass in mass SDOF subsystems, periodic two-mass spring-mass-damper inserts, periodic and graded chiral lattices, and the zigzag inserts. Many research investigate these types of resonators and the vibration attenuation characteristics of the proposed metastructures [3-25]. Theory and overview of the metastructures are well explained in these studies [3-5]. Since the concept of the vibration absorber is utilized and its theory is in good agreement with the metamaterial concept, the basic design idea is that these subunits are tuned to excite at one of its fundamental frequencies where

frequency bandgaps are occurred. Therefore, the proper design of internal resonators is the main objective where the geometrical parameters of the resonators are tuned.

The distributed vibration absorbers as internal resonators are studied for the vibration control of the metastructures in detail as in [6-11]. Chen et al. investigated the dynamic behavior of sandwich structure analytically and experimentally, where it is modeled as a metastructure. The effect of the geometrical parameters on frequency bandgaps is examined. It was found that higher internal mass is widened the frequency bandgap while the spring constant does not affect at all [6]. Borgi et al. utilized MDOF resonators where local resonators are excited at their different resonant frequencies to study multiple bandgap formation of metastructures. It was found that bandwidths of the bandgaps are affected by overall mass ratios of the resonators, distribution of mass of the different resonators, and the minimum number of resonators attached along the beam [7]. Hobeck and Inman created unique SDOF spring-mass oscillators embedded inside the primary structure where the proposed design is manufactured by 3D printing. The proposed design is superior to the conventional vibration absorbers considering no additional mass is required to achieve the same performance by applying the VE material layer [8]. Later, Reichl and Inman proposed a unique constant mass metastructure. Distributed vibration absorbers are created by linearly varying natural frequencies and distributing the mass of the absorbers along the beam while the total mass is the same. It was found that distributed vibration absorbers with linearly varying frequencies can suppress vibrations and superior, varying the mass of the absorbers at higher mass ratios is superior, and metastructure performs slightly better than the TMDs for lower mass ratios for vibration suppression [9-11].

The chiral lattice inserts as internal resonators are studied for the vibration control of the metastructures in detail as in [12-16]. Bettini et al. proposed the composite morphing airfoil structure using a chiral topology. The research group has an excellent effort to design chiral topology using traditional manufacturing techniques considering that 3D printing methodologies were not accessible and reliable. They conclude that the chiral core topology is a possible application in smart morphing

structures [12]. Baravelli and Ruzzene investigate periodic and graded chiral lattice designs. It was concluded that locally resonant subunits behave as periodic vibration absorbers, out-of-phase motion is the leading mechanism to vibration reduction, and graded lattice geometry is expected to be more effective in a broader frequency range [13]. Abdeljaber et al. investigated the effect of the geometric parameters of the chiral topology, such as the characteristic angle Φ and the radius of the nodes R. Since effects of the various design parameters used, a genetic algorithm is developed to optimize design parameters via using MATLAB Genetic Algorithm Toolbox. Optimized chiral lattice configurations show that non-periodic or graded inserts need to be used for low-frequency vibration attenuation [14]. Later, they compared the various optimal design of chiral lattices found with Baravelli&Ruzzene's proposed design [13] which is based on a trial-error approach rather than optimization developed using genetic algorithm as in [14,15]. It is shown that optimal designs found in [14,15] are superior to [13]. Later, Essink and Inman manufactured two of these optimized designs to validate vibration attenuation characteristics of proposed metastructures experimentally. Both optimized metastructures are achieved very good vibration attenuation [16].

The zigzag inserts as internal resonators are studied for the vibration control of the metastructures in detail as in [17-21]. In these studies, the concept of the vibration absorber is extended to examine energy harvesting and nonlinearity on metastructures. Chiral lattices have disadvantages in finding closed-form analytical solutions, computational inefficiency, geometrical restrictions of the ligaments, and manufacturing. Abdeljaber et al. proposed zigzag beam inserts to solve these issues. After a closed-form solution is found, an optimization procedure based on a genetic algorithm is developed using geometrical parameters. It was concluded that zigzag inserts are excellent to chiral lattice inserts, graded tip masses should be used, and nonlinear zigzag inserts can have better vibration suppression characteristics [17]. Later, they use a very similar approach to tune geometrical parameters of zigzag inserts for low-frequency vibration attenuation. It was shown that global vibration amplitudes are reduced considerably within a broader frequency range [18]. Essink

et al. created metastructure, which consists of a primary beam with internal zigzag beams where piezo patches are glued on top of it to harvest energy. They also added nonlinearity to the structure, placing magnets on both sides of the zigzag inserts. The mathematical model is developed for both cases using extended Hamilton's principle. They concluded that the nonlinear system has not the highest power output. However, it can achieve a broadband energy harvesting range, so it is desirable to have nonlinearity in the system for this type of design [19]. Hobeck and Inman also investigate nonlinearity where opposing magnets are placed on top of zigzag inserts. The linear and nonlinear models of the proposed design are developed and verified by the experiment. It is concluded that nonlinear zigzag inserts are superior, and the mathematical model agrees with the experimental results [20]. Later, they added piezo patches on top of the zigzag inserts to harvest energy. Comparing [19], they investigate multi-objective optimization tasks using Pareto Frontier plots. They found that a multifunctional metastructure can maximize power output while minimizing host structure vibrations [21].

Although these studies have promising results, few studies examine damping and frequency-dependent properties of materials used in metastructures [22-25]. Essink and Inman investigated the effectiveness of the absorber design and damping properties of chosen materials rather than the geometry of the absorber design as in the literature. It is shown that if the primary damping ratio is three and above, the effect of the absorber parameters is overpowered [22]. An exact analytical approach is developed to calculate the dynamic for the locally resonant beams where frequency-dependent properties are included in the model by Failla et al. using SDOF and MDOF mass-spring subunits. They concluded that different placements of masses/springs/dashpots might lead to different bandgaps and modal contributions on different modes that need to be investigated to minimize these contributions [23]. Ghachi et al. proposed the metamaterial with periodic viscoelastic subunits to lower vibration transmission at the low frequencies. The linear viscoelasticity concept is used to model VE metamaterial. Since experimental validations are very rare in literature, they manufacture these specimens for this purpose. They developed a

multi-objective optimization task for choosing geometrical parameters and VE layers using a genetic algorithm. It is concluded that the multi-objective optimization algorithm is very reliable where it lowers the weight with high vibration attenuation [24]. Since 3D printing is used to manufacture these metastructures, it is essential to investigate how the properties of polymers are affected by the temperature changes. Liu et al. included viscoelastic properties of 3D printing materials in the model of the metastructure. The effect of the printing directions and testing methodology are both investigated by the experimental setup. It is concluded that printing directions do not affect at all, but the testing configuration has a clear distinction for vibration attenuation characteristics [25].

Free layer damping treatment and constrained layer damping treatment are well studied in literature. Thus, effects of using viscoelastic materials as a damping layer in these treatments are well explained. Passive standoff layer damping treatment is rarely studied so proposed analytical models and experimental studies are very recent. Although adding standoff layer between the base and the damping layer considered first in 1959 by Whittier, it was not studied until the late 80's. Whittier shows that standoff layer can be used as a strain magnifier by increasing shear deformation on viscoelastic layer [26]. Later, Yellin, et al. extensively studied PSLDT to model analytically and verify numerically effects of adding standoff layer to the structure. They developed 1-D analytical model with Euler-Bernoulli beam assumption. The main goal of this is predicting damping performance of the PSLDT correctly. Also, they developed finite element model for both uniform and slotted standoff layer damping treatment to compare analytical and experimental results found. It was found that bonding between layers is very important for the frequency response and standoff layer have infinite shear stiffness and zero bending stiffness in ideal case is very inaccurate assumption made for certain beam configurations [27-28]. Later, the formulation for passive standoff layer treated cantilever beam was developed using a transfer function model by Chaudry. He also developed the finite element model by modifying 4^{th} order equation of motion. The results show that approaches developed for both analytical and finite element model are well agreed

with each other and experiments [29]. Trindade proposed a genetic algorithm-based optimization technique to maximize damping and minimize weight added to structure using both standoff layer and piezoelectric actuators. It is hybrid passive-active vibration control approach where the damping layer thickness and the location of the piezoelectric actuators are design parameters used in optimization. It was shown that damping performance of the hybrid treatment is effective in the higher added mass regions [30]. Eyyupoglu developed novel damping treatment designs for beams using various standoff layer designs. Since analytical model developed does not include complex geometries, finite element model is developed. The main objective was to increase strains in viscoelastic layers which results in higher damping performance. Adding standoff layer introduces significant amount of mass to the structure. Therefore, he also aims to optimize standoff layer geometry while minimizing added weight to the system with high damping performance. Topology optimization methodology is found the most suitable one considering software capabilities of ANSYS and MATLAB. After evaluating all the cases in his study, the optimized standoff layer with multiple constrained layer damping treated beam is found to be superior. As a final step, he selects a sample to verify his model and numerical results by the experiment. It was shown that theoretical, finite element and experimental results are agreed well [31]. Later, the best standoff layer layout of his study is compared with designs proposed in this study.

1.4 Outline of the Thesis

The introduction of vibration control methods used in literature is given in chapter 1. Surface damping treatments and metastructure concept is explained in detail. The scope and objectives of the thesis are briefly mentioned. Literature surveys about metamaterials and passive standoff layer damping treatment are given extensively.

Surface damping treatment and metastructure concept are explained theoretically in chapter 2. Also, various types of viscoelastic modelling approach are presented.

The finite element modeling of the base structure with added surface damping treatments is developed in chapter 3. The ANSYS finite element modelling software is used to develop models. The element types, damping matrix, viscoelastic modelling of the damping layer and contact types are investigated to observe effects of these parameters and whether it can physically represent expected dynamic behavior of the structure. Then, the proposed methodology and finite element models are verified comparing with analytical results and experimental results of previous studies. After verifying the finite element model, the thickness of standoff layer is optimized, and reference CLDT beam with a uniform thickness standoff layer was developed.

Various novel design alternatives are developed using structural and parametric optimization in chapter 4. These novel design alternatives are compared with reference baseline configurations and previous design alternatives from literature considering performance metric defined that describes best damping performance of the structure. Thus, the best novel design alternative is found. Later, a comprehensive comparison of proposed novel design alternatives, metastructures and previous design alternatives from literature is performed.

The conclusion and future recommendations to improve thesis study are given in chapter 5.

CHAPTER 2

THEORETICAL BACKGROUND

2.1 Vibration Damping

Adding any form of damping to the structure results in eliminating vibrations with time. However, quantity, measures and design considerations are differed from one system to another. The main mechanism of the damping is the dissipation of any form of energy as a heat, which actually reduces total vibrational energy of the structure. Thus, it is essential adding damping to the structure to reach desired vibration amplitudes throughout the operating cycle. The main mechanism of eliminating vibrations at resonances or specific frequencies is inertial forces balanced out by damping forces since elastic forces are quite small. Therefore, damping forces are the only resistance to eliminate these vibrations. Damping can be achieved by internally or externally. Material damping is occurred through deformation of the structure, which depends strongly mechanical properties of materials used in the structure. Structural damping, viscous damping, friction damping, viscoelastic damping etc. are other types of damping which have their own damping mechanisms. In this study, viscoelastic vibration damping is the main concern since surface damping treatment designs are developed using viscoelastic material layer as a damping layer.

2.1.1 Viscoelastic Vibration Damping

Viscoelastic materials are polymeric, elastomeric, and amorphous materials that possess both elastic and viscous material behaviors. Damping and stiffness properties of these structures are strongly dependent on the atomic compositions they have. Generally, these rubber-like structures are very soft. Thus, they can not be used

as a structural member to carry loads applied. The structure can have both good damping performance and structural rigidity if added viscoelastic material is properly designed. Thus, modeling of viscoelastic material is a very important research interest for years. Maxwell model, Kelvin – Voigt model, Standard linear model and generalized Maxwell model are developed with attaching spring and mass in serial and parallel and describing constitutive relationships. Partial fraction models are also developed considering stress and strain relationship to describe mathematically. Combining concepts of these models with reduced frequency approach viscoelastic material data can be found in a related frequency region based on the test data. Some of these concepts and models are explained in this section below and given in figure 2.1. Derivation of the constitutive equations of these models are well studied in the literature.

Maxwell model is developed simply connecting spring and dashpot in series and the model is given in figure 2.1. The complex modulus is given in equation 1 [32].

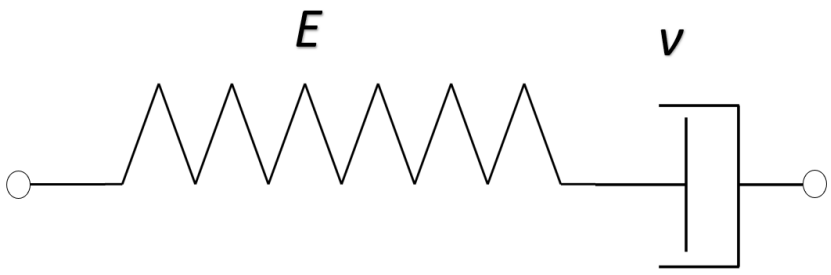

Figure 2.1. Maxwell Model

$$E^*(i\omega) = \frac{i\omega\nu E}{E+i\omega\nu} \quad (1)$$

Kelvin - Voigt model is developed simply connecting spring and dashpot in parallel and the model is given in figure 2.2. The complex modulus is given in equation 2 [32].

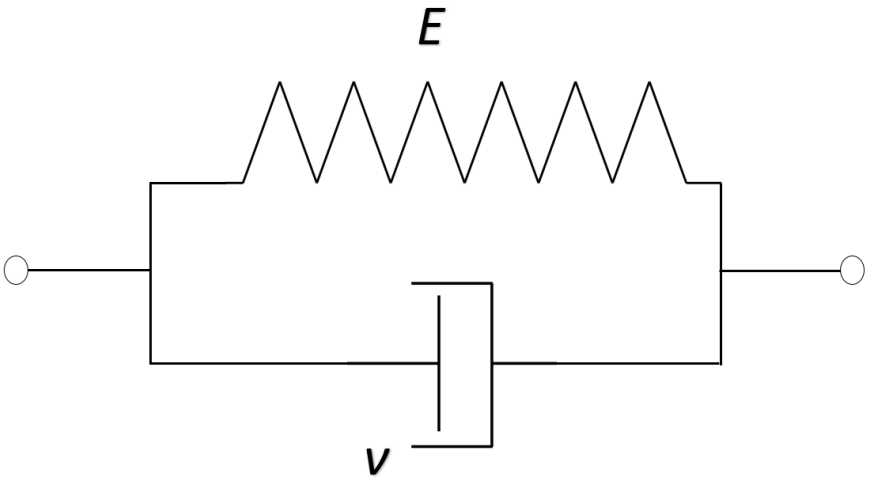

Figure 2.2. Kelvin – Voigt Model

$$E^*(i\omega) = E + i\omega v \tag{2}$$

Standard linear model is developed simply connecting spring and dashpot and spring in parallel and the model is given in figure 2.3. The model can accurately represent real material behavior except the variation of storage and loss modulus with frequency. The complex modulus is given in equation 3 [32].

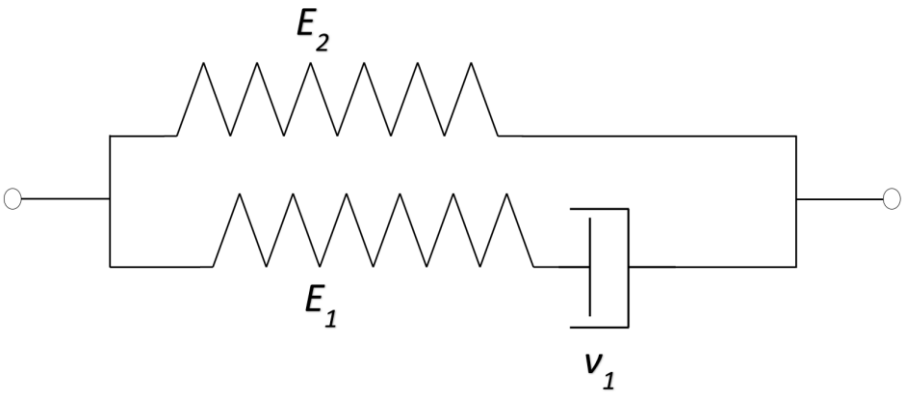

Figure 2.3. Standard Linear Model

$$E^*(i\omega) = \frac{i\omega v_1 E_1}{E_1 + i\omega v_1} + E_2 + i\omega v_2 \tag{3}$$

Based on these simple models, the number of elements are increased to derive more generalized and accurate models. For example, generalized standard model is developed by including additional derivatives terms for stress and strain. Thus, the stress and strain relation can be given in equation 4.

$$\sigma + \sum_{n=1}^{\infty} \alpha_n \frac{d^n \sigma}{dt^n} = E\varepsilon + E \sum_{n=1}^{\infty} \beta_n \frac{d^n \varepsilon}{dt^n} \quad (4)$$

For harmonic forcing, harmonic stress and strain functions can be rewritten as in equation 5.

$$\sigma = \sigma_0 e^{i\omega t}; \varepsilon = \varepsilon_0 e^{i\omega t} \quad (5)$$

Putting and arranging these harmonic forms into equation 4 yields to equation 6.

$$\sigma_0 = \frac{E\varepsilon_0[1+\sum_{n=1}^{\infty} \beta_n (i\omega)^n]}{[1+\sum_{n=1}^{\infty} \alpha_n (i\omega)^n]} = (E' + iE'')\varepsilon_0 \quad (6)$$

Although it is more complicated, the material data can be fitted by properly choosing α_n and β_n. Then, expressions for storage and loss modulus are given in equations 7 and 8 respectively.

$$\frac{E'}{E} = \frac{AC+BD}{C^2+D^2} \quad (7)$$

$$\frac{E''}{E} = \frac{BC+AD}{C^2+D^2} \quad (8)$$

The unknown terms are given in equation 9, 10, 11 and 12.

$$A = 1 - \beta_2\omega^2 + \beta_4\omega^4 \cdots i^{2n-2}\beta_{2n-2}\omega^{2n-2} \quad (9)$$

$$B = \beta_1\omega - \beta_3\omega^3 + \beta_5\omega^5 \cdots i^{2n-1}\beta_{2n-1}\omega^{2n-1} \quad (10)$$

$$C = 1 - \alpha_2\omega^2 + \alpha_4\omega^4 \cdots i^{2n-2}\alpha_{2n-2}\omega^{2n-2} \quad (11)$$

$$D = \alpha_1\omega - \alpha_3\omega^3 + \alpha_5\omega^5 \cdots i^{2n-1}\alpha_{2n-1}\omega^{2n-1} \quad (12)$$

Partial fraction models are developed to reduce the number of terms used in generalized standard model. The relation between stress and strain is given in equation 13.

$$\sigma(t) + \sum_{n=1}^{\infty} a_n D^{\alpha_n}[\sigma(t)] = E\varepsilon(t) + E\sum_{n=1}^{\infty} b_n D^{\beta_n}[\varepsilon(t)] \quad (13)$$

The generalized derivatives can be defined as in equation 14 using gamma function.

$$D^{\alpha_n}[x(t)] = \frac{1}{\Gamma(1-\alpha_n)} \frac{d}{dt} \int_0^t \frac{x(\tau)}{(t-\tau)^{\alpha_n}} dt \quad (14)$$

For harmonic forcing, harmonic stress and strain functions can be rewritten as in equation 15.

$$\sigma_0[1 + \sum_{n=1}^{\infty} a_n (i\omega)^{\alpha_n}] = E\varepsilon_0\left[1 + \sum_{n=1}^{\infty} b_n (i\omega)^{\beta_n}\right] \quad (15)$$

The initial stress can be represented in the complex form as in equation 16.

$$\sigma_0 = E^* \varepsilon_0 = (E' + iE'')\varepsilon_0 \quad (16)$$

Therefore, the relations for storage and loss modulus can be represented as in equation 17 and 18 respectively.

$$\frac{E'}{E} = Re\left[\frac{1+\sum_{n=1}^{\infty} b_n (i\omega)^{\beta_n}}{1+\sum_{n=1}^{\infty} a_n (i\omega)^{\alpha_n}}\right] \quad (17)$$

$$\frac{E''}{E} = Im\left[\frac{1+\sum_{n=1}^{\infty} b_n (i\omega)^{\beta_n}}{1+\sum_{n=1}^{\infty} a_n (i\omega)^{\alpha_n}}\right] \quad (18)$$

Using regular complex number, i.e., $i=e^{i\pi/2}$, and N=1, the complex modulus can be written as in equation 19.

$$\frac{E^*}{E_e} = \frac{1+b_1(i\omega)^{\beta_1}}{1+a_1(i\omega)^{\alpha_1}} = \frac{A+iB}{C+iD} \quad (19)$$

The unknown terms are given in equation 20, 21, 22 and 23.

$$A = 1 + b_1 \cos\left(\frac{\beta_1 \pi}{2}\right)\omega^{\beta_1} \quad (20)$$

$$B = b_1 \sin\left(\frac{\beta_1 \pi}{2}\right)\omega^{\beta_1} \quad (21)$$

$$C = 1 + a_1 \cos\left(\frac{\alpha_1 \pi}{2}\right)\omega^{\alpha_1} \quad (22)$$

$$D = a_1 \sin\left(\frac{\alpha_1 \pi}{2}\right)\omega^{\alpha_1} \quad (23)$$

The storage modulus and the loss factor of the viscoelastic materials are highly dependent on both temperature and frequency. However, they show similar behavior while increasing. Therefore, reduced frequency concept is introduced using similarity between frequency and temperature dependence of viscoelastic materials. The approach based on complex modulus at some distinct temperature and frequency are identical to each other. Starting from the reference temperature, the complex modulus and the loss factor values are determined along the reduced frequency axis. Then, these values are curve fitted to determine master curve which represents viscoelastic material data in reduced frequency domain. The reduced frequency curves are given in figure 2.4 as an example [32].

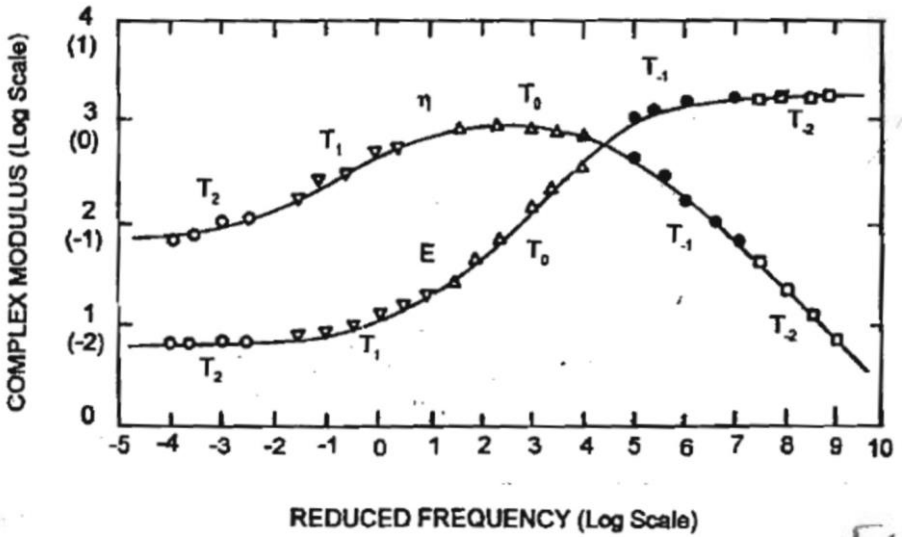

Figure 2.4. The Reduced Frequency Curves [32]

Also, the well-known shift factor equation, namely, The Arrhenius shift factor equation is given in equation 24.

$$\log[\alpha(T)] = T_A(\frac{1}{T} - \frac{1}{T_0}) \quad (24)$$

Combining reduced frequency approach with the mathematical models, the complex modulus and loss factor values for viscoelastic materials can be found. Replacing frequency with reduced frequency in partial fraction model, the complex modulus and the reduced frequency can be represented as in equation 25 and 26 respectively.

$$E^* = \sum_{n=1}^{N} \frac{a_n + b_n(i\omega_R)^{\beta n}}{1 + c_n(i\omega_R)^{\alpha n}} \quad (25)$$

$$\omega_R = \omega\alpha(t) \quad (26)$$

2.2 Surface Damping Treatments

Surface damping treatments are developed in such an approach that viscoelastic materials can be used to add damping to the structure if it is designed properly. These treatments are explained in detail in this section.

2.2.1 Free Layer Damping Treatment (FLDT)

FLDT is simply applied to the base structure by coating with constant thickness. The viscoelastic layer deforms in flexure which increases the dissipation of the energy by deforming VE layer. FLDT and deformation pattern are shown in figure 2.5 [32]. A mathematical model of the FLDT is developed considering pure bending of two-layer composite beam. Oberst and Ross – Kerwin – Ungar (RKU) equations are used most to mathematically describe FLDT. These equations are given in equations 27 and 28 respectively.

$$\frac{(EI)^*}{E_1 I_1} = 1 + \frac{E_2^*}{E_1}\left(\frac{H_2}{H_1}\right)^3 + 3\left(1 + \frac{H_2}{H_1}\right)^2 \frac{\frac{E_2^*}{E_1}\left(\frac{H_2}{H_1}\right)}{1 + \frac{E_2^*}{E_1}\left(\frac{H_2}{H_1}\right)} \quad (27)$$

The unknown parameters in this equation are "*E*" for Young's Modulus of the layer, "*H*" for thickness of the layer, "*I*" for moment of inertia of the layer and "*" for complex form. Equation 28 is developed considering thickness of the third layer is zero in RKU equation.

$$\frac{(EI)^*}{E_1 I_1} = 1 + e_2(h_2)^3 + 3(1 + h_2)^2 \frac{e_2 h_2}{1 + e_2 h_2} \quad (28)$$

The unknown parameters are given in equation 29.

$$e_2 = \frac{E_2^*}{E_1}; h_2 = \frac{H_2}{H_1}; I_1 = \frac{1}{12} b(H_1)^3 \quad (29)$$

It can be seen that equations 27 and 28 are exactly the same.

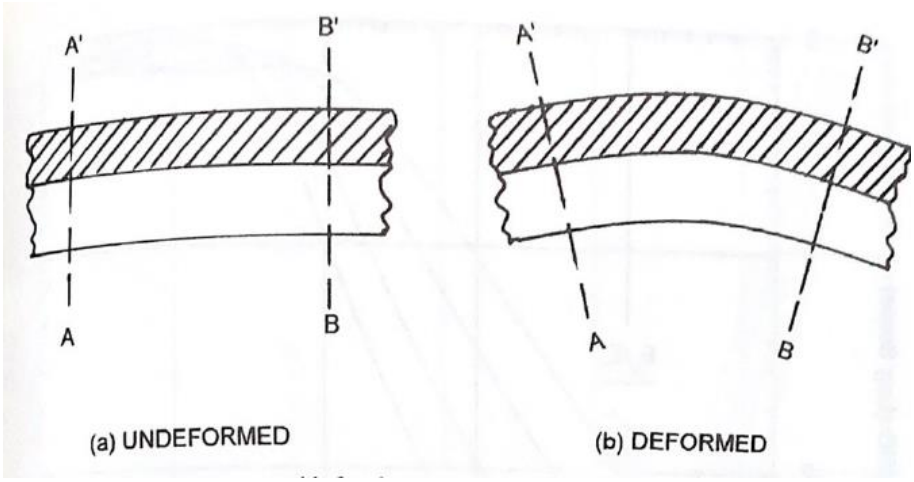

Figure 2.5. Free Layer Damping Treatment [32]

2.2.2 Constrained Layer Damping Treatment (CLDT)

VE layer is constrained by another stiff layer from the top in CLDT. Therefore, it is sandwiched between stiff layers which results in the changing deformation pattern of VE layer. Thus, VE layer deforms in shear mode. It is found that CLDT is superior considering weight and damping performance than FLDT. CLDT and deformation pattern are shown in figure 2.6 [32]. RKU equations are developed for only pinned - pinned boundary condition to explain CLDT mathematically. Later, the correction factors are defined for other boundary conditions. A more accurate form of these equation was developed by Rao using Euler - Bernoulli beam theory. RKU equations for single layer constrained damping layer treatment is given below in equation 30.

$$(EI)^* = \frac{E_1 {H_1}^3}{12} + \frac{{E_2}^* {H_2}^3}{12} + \frac{E_3 {H_3}^3}{12} - \frac{{E_2}^* {H_2}^2}{12}\left(\frac{H_{31}-D}{1+g^*}\right) + E_1 H_1 D^2 + {E_2}^* H_2 (H_{21}-D)^2 +$$

$$\cdots E_3 H_3 (H_{31}-D)^2 - \left(0.5 {E_2}^* H_2 (H_{21}-D) + E_3 H_3 (H_{31}-D)\right)\left(\frac{H_{31}-D}{1+g^*}\right) \quad (30)$$

The unknown parameters in this equation are given in equation 31, 32, 33 and 34 respectively.

$$H_{31} = H_2 + 0.5(H_1 + H_3) \tag{31}$$

$$H_{21} = 0.5(H_1 + H_2) \tag{32}$$

$$D = \frac{E_2{}^* H_2(H_{21} - 0.5H_{31}) + g^*(E_2{}^* H_2 H_{21} + E_3 H_3 H_{31})}{E_1 H_1 + 0.5E_2{}^* H_2 + g^*(E_1 H_1 + E_2{}^* H_2 + E_3 H_3)} \tag{33}$$

$$g^* = \frac{G_2{}^* \lambda^2}{E_3 H_2 H_3 \pi^2} \tag{34}$$

Rao's correction factor for the specific mode and boundary conditions needs to be used in RKU equations to model accurately other boundary conditions as given in table 2.1 [32]. Therefore, modified shear parameter and the semi-wavelength for any mode are replaced in RKU equation. These modified parameters are given in equation 35 and 36.

$$g^* = \frac{G_2{}^* L^2}{E_3 H_2 H_3 \xi_n{}^2 \sqrt{C_n}} \tag{35}$$

$$\lambda = \frac{\pi L}{\xi_n \sqrt{C_n}} \tag{36}$$

Table 2.1 Corrections to Shear Parameter for Various Beam Boundary Conditions[32]

Boundary Conditions	Correction Factor	
	Mode 1	Mode 2+
Pinned-Pinned	1	1
Clamped-Clamped	1.4	1
Clamped-Pinned	1	1
Clamped-Free	0.9	1
Free-Free	1	1

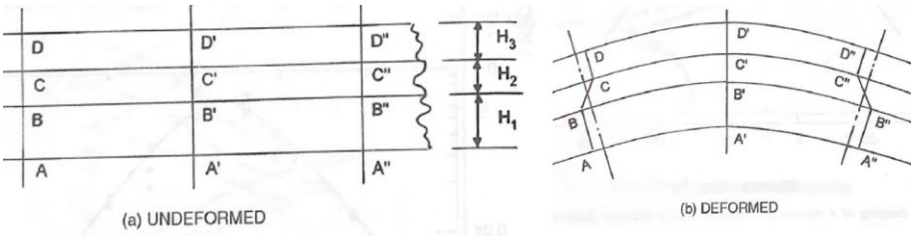

Figure 2.6. Constrained Layer Damping Treatment [32]

2.2.3 Passive Standoff Layer Damping Treatment (PSLDT)

PSLDT is developed using standoff layer between the base and VE layer which increases distance between damping layer and neutral axis. Induced strains are magnified so damping performance of the structure can be increased if it is properly designed. PSLDT and deformation pattern are shown in figure 2.7 [33]. Yellin and her research group investigate the mathematical model of passive standoff layer beam using the method of distributed transfer functions. In their model, they assumed that the base and the constraining layer do not deform in shear while the VE layer deforms only in shear. They demonstrate that the dynamic behavior of the structure can be improved by adding the standoff layer. The reader can further examine mathematical models in their research paper [28].

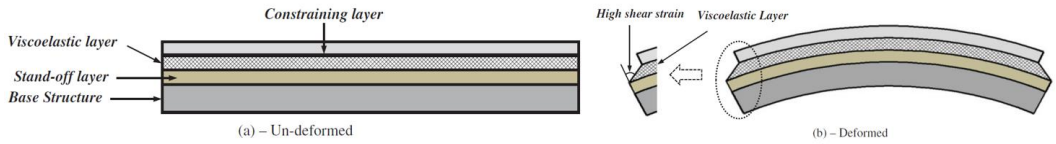

Figure 2.7. Passive Standoff Layer Damping Treatment [33]

2.3 Metastructures

Metastructures that consist of the primary structure and locally resonant subunits are created by embedding these subunits to the primary structure rather than attaching them to reduce vibration levels of the main structure. These internal locally resonant

subunits can be spring-mass, mass in mass SDOF subsystems, periodic two-mass spring-mass-damper inserts, periodic and graded chiral lattices, and the zigzag inserts. The main mechanism behind reducing vibration level is found to be local resonance mechanism structure have from embedded local resonators. The theory of metastructure is explained below [3].

Negative effective mass concept is demonstrated considering two-degree-of-freedom mass-in-mass structure as shown in figure 2.8 [3].

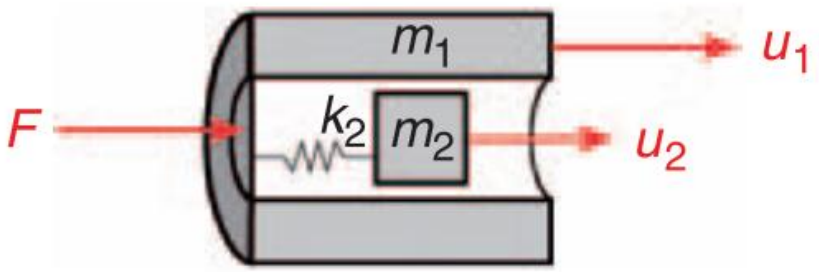

Figure 2.8. 2-DOF mass-in-mass structure [3]

Equation of the motion of the structure is given in equation 37 in matrix form.

$$\begin{bmatrix} m_1 & 0 \\ 0 & m_2 \end{bmatrix} \begin{Bmatrix} \ddot{u_1} \\ \ddot{u_2} \end{Bmatrix} + \begin{bmatrix} k_2 & -k_2 \\ -k_2 & k_2 \end{bmatrix} \begin{Bmatrix} u_1 \\ u_2 \end{Bmatrix} = \begin{Bmatrix} F \\ 0 \end{Bmatrix} \tag{37}$$

Assuming harmonic motion, the forcing and response are in the form of equation 38.

$$F = F_0 e^{i\omega t}; \begin{Bmatrix} u_1 \\ u_2 \end{Bmatrix} = \begin{Bmatrix} a_1 \\ a_2 \end{Bmatrix} e^{i\omega t} \tag{38}$$

Then, the frequency response functions and the dynamical effective mass can be found as in equation 39, 40 and 41 respectively.

$$H_{11} = \frac{a_1}{F_0} = \frac{k_2 - m_2\omega^2}{(k_2 - m_1\omega^2)(k_2 - m_2\omega^2) - {k_2}^2} \tag{39}$$

$$H_{21} = \frac{a_2}{F_0} = \frac{k_2}{(k_2 - m_1\omega^2)(k_2 - m_2\omega^2) - {k_2}^2} \tag{40}$$

$$\widetilde{m_1} = \frac{F}{\ddot{u_1}} = \frac{F_0}{-\omega^2 a_1} = m_1 + \frac{m_2}{1-(\omega^2/{\omega_2}^2)}; \omega_2 = \sqrt{\frac{k_2}{m_2}} \quad (41)$$

It can be understood that if the excitation frequency is equal to the local resonance frequency of the spring-mass subsystem, the effective mass tends to infinity theoratically. Then, arranging given equations the external force and the inertia force can be found that as in equation 42.

$$F_0 = -k_2 a_2; F(t) = -k_2 u_2(t) = m_2 \ddot{u_2}(t) \quad (42)$$

From this equality, it is shown that the external force is cancelled out by the inertia force which is the same mechanism in the vibration absorbers. The responses are out of phase in an optical mode where $\omega > \omega_2$ and the effective mass is negative. Also, the responses are in phase in an acoustic mode where $\omega < \omega_2$ and the effective mass is positive.

Numerical examples show that the embedded local resonators can be used to reduce peak vibration response values at resonance frequencies. Therefore, the broadband vibration absorption can be achieved if the local resonators are properly designed. It is relatively simple considering required natural frequency of the absorbers which is equal or very close to the one of the natural frequency of the structure can achieved with tuning the mass and stiffness of the vibration absorber along the structure.

CHAPTER 3

FINITE ELEMENT MODELING OF THE BASE STRUCTURE WITH ADDED SURFACE DAMPING TREATMENTS

3.1 Introduction

With advancing technology, lightweight structures can be easily manufactured using additive manufacturing techniques. However, this leads to modelling complexity of the designed system which leads to finding an analytical solution being very complicated. Numerical approximation methods and finite element modelling can be beneficial in this context. Since topology optimization generally results in very complex geometries in boundaries, finite element modelling is used to model these geometries. The proposed methodology and verification of the developed models are explained in this chapter.

3.2 Methodology

ANSYS simulation software is chosen for finite element modelling. There is various software in industry which have their own capabilities, element types, analysis types and modelling techniques. Therefore, it can be noted that description of the element types and which analysis types support them is very important. The simply supported beam configuration is chosen to compare finite element model with analytical model. Further, the fixed-free beam configuration is chosen to validate finite element model using results in literature. After the developed model is verified, the fixed-fixed beam configuration is used to find optimum thickness of the standoff layer. Boundary conditions for the optimization are defined according to the effective beam length is restricted on both ends which resembles inner section of the fuselage geometry is constrained by stinger and frames as in Ulubalci's previous work [36]. Harmonic analysis system is used in ANSYS since frequency and temperature dependent

properties can be best modelled in this module. The material properties used throughout this study in analysis are shown in table 3.1. The ISD – 112 material by 3M Company is chosen as a viscoelastic material for practical purposes. The damping material properties are found using equations given in [34]. Soovere and Drake extensively measure numerous industrial damping material properties in their book. Equations found are based on these curve-fitted experimental data. The complex shear modulus and the shift factor formulation are given in equation 43 and 44 respectively.

$$G^* = G(1 + i\eta) = G_e + \frac{G_1}{1+c_1(i\frac{f_R}{f_1})^{-\alpha_1}+(i\frac{f_R}{f_1})^{-\beta_1}} \quad (43)$$

$$\log\big(\alpha(T)\big) = a\left(\frac{1}{T} - \frac{1}{T_o}\right) + 2.303\left(\frac{2a}{T_o} - b\right)\log\left(\frac{T}{T_o}\right) + (\frac{b}{T_o} - \frac{a}{{T_o}^2} - S_{AZ})(T - T_o) \quad (44)$$

The unknown parameters a and b in equation 44 can be found using equations 45-51 respectively.

$$C_A = \left(\frac{1}{T_L} - \frac{1}{T_o}\right)^2 \quad (45)$$

$$C_B = \left(\frac{1}{T_L} - \frac{1}{T_o}\right) \quad (46)$$

$$C_C = \left(\frac{1}{S_{AL}} - \frac{1}{S_{AZ}}\right) \quad (47)$$

$$D_A = \left(\frac{1}{T_H} - \frac{1}{T_o}\right)^2 \quad (48)$$

$$D_B = \left(\frac{1}{T_H} - \frac{1}{T_o}\right) \quad (49)$$

$$D_C = \left(\frac{1}{S_{AH}} - \frac{1}{S_{AZ}}\right) \quad (50)$$

$$D_E = (D_B C_A - D_A C_B) \quad (51)$$

$$a = (D_B C_C - D_C C_B)/D_E \quad (52)$$

$$b = (D_C C_A - D_A C_C)/D_E \quad (53)$$

The other unknown parameters for both equations are given in table 3.2. Therefore, the complex shear modulus can be found at any given frequency and temperature using these equations.

Table 3.1 Material Properties

Material	Property	Value	Units	Symbol
Aluminum	Density of the Base Layer	2700	kg/m^3	ρ_1
	Young's Modulus of the Base Layer	70000	MPa	E_1
	Poisson's Ratio of the Base Layer	0.33	-	ν_1
ABS M30	Density of the Standoff Layer	1040	kg/m^3	ρ_2
	Young's Modulus of the Standoff Layer	2400	MPa	E_2
	Poisson's Ratio of the Standoff Layer	0.45	-	ν_2
ISD 112	Density of the Viscoelastic Layer	900	kg/m^3	ρ_3
	Young's Modulus of the Viscoelastic Layer	Freq. Dep.	MPa	E_3
	Poisson's Ratio of the Viscoelastic Layer	0.49	-	ν_3
Aluminum	Density of the Constraining Layer	2700	kg/m^3	ρ_4
	Young's Modulus of the Constraining Layer	70000	MPa	E_4
	Poisson's Ratio of the Constraining Layer	0.33	-	ν_4

Table 3.2 The Unknown Parameter for Equations 43 and 44

Property	Value	Units
G_e	0.4307	MPa
G_1	1200	MPa
f_1	0.1543×10^7	Hz
c_1	3.241	-
a_1	0.18	-
β_1	0.6847	-
T	Reference	K
T_0	290	K
T_H	360	K
S_{AZ}	0.05956	K^{-1}
S_{AL}	0.1474	K^{-1}
S_{AH}	0.009725	K^{-1}

After defining material properties, it is essential to import these values into the finite element model. Elastic materials can be defined easily since material properties remain the same in all directions when they deform. However, the frequency dependent complex modulus and loss factor values need to be carefully assigned in ANSYS. ANSYS introduced various damping matrices for specific types of problems. ANSYS defines the damping matrix given in equation 54 for the harmonic analysis module where the full equation of motion is solved directly [35].

$$[C] = \alpha[M] + \left(\beta + \frac{g}{\omega}\right)[K] + \sum_{i=1}^{N_{ma}} \alpha_i^m [M_i] + \sum_{i=1}^{N_{ma}^{MD}} \sum_{k=1}^{N_{sa}} \alpha_p [M_k]_i + \cdots + \sum_{j=1}^{N_m} \left(\beta_j^m + \frac{m_j}{\omega} + \frac{g_j^E}{\omega}\right)[K_j] + \sum_{j=1}^{N_{mb}^{MD}} \sum_{n=1}^{N_{sb}} \beta_q [K_n]_j + \sum_{k=1}^{N_e} [C_k] + \cdots + \sum_{m=1}^{N_v} \frac{[K_m]}{\omega} + \sum_{l=1}^{N_g} [G_l] + \frac{1}{\omega} \sum_{k=1}^{N_e^*} [K_k{}^*] \quad [54]$$

Since the frequency-dependent structural damping coefficient for damping material is the only damping source, the damping matrix is reduced to equation 55.

$$[C] = \sum_{j=1}^{N_m} \left(\frac{g_j^E}{\omega}\right)[K_j] \; where \qquad [55]$$

$$g_j^E = structural\ damping\ coefficient\ for\ material\ j$$

$$N_m = number\ of\ materials, \omega = excitation\ circular\ frequency$$

$$[K_j] = portion\ of\ structural\ stiffness\ matrix\ based\ on\ material\ j$$

The structural damping coefficient can be defined using "TB, SDAMP," command. However, this command also needs "TBFIELD, FREQ" command for defining certain frequency values and "TBDATA" command for importing data in table. Thus, the structural damping command combined with frequency command for each frequency point is defined. The example of defining damping values with respect to frequency is given in figure 3.1. The elastic modulus is also defined in a similar manner using "TB, ELASTIC," command as given in figure 3.2. Thus, frequency dependent elastic modulus and loss factor values can be defined in any frequency range with proper units selected.

```
20020  TB,SDAMP,MATID      → The structural damping is applied to the material.
20021  TBFIELD,FREQ,1      → The frequency is defined.
20022  TBDATA,1,0.0672     → The value of the coefficient is defined in table.
20023  TBFIELD,FREQ,2
20024  TBDATA,1,0.1056
20025  TBFIELD,FREQ,3
20026  TBDATA,1,0.1368
20027  TBFIELD,FREQ,4
20028  TBDATA,1,0.1639
20029  TBFIELD,FREQ,5
20030  TBDATA,1,0.1881
```

Figure 3.1. Defining damping values in ANSYS

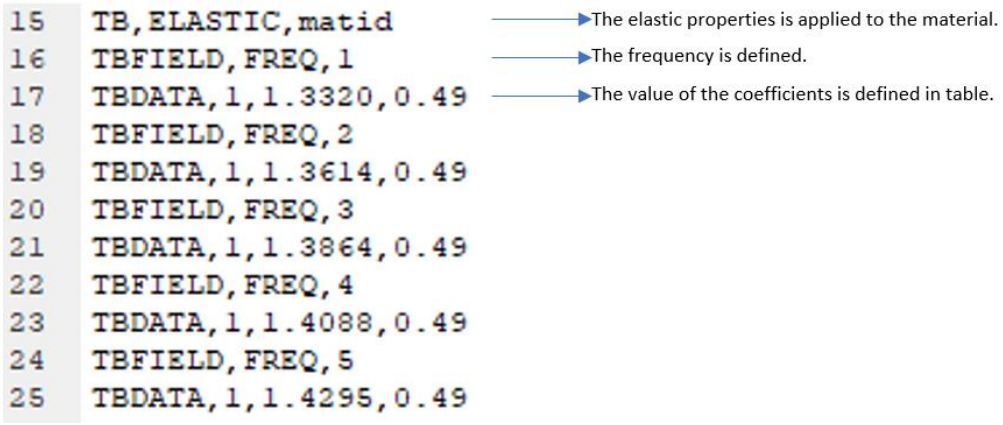

Figure 3.2. Defining elastic properties in ANSYS

It is also worth mentioning that SOLID 185 - 187 and PLANE 182/183 elements support material dependent structural damping in ANSYS. Therefore, the effects of mesh density, the element type and the element order are observed considering the computation time required and whether the structural damping is applied to the structure properly. The reference case for this comparison analysis is chosen from Eyyupoglu's study [31]. The geometric properties of this reference beam are given in table 3.3. Seven different cases are defined in the analysis. The frequency dependent damping is only added to the damping layer while the global damping is applied to the structure. The frequency range is defined as 0 to 130 Hz considering the first natural frequency of the reference beam. The properties of these cases are given in figure 3.3. Also, the frequency response function comparison is given in figure 3.4.

Table 3.3 Geometric Properties of the Reference CLDT Beam

Property	Value	Units	Symbol
Thickness of the Base Layer	3	mm	H_1
Thickness of the Viscoelastic Layer	0.127	mm	H_2
Thickness of the Constraining Layer	0.254	mm	H_3
Width of the Beam	12.7	mm	w_b
Length of the Beam	150	mm	L_b

Property	Case-1	Case-2	Case-3	Case-4	Case-5	Case-6	Case-7
The element number	6000	6000	6000	4800	2400	2400	4800
The node number	8305	8305	8305	25021	7817	7817	6795
The element type	SOLID185	SOLID185	SOLID186	SOLID186	PLANE183	PLANE183	SOLID185
The element order	linear	linear	linear	quadratic	quadratic	quadratic	linear
Global damping	yes	yes	yes	yes	yes	yes	yes
Structural damping	no	yes	yes	yes	no	yes	yes
The computation time	3 min 37 sec	5 min 31 sec	5 min 23 sec	11 min 11 sec	35 sec	1 min	4 min 44 sec
The natural frequency [Hz.]	120	118	123	118	107	107	118

Figure 3.3. Comparison Table for Cases in Analysis

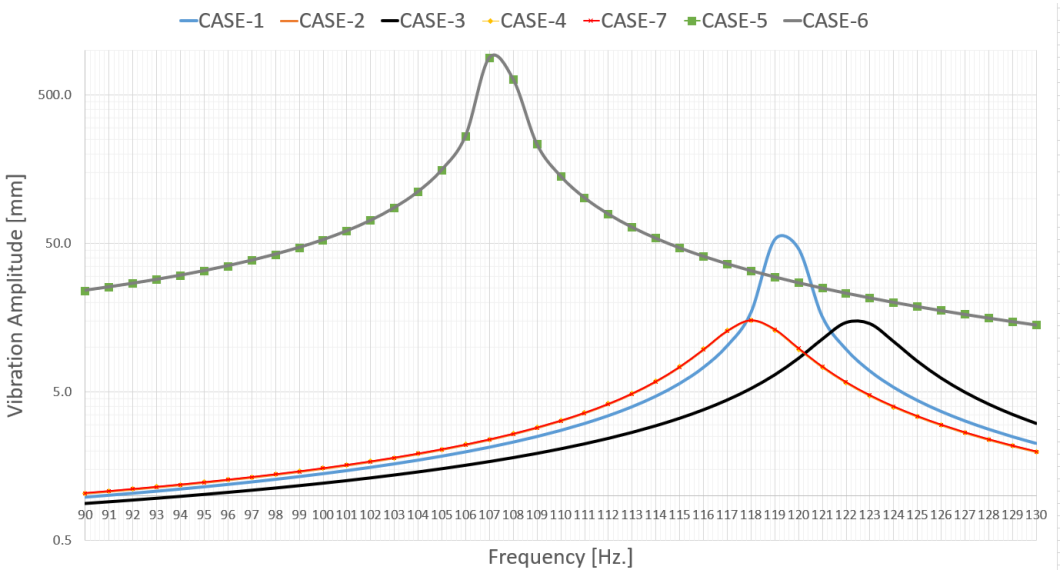

Figure 3.4. The FRF Comparison for Cases in Analysis

Comparing FRF results, it is found that case-2, case-4, and case-7 have well agreed each other with slightly differences in vibration amplitudes, SOLID186 element needs to be used in quadratic order since this element displays quadratic displacement behavior and the structural damping can not be added to PLANE183 elements using commands. Also, case-2, case-4 and case-7 have very close first natural frequency with the analytical result for reference beam. The comparison is given in table 3.4. Thus, considering all of the results mentioned, SOLID185 element with linear element order is found to be the best choice to use in finite element modelling.

Table 3.4 The Comparison with Analytical Results

Case in Analysis	Nat. Freq. [Hz.]	Loss Factor [-]	Error [%]	Error [%]
CASE-2	118.00	0.02864	0.55	11.19
CASE-4	118.00	0.02856	0.55	11.45
CASE-7	118.00	0.02873	0.55	10.92
Analytical Result	117.36	0.03225	NA	NA

The bonding between layers in surface damping treatment applications is another important factor. Generally, the layers are bonded together using very thin and stiff adhesive as possible in real damping treatment applications. Thus, the connections between layers must be well defined in the finite element model. However, it is assumed that perfect bonding has occurred between layers in developed analytical models. Generally, it is preferred that the adhesive layer is added to the finite element model for only practical purposes when necessary. Thus, the connections between layers are assumed to be perfectly rigid. Pure penalty, multi-point constraint (MPC), normal Lagrange, and augmented Lagrange are contact types used in ANSYS. Also, the shared topology option in SCDM can be used to define rigid connection between layers. All of them have their own computational capabilities and simplifications. Therefore, it is essential to observe the effects of these contact types. The geometric properties of the beam used in contact type analysis are given in table 3.5. Also, the frequency response function comparison is given in figure 3.5.

Table 3.5 The Geometric Properties of the Reference PSLDT Beam

Property	Value	Units	Symbol
Thickness of the Base Layer	3	mm	H_1
Thickness of the Standoff Layer	4	mm	H_2
Thickness of the Viscoelastic Layer	0.127	mm	H_3
Thickness of the Constraining Layer	0.254	mm	H_4
Width of the Beam	12.7	mm	w_b
Length of the Beam	150	mm	L_b

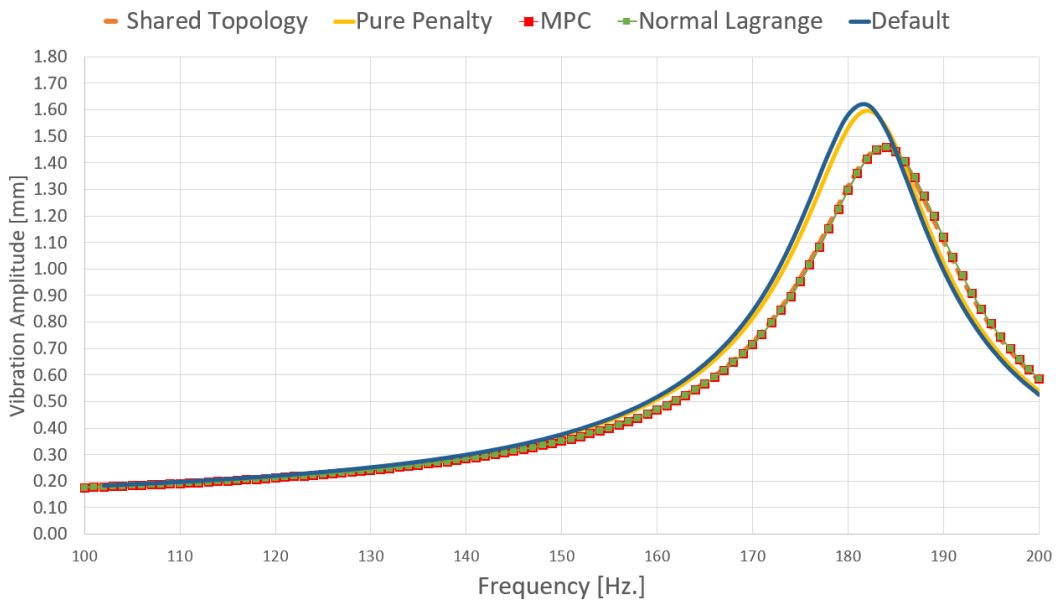

Figure 3.5. The FRF Comparison for Contact Types Analysis

Comparing FRF results, it is found that MPC, normal Lagrange and the shared topology contact methods have well agreed each other, the augmented Lagrange method is the default for this harmonic analysis problem, and the pure penalty method has higher vibration amplitudes since it does not encounter contact between surfaces. Thus, considering all of the results mentioned, the shared topology method is found to be the best choice to use in finite element modelling considering the computation time is lesser than MPC and the normal Lagrange methods.

In summary, the frequency dependent damping is added using commands, SOLID185 element with linear element order and the shared topology method for contacting layers are chosen to develop finite element models throughout this study.

3.3 Comparison with Analytical Results

The finite element model and analytical results are compared to verify developed model. The CLDT beam is chosen since the analytical results can be easily computed

by solving forced vibration analysis problem for the simply supported beam. Since frequency dependent material properties are also a function of the frequency itself, iterative procedure is required to find loss factor and natural frequency values. MATLAB software is used to compute analytical results and the FRF of the CLDT beam. Iterative solution procedure of analytical model is given in figure 3.6. Also, the frequency parameter table which can be used to find βn values for different boundary condition is given in figure 3.7 [37].

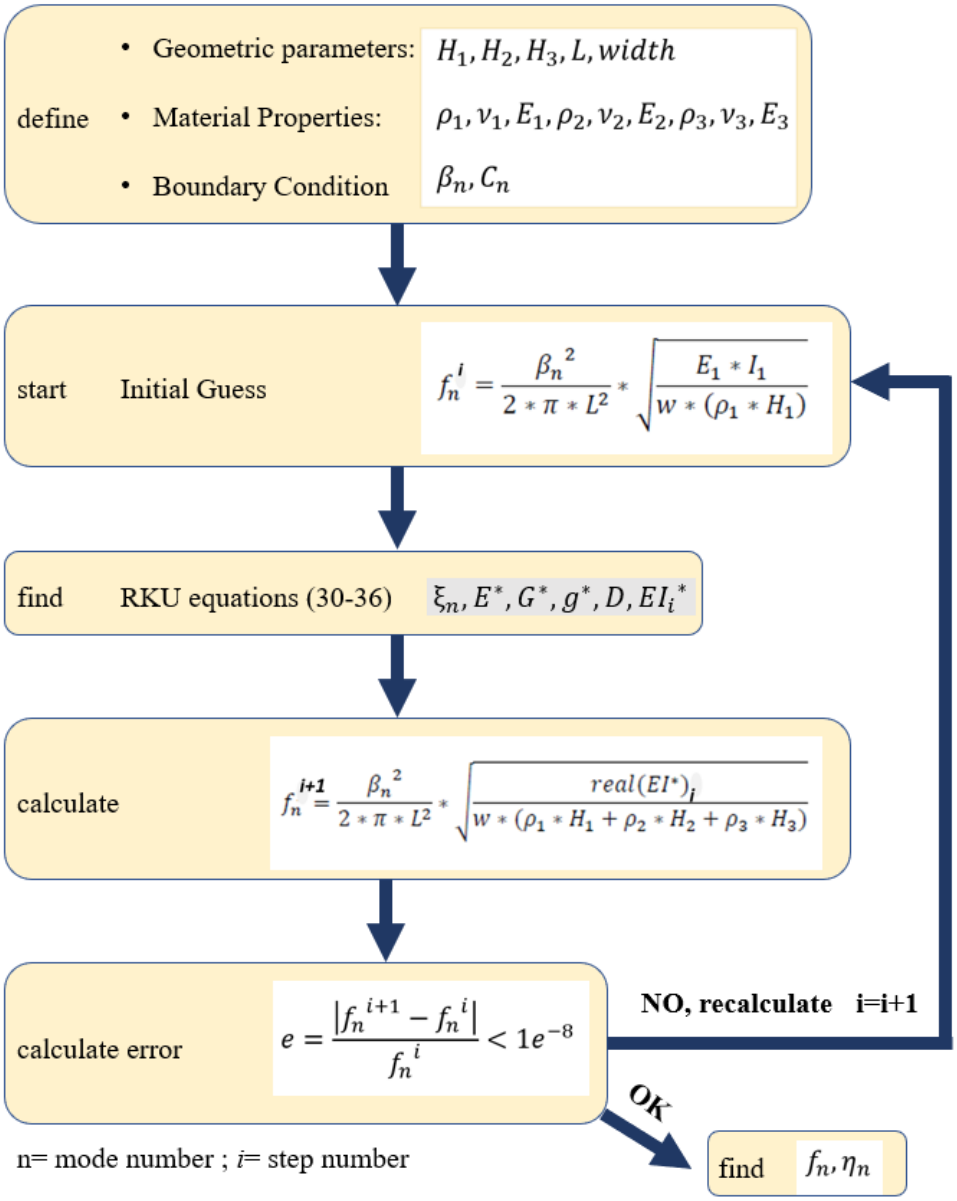

Figure 3.6. Iterative Solution Procedure of Analytical Model

m	C-C	C-SS	C-F	SS-SS	SS-F	F-F
1	22.373	15.418	3.516	9.8696	Same as	Same as
2	61.673	49.965	22.034	39.478	C-SS cases	C-C
3	120.903	104.248	61.697	88.826	Plus one	Plus two
4	199.859	178.270	120.902	157.914	Zero root	Zero roots
5	298.556	272.031	199.860	246.740		
> 5	$(2m+1)^2\pi^2/4$	$(4m+1)^2\pi^2/16$	$(2m-1)^2\pi^2/4$	$m^2\pi^2$		

** C: Clamped SS: Simply Supported F: Free

Table: Frequency Parameters $\beta_i^2=(\alpha_i l)^2=\omega_i l^2\sqrt{\rho A/EI}$ for beams with elementary boundary condition.

Figure 3.7. The Frequency Parameter Table for Different Boundary Conditions[37]

After error condition is satisfied, the loss factor and natural frequency values can be found as in equation 56 and 57.

$$\eta_n^i = \frac{imag(EI_i^*)}{real(EI_i^*)} \tag{56}$$

$$f_n^i = \frac{{\beta_n}^2}{2\pi L^2} * \sqrt{\frac{real(EI_i^*)}{width*(\rho_1 H_1+\rho_2 H_2+\rho_3 H_3)}} \tag{57}$$

The finite element model developed for comparison is shown in figure 3.8. The unit harmonic forcing is applied to middle section while simply supported boundary conditions are defined both ends of the CLDT beam. The geometric properties of this CLDT beam are given in table 3.6.

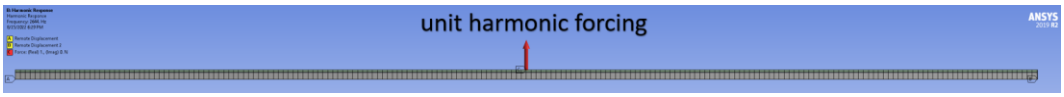

Figure 3.8. The FEM for Simply Supported CLDT Beam

Table 3.6 The Geometric Properties of the CLDT Beam

Property	Value	Units	Symbol
Thickness of the Base Layer	1	mm	H_1
Thickness of the Viscoelastic Layer	0.127	mm	H_2
Thickness of the Constraining Layer	0.254	mm	H_3
Width of the Beam	12.7	mm	w_b
Length of the Beam	150	mm	L_b

The problem is solved in 0-3200 Hz. frequency range considering computation time required to get high frequency modes in the FEM. Thus, the first three modes of the CLDT beam are found. The FRF comparison plot and results are given in figure 3.9 and table 3.7 respectively.

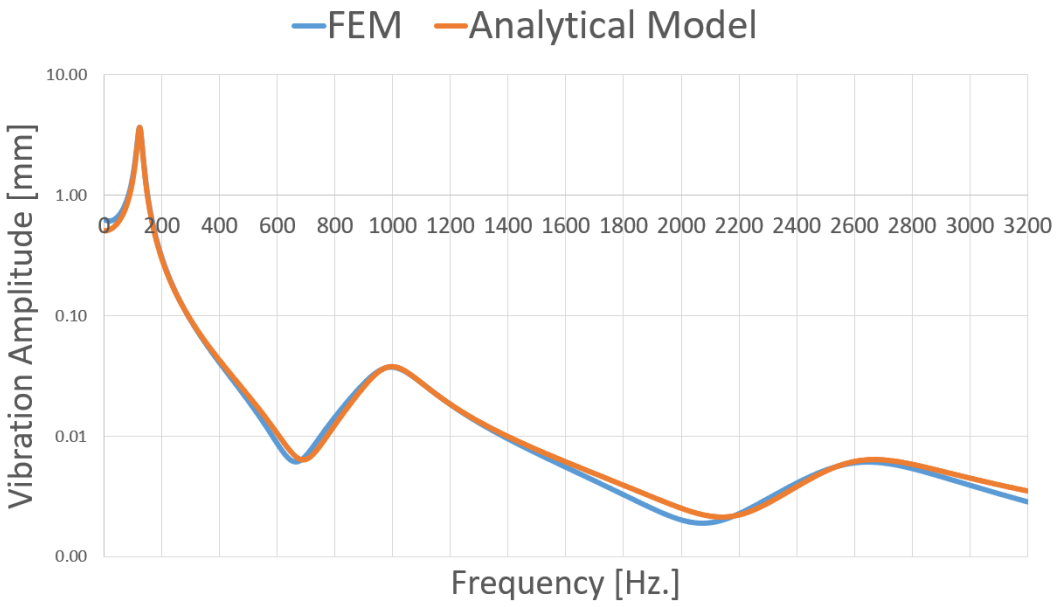

Figure 3.9. The FRF Comparison for the CLDT Beam

Table 3.7 The FRF Results

		FEM	Analytical	Error [%]
1st Mode	The Natural Frequency [Hz.]	123.00	123.00	0.00
	Loss Factor [-]	0.1466	0.1376	6.50
2nd Mode	The Natural Frequency [Hz.]	994.00	997.00	0.30
	Loss Factor [-]	0.2177	0.2026	7.43
3rd Mode	The Natural Frequency [Hz.]	2648.00	2669.00	0.79
	Loss Factor [-]	0.19726	0.2019	2.31

It can be concluded that the FEM and analytical results have agreed well with each other with slight differences for loss factor values. Hence, the proposed methodology to develop finite element model is quite accurate.

3.4 Comparison with Previous Studies

In order to further validate the FEM, the results of the reference CLDT beam in literature are compared. Eyyupoglu in his thesis study proposed a cantilever CLDT beam where the developed model experimentally verified [31]. Therefore, the experimental and FEM results of the CLDT reference beam in his study will be compared with the results found from the FEM proposed in this study. Also, it is worth to mention that the 2D FEM developed using PLANE183 elements in his work. Thus, it is expected to observe similar dynamic behavior in experiments with the 3D FEM developed in this study. The geometric properties are given in table 3.3. The problem is solved in 0-2500 Hz. frequency range considering only the first three modes of the reference CLDT beam. The FRF comparison plot and results are given in figure 3.10 and table 3.8 respectively.

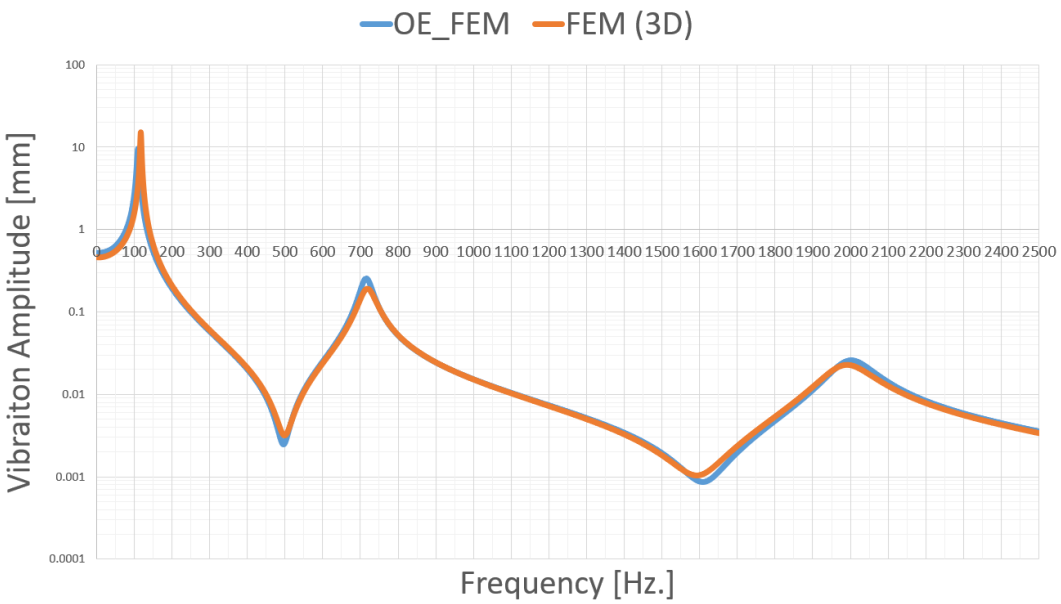

Figure 3.10. The FRF Comparison of the FEM Models

Table 3.8 The FRF Results for the FEMs

		FEM (3D)	OE_FEM	Error [%]
1st Mode	The Natural Frequency [Hz.]	118.00	115.60	2.08
	Loss Factor [-]	0.0287	0.0393	26.90
2nd Mode	The Natural Frequency [Hz.]	719.00	737.30	2.48
	Loss Factor [-]	0.0600	0.0478	25.49
3rd Mode	The Natural Frequency [Hz.]	1991.00	2051.50	2.95
	Loss Factor [-]	0.06654	0.0617	7.85

Comparing the results found, the first three natural frequency values are in close agreement while only the loss factor of the third mode is very close. Due to differences between loss factor values, the analytical model verified in section 3.3 is used to compare the results of the 3D FEM used in this case. The FRF results are given in table 3.9.

Table 3.9 The FRF Results for the FEM and Analytical Model

		FEM (3D)	Analytical	Error [%]
1st Mode	The Natural Frequency [Hz.]	118.00	117.36	0.55
	Loss Factor [-]	0.0287	0.0323	10.93
2nd Mode	The Natural Frequency [Hz.]	719.00	718.69	0.04
	Loss Factor [-]	0.0600	0.0634	5.34
3rd Mode	The Natural Frequency [Hz.]	1991.00	1981.44	0.48
	Loss Factor [-]	0.06654	0.0720	7.62

Comparing the results found, the first three natural frequency values are very close while loss factor values are well agreed to each other. The difference between loss factors for the FEMs can be due to element type, contact method and the reference temperature chosen.

After comparing the FEM results, the experimental result can be compared with the developed FEM in this study. The geometric properties of the reference CLDT beam in experiment is given in table 3.10. The FRF comparison plot and results are given in figure 3.11 and table 3.11 respectively.

Table 3.10 The Geometric Properties of the Reference CLDT Beam in Experiment

Property	Value	Units	Symbol
Thickness of the Base Layer	3.15	mm	H_1
Thickness of the Viscoelastic Layer	0.127	mm	H_2
Thickness of the Constraining Layer	0.254	mm	H_3
Width of the Beam	12.7	mm	w_b
Length of the Beam	151.7	mm	L_b

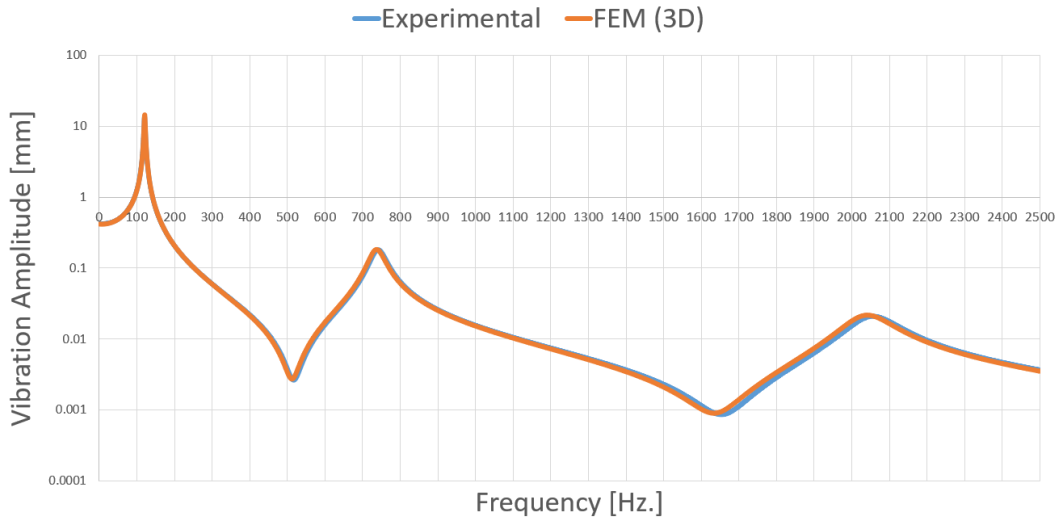

Figure 3.11. The FRF Comparison with the Experiment

Table 3.11 The FRF Results for the FEM and the Experiment

		FEM	Experimental	Error [%]
1st Mode	The Natural Frequency [Hz.]	121.00	118.50	2.11
	Loss Factor [-]	0.0274	0.0243	12.91
2nd Mode	The Natural Frequency [Hz.]	719.00	737.00	2.44
	Loss Factor [-]	0.0581	0.0640	9.16
3rd Mode	The Natural Frequency [Hz.]	2041.00	2052.30	0.55
	Loss Factor [-]	0.06308	0.0644	2.05

Comparing the results found, the first three natural frequency values are very close while loss factor values are well agreed to each other.

3.5 The Performance Metric

The damping ratio and the loss factor are the most used damping measures in literature. The half-power bandwidth method is the most practical and simplest to measure these values from both measured test data and calculated FRFs of developed models. It is simply finding corresponding natural frequencies of peak response values and half-power bandwidth frequencies where the vibration amplitude is $2^{1/2}$

less than peak response values in a given frequency range. The half-power method is illustrated in figure 3.12. The relationship between the damping ratio and loss factor is given in equation 58.

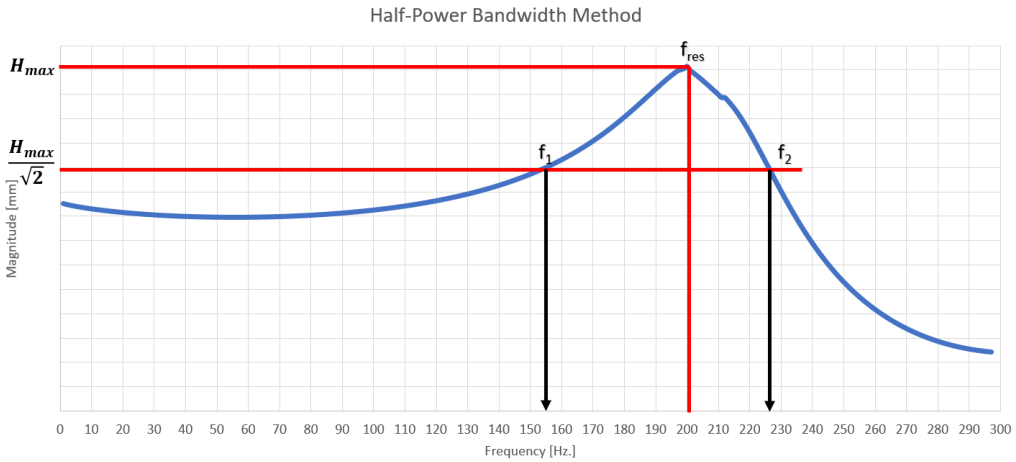

Figure 3.12. Half-Power Bandwidth Method

$$\xi \cong \frac{f_2 - f_1}{2 * f_{res}}; where\ \eta = 2\xi \quad (58)$$

Although identifying damping is straight forward, evaluating damping performance and vibration characteristics can be complicated. For instance, increasing the damping ratio may result in decreasing vibration amplitudes around resonance. However, the total vibration response can still increase. Moreover, unwanted vibrations can appear at unexpected frequency regions. Also, the total weight of the structure is expected to be at a certain level where vibration control techniques cannot be easily applied to the structure due to weight limitations and design complexity. Therefore, it is essential to define a suitable performance metric which quantifies the vibration damping performance of the structure more precisely. Hence, the performance metric defined in this study, total added mass, total added standoff layer mass, total vibration response and the average of the damping values of the first three modes in certain frequency range of the structure are used to evaluate damping performance. This performance metric and these parameters are used to find optimum design configuration.

Ulubalci in his thesis defined performance metric which relates the total energy of the output signal with given input signal [36]. This metric can be simply calculated using the area under frequency response function in any frequency region of interest. Similarly in this thesis, performance metric can be defined for a unit loading as given in equation 59.

$$E[y^2]_{defined\ frequency\ range} = \int_{f_l}^{f_u} S_y(f)df = \sum_{f_l}^{f_u} |H(f)|^2 \quad (59)$$

The area under the frequency response function can be calculated using numerical methods. Therefore, Simpson's 1/3 general rule is applied to calculate performance metric which is called "Power Value" throughout this thesis study. The general form of Simpson's 1/3 general rule is given in equation 60.

$$I = \int_a^b f(x)dx \approx \frac{b-a}{3n}(f(a) + 4\sum_{3,5,7\ldots}^{n-1} f(x) + 2\sum_{2,4,6\ldots}^{n-1} f(x) + f(b)) \quad (60)$$

For a defined frequency range, equation 60 becomes:

$$I = Power\ Value = \frac{h}{3}(|H(f_l)|^2 + 4\sum_{3,5,7\ldots}^{n-1} |H(f_x)|^2 + 2\sum_{2,4,6\ldots}^{n-1} |H(f_x)|^2 + |H(f_u)|^2) \quad (61)$$

Where $h = frequency\ spacing = \frac{b-a}{n}; n = number\ of\ point$

Finally, total added weight and total added standoff layer weight can be calculated as given in equation 62 and 63 where material properties given in table 3.1 used.

$$Total\ Added\ Mass = \rho_2 V_2 + \rho_3 V_3 + \rho_4 V_4 \quad (62)$$

$$Total\ Added\ Standoff\ Layer\ Mass = \rho_2 V_2 \quad (63)$$

Hence, the evaluation of the damping performance will be achieved considering the performance metric, total added masses, and the loss factor values of the structure in a defined frequency region of interest throughout this thesis. The proposed methodology and procedure to calculate all of these parameters are given in figure 3.13.

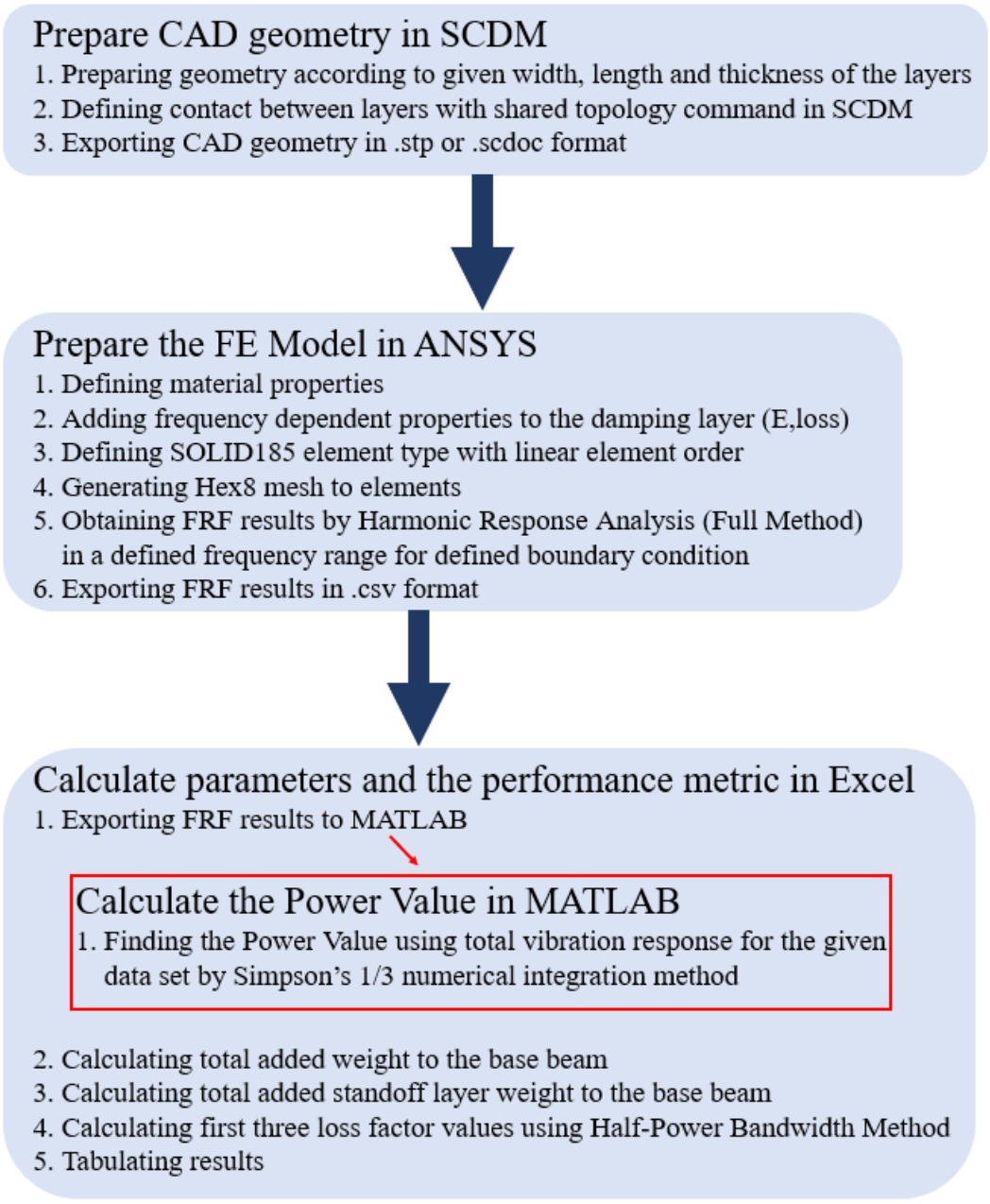

Figure 3.13. The Proposed Methodology to Find Unknown Parameters

The proposed methodology is used to find results in section 3.6 and chapter 4. The developed finite element models for any case will have similar mesh densities, computation time and same boundary conditions.

3.6 Thickness Optimization of the Standoff Layer

Although increasing thickness of the damping layer improves damping performance, it also increases total weight of the structure. In a similar approach, increasing thickness of the standoff layer does not result required static and dynamic properties of the system. Therefore, there is always an optimum design point where the required properties are satisfied best. However, there might still be challenging to design and manufacture such a system. The thickness of the standoff layer is optimized for PSLDT where it introduces the best damping performance and is easy to manufacture. Considering surface damping treatment designs mostly used in very thin sheet metals, the base layer thickness is decided to be 1 mm thick. The thickness of the base beam will be used in reference base beam configuration after other geometrical parameters are decided. The fixed-free and the fixed-fixed boundary condition is chosen to find optimum thickness of the standoff layer and reference geometrical properties. The results and developed models are explained in the following sections.

3.6.1 The Fixed-Free Beam Configuration

The fixed-free beam configuration was used to validate develop finite element model. Similarly, length and width of the beam are also chosen reference CLDT beam given in table 3.3. The example of finite element model is given in figure 3.14. The geometric properties of the PSLDT configurations are given in table 3.12.

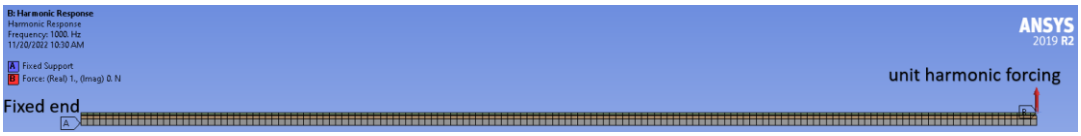

Figure 3.14. The Fixed-Free Beam Configuration

Table 3.12 The Geometric Properties of the PSLDT Configurations

Property	Value	Units	Symbol
Thickness of the Base Layer	1	mm	H_1
Thickness of the Standoff Layer	0.5-4	mm	H_2
Thickness of the Viscoelastic Layer	0.127	mm	H_3
Thickness of the Constraining Layer	0.254	mm	H_4
Width of the Beam	12.7	mm	w_b
Length of the Beam	150	mm	L_b

The finite element model is developed using similar mesh densities as possible due to prevent modeling differences. The average of loss factor values, total added masses, the percentage of total added mass to base beam mass in structure and power value are calculated for 19 cases in analysis where the uniform standoff layer thickness varies between 0.5-4 mm. These results are given in table 3.13. The developed FEMs are based on methodology introduced before.

Table 3.13 The Results for Various PSLDT Designs

Case	Thickness of the SOL[mm]	Total Added Standoff Layer Mass [g]	Total Added Mass [g]	Total Added Mass [%]	Avg. of First Three Loss Factor [-]	Power Value
1	0.5	0.99	2.51	48.89	0.22	1935.8
2	0.75	1.49	2.94	57.23	0.24	1094.9
3	1	1.98	3.93	76.31	0.25	674.3
4	1.25	2.48	4.91	95.39	0.25	441.8
5	1.5	2.97	5.89	114.47	0.25	304.0
6	1.75	3.47	6.87	133.55	0.24	217.7
7	2	3.96	7.85	152.63	0.24	161.0
8	2.25	4.46	8.83	171.70	0.23	122.3
9	2.5	4.95	9.81	190.78	0.23	95.0
10	2.75	5.45	10.79	209.86	0.22	75.2
11	3	5.94	11.78	228.94	0.21	60.6
12	3.25	6.44	12.76	248.02	0.21	49.5
13	3.5	6.93	13.74	267.10	0.20	40.9
14	3.75	7.43	14.72	286.17	0.19	34.2
15	4	7.92	15.70	305.25	0.19	28.9
16	0.8	1.58	3.14	61.05	0.24	988.5
17	0.9	1.78	3.53	68.68	0.24	811.4
18	1.1	2.18	4.32	83.94	0.24	565.7
19	1.2	2.38	4.71	91.58	0.25	478.7
Base	NA	NA	NA	NA	NA	NA
1x	NA	NA	1.52	29.63	NA	NA
2x	NA	NA	3.05	59.27	NA	NA
3x	NA	NA	4.57	88.9	NA	NA

From the results given in table 3.13, it can be understood that increasing thickness of the standoff layer improves damping performance at certain design points as expected. After reaching its optimum design value, the loss factor value introduced in the structure tends to be the loss factor value of the standoff layer itself. Also, single, double and triple constrained layer damping treatment without any standoff layer is used to constraint total added mass percentage. Therefore, the total added

mass percantage is decided to be around sixty percent of the baseline structure. Hence, it is found that optimum thickness is in between 0.5-0.8 mm. The FRF comparison is given for this thickness range in figure 3.15.

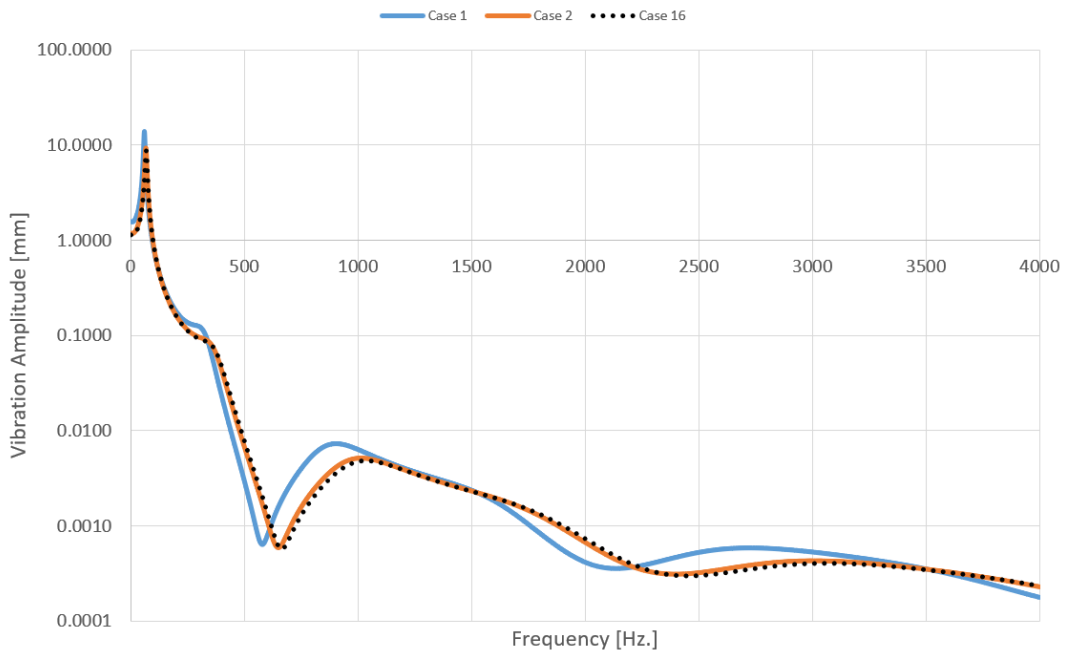

Figure 3.15. The FRF Comparison for Optimized PSLDT Designs

Comparing the FRF results, it can be concluded that although the total added mass percentage of case 2 is slightly less than case 16, case 16 is still superior to case 2 since it has lower power value while it has almost same mass with multiple constrained layer damping treated beam.

3.6.2 The Fixed-Fixed Beam Configuration

Ulubalci in his thesis studied various standoff layer geometries to improve damping performance of plates [36]. He proposed a fuselage geometry which is composed of outer skin plate, stringer, C-frame, and L-bracket. These parts are assembled together by riveting process. The proposed standoff layer geometries with single CLDT are

applied to the outer skin plate to improve damping performance. The geometric properties of the fuselage geometry are given in table 3.14.

Table 3.14 The Geometric Properties of the Fuselage Geometry

	Length [mm]	Width [mm]	Depth [mm]	Thickness [mm]
Stringer	260	30	25	1
C-Frame	300	20	40	1.6
L-Bracket	15	15	15	1
Outer Skin Plate	300	300	-	1

For this study, the proposed fixed-fixed beam configuration is defined considering the fuselage geometry given above. The length of the beam portion is defined such that the outer skin plate and C-frames are riveted on both sides with a width of 20 mms. Therefore, the effective length of the beam becomes to be 260 mm long with the fixed-fixed boundary condition which is shown in figure 3.16. The width of the beam is decided to be 10 mm, considering the computation time required in the finite element model and practical purposes for the experiment. The design strategy aims that if the damping performance of the fixed-fixed beam can be improved, the proposed optimized designs can be periodically placed along the fuselage geometry to improve the damping performance of the fuselage geometry. The logic resembles a metastructure design where internal absorbers are placed periodically to the base structure. In this section, the geometric properties of the reference baseline and constrained layer damping geometry are decided. Moreover, defining reference constrained layer damping treatment with a uniform standoff layer is another objective of this study. Therefore, the optimum thickness of the standoff layer is decided considering both the fixed-free and fixed-fixed boundary conditions in this section using the proposed methodology explained before. The results of the finite element model of the reference base and CLDT beam are given in detail in this section.

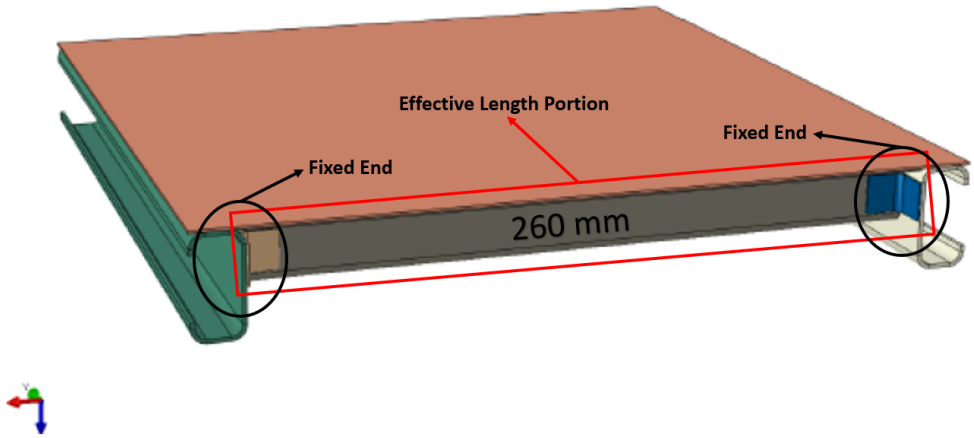

Figure 3.16. The Effective Beam Portion [36]

3.6.2.1 Vibration Characteristics of the Reference Base Beam

The reference base beam is fixed on both ends. The loading is applied between 1/5 and 1/4 of the beam length from the left tip in order to capture the first three mode shapes. The frequency response function results are found by measuring the displacement at the same location. Also, global damping is applied to the structure to prevent higher vibration amplitudes at resonance. The finite element model of the base beam and the boundary condition are given in figure 3.17. The geometric properties of the base beam are given in table 3.15.

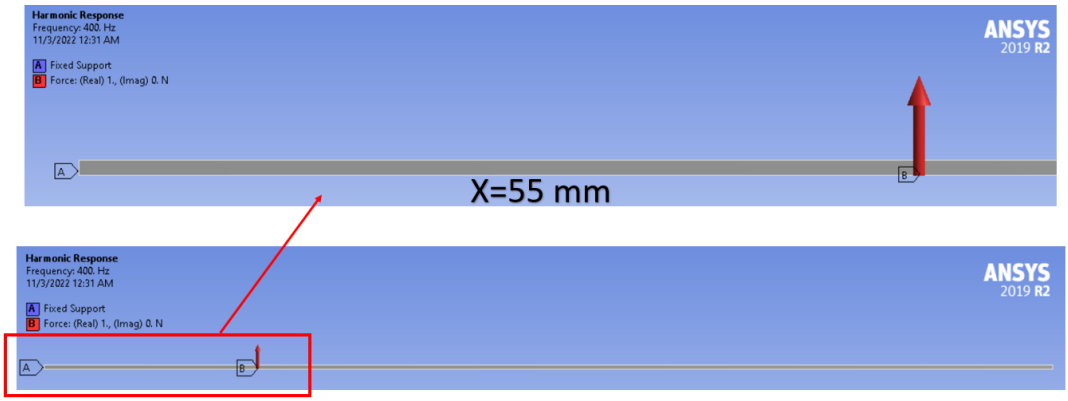

Figure 3.17. The Finite Element Model of the Reference Base Beam

Table 3.15 The Geometric Properties of the Base Beam

Property	Value	Units	Symbol
Thickness of the Base Layer	1	mm	H_1
Width of the Beam	10	mm	w_b
Length of the Beam	260	mm	L_b

The FRF plot and results are given in table 3.16 and figure 3.18 respectively. It can be concluded that the average of the loss factor values seems quite reasonable since most metals have very low structural damping. Also, the finite element model and analytical results have agreed well with each other. Here, only the first three modes of the base beam are considered. However, the FEM is solved in a 0-800 Hz. frequency range considering novel design alternatives in chapter 4 need at least 800 Hz. to capture the first three natural frequencies and mode shapes. Therefore, another resonance peak is occurred around 690 Hz. in the FRF plot since the fourth mode shape of the base beam is 691.63 Hz..

Table 3.16 The FEM Results of Reference Base Beam

Base Beam		FEM (Modal)	FEM (Harmonic)	Analytical	Error [%]	Loss Factor
1st Mode	The Natural Frequency [Hz.]	77.88	78.00	77.42	0.74	0.009
2nd Mode	The Natural Frequency [Hz.]	214.66	215.00	213.42	0.74	0.005
3rd Mode	The Natural Frequency [Hz.]	420.88	421.00	418.40	0.62	0.002

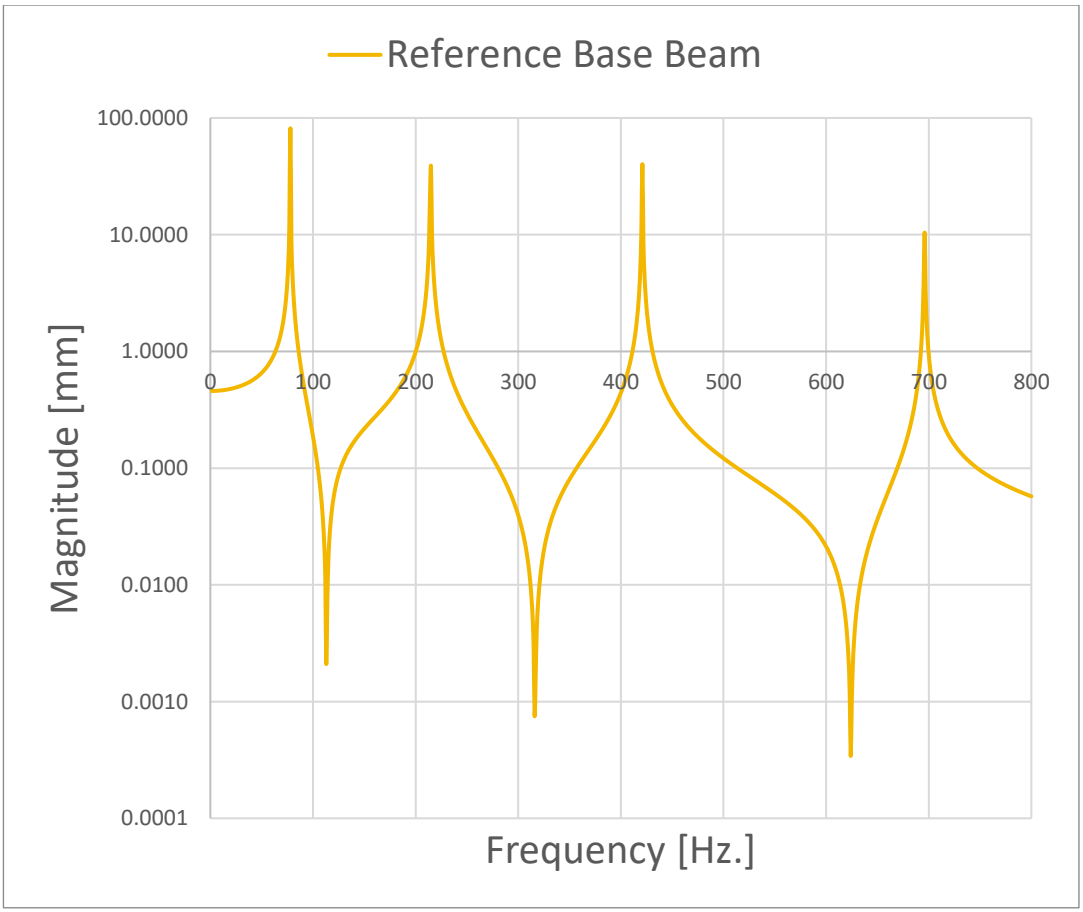

Figure 3.18. The FRF Plot of the Reference Base Beam

3.6.2.2 Vibration Characteristics of the Reference Single CLDT Beam

The boundary conditions and properties of the finite element model of the reference single layer constrained layer damping treated beam is same with the finite element model of the reference base beam. The frequency response function results are found by measuring the displacement at the same location. The finite element model of the base beam and the boundary conditions are given in figure 3.19. The geometric properties of the reference base beam are given in table 3.17.

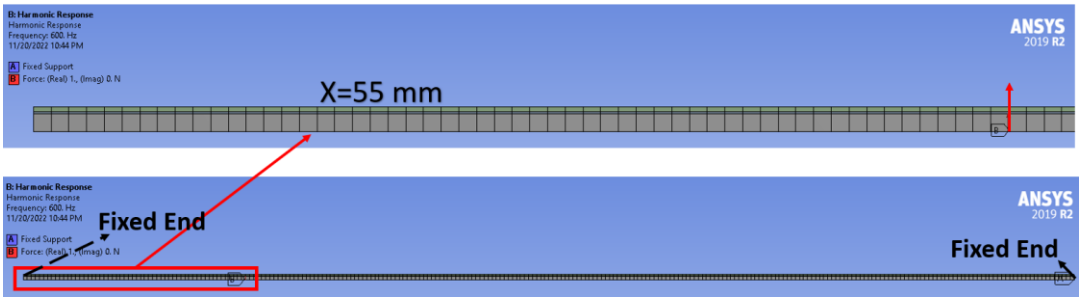

Figure 3.19. The Finite Element Model of the Reference Single CLDT Beam

Table 3.17 The Geometric Properties of the Reference Single CLDT Beam

Property	Value	Units	Symbol
Thickness of the Base Layer	1	mm	H_1
Thickness of the Viscoelastic Layer	0.127	mm	H_3
Thickness of the Constraining Layer	0.254	mm	H_4
Width of the Beam	10	mm	w_b
Length of the Beam	260	mm	L_b

The FRF plot and results are given in table 3.18 and figure 3.20 respectively. It can be concluded that the finite element model and analytical results have agreed well with each other. Moreover, applying constrained damping layer to the base beam improves loss factor values as expected.

Table 3.18 The FEM Results of Reference Single CLDT Beam

Single CLDT Beam		FEM (Harmonic)	Analytical	Error [%]	Loss Factor
1st Mode	The Natural Frequency [Hz.]	87.00	90.96	4.35	0.162
2nd Mode	The Natural Frequency [Hz.]	233.00	242.11	3.76	0.193
3rd Mode	The Natural Frequency [Hz.]	454.00	458.45	0.97	0.192

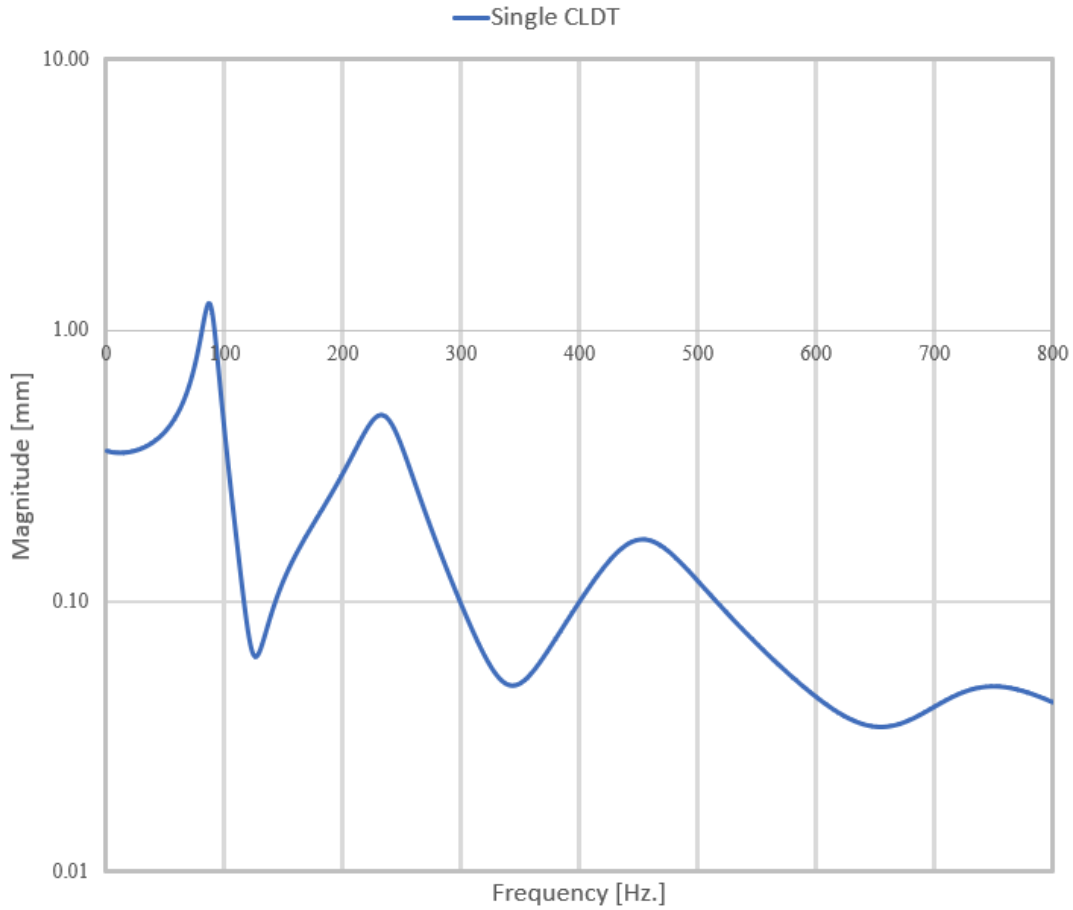

Figure 3.20. The FRF Plot of the Reference Single CLDT Beam

After FRF plots and FEM results of the reference base and CLDT beam are introduced, optimum thickness of the uniform standoff layer can be found. Consequently, the reference constrained layer damping treatment with a uniform standoff layer beam configuration can be decided. The scaled baseline geometries and the geometric properties are given in figure 3.21 and table 3.19 respectively. The finite element model is developed using similar mesh densities as possible due to prevent modeling differences for the fixed-fixed boundary condition in ANSYS. The average of loss factor values, total added masses, the percentage of total added mass to base beam mass in structure and power value are calculated for 7 cases in analysis where the uniform standoff layer thickness varies between 0.5-1 mm. In order to

constrain the percentage of total added mass, the multiple and triple CLDT beam cases are also included to compare them with a uniform PSLDT cases.

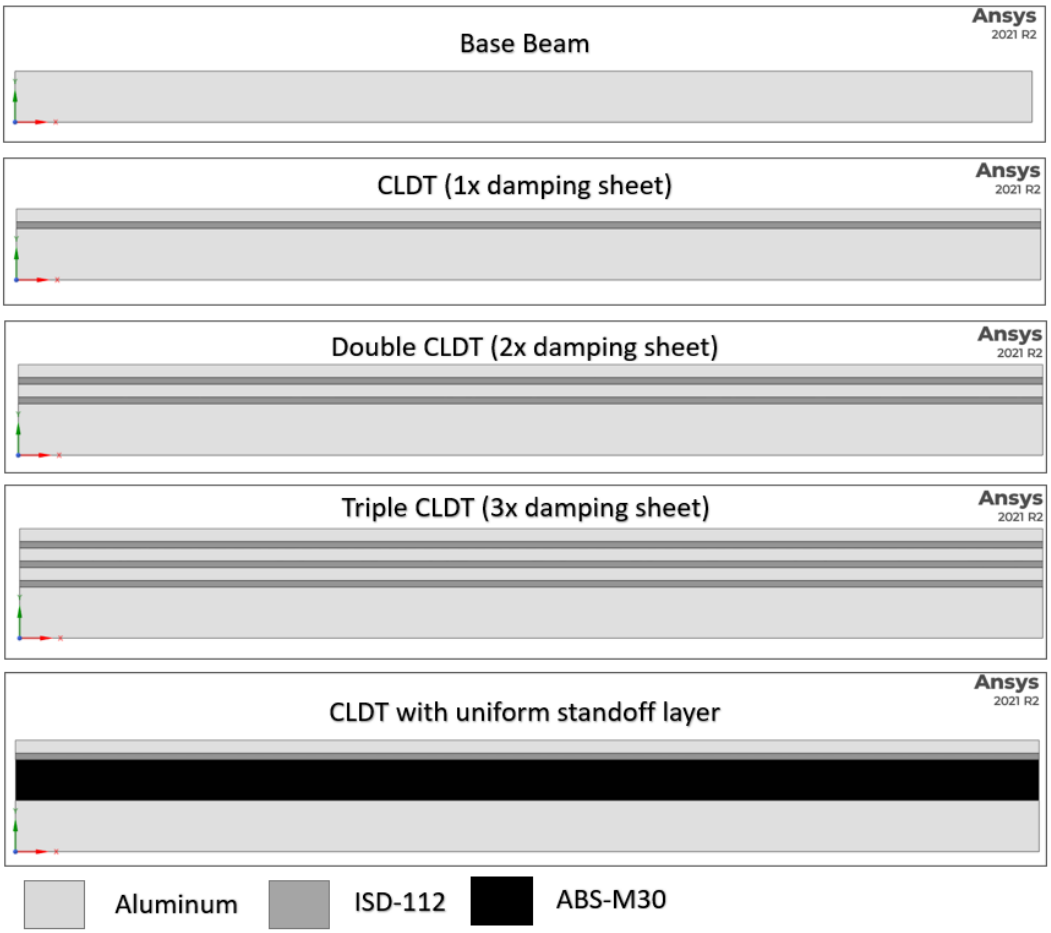

Figure 3.21. The Scaled Baseline Geometries

Table 3.19 The Geometric Properties of the PSLDT Configurations

Property	Value	Units	Symbol
Thickness of the Base Layer	1	mm	H_1
Thickness of the Standoff Layer	0.5-1	mm	H_2
Thickness of the Viscoelastic Layer	0.127	mm	H_3
Thickness of the Constraining Layer	0.254	mm	H_4
Width of the Beam	10	mm	w_b
Length of the Beam	260	mm	L_b

The results for the fixed-fixed PSLDT beam and the FRF comparison between cases are given in table 3.20 and figure 3.22 respectively. Comparing the results, the calculated power value is reduced so that the damping performance is improved while thickness of the standoff layer is increasing. However, the amount of the total added mass has also increased. Comparing the total added mass of single CLDT, double CLDT and triple CLDT beam with cases proposed here, the total added mass percentage of double CLDT beam decided to be a reference value. Comparing the FRF results, it can be concluded that although the total added mass percentage of case 4 is slightly less than case 5, case 5 is still superior to case 4 since it has lower power value while it has almost same mass with multiple constrained layer damping treated beam. Thus, the optimum standoff layer thickness of the reference PSLDT configuration is decided to be 0.8 mm thick. After geometric properties of the reference PSLDT beam are decided, the novel standoff layer geometries will be proposed and explained in detail in chapter 4.

Table 3.20 The Results for The Fixed-Fixed PSLDT Cases

CASE	Total Mass[g]	Total Added Mass[g]	Added SOL Mass[g]	Added Total Mass[%]	Avg. of First Three Loss Factor	Power Value
Base Beam	7.02	NA	NA	NA	0.005	10000.07
Single CLDT	9.10	2.08	NA	29.63	0.18	54.13
Double CLDT	11.18	4.16	NA	59.27	0.28	29.34
Triple CLDT	13.26	6.24	NA	88.90	0.29	19.23
Case 1 (H2=0.5)	10.45	3.43	1.35	48.89	0.32	17.66
Case 2 (H2=0.6)	10.72	3.70	1.62	52.74	0.35	14.63
Case 3 (H2=0.7)	10.99	3.97	1.89	56.60	0.36	12.20
Case 4 (H2=0.75)	11.13	4.11	2.03	58.52	0.37	11.16
Case 5 (H2=0.8)	11.26	4.24	2.16	60.45	0.38	10.22
Case 6 (H2=0.9)	11.53	4.51	2.43	64.30	0.38	8.61
Case 7 (H2=1)	11.80	4.78	2.70	68.15	0.39	7.28

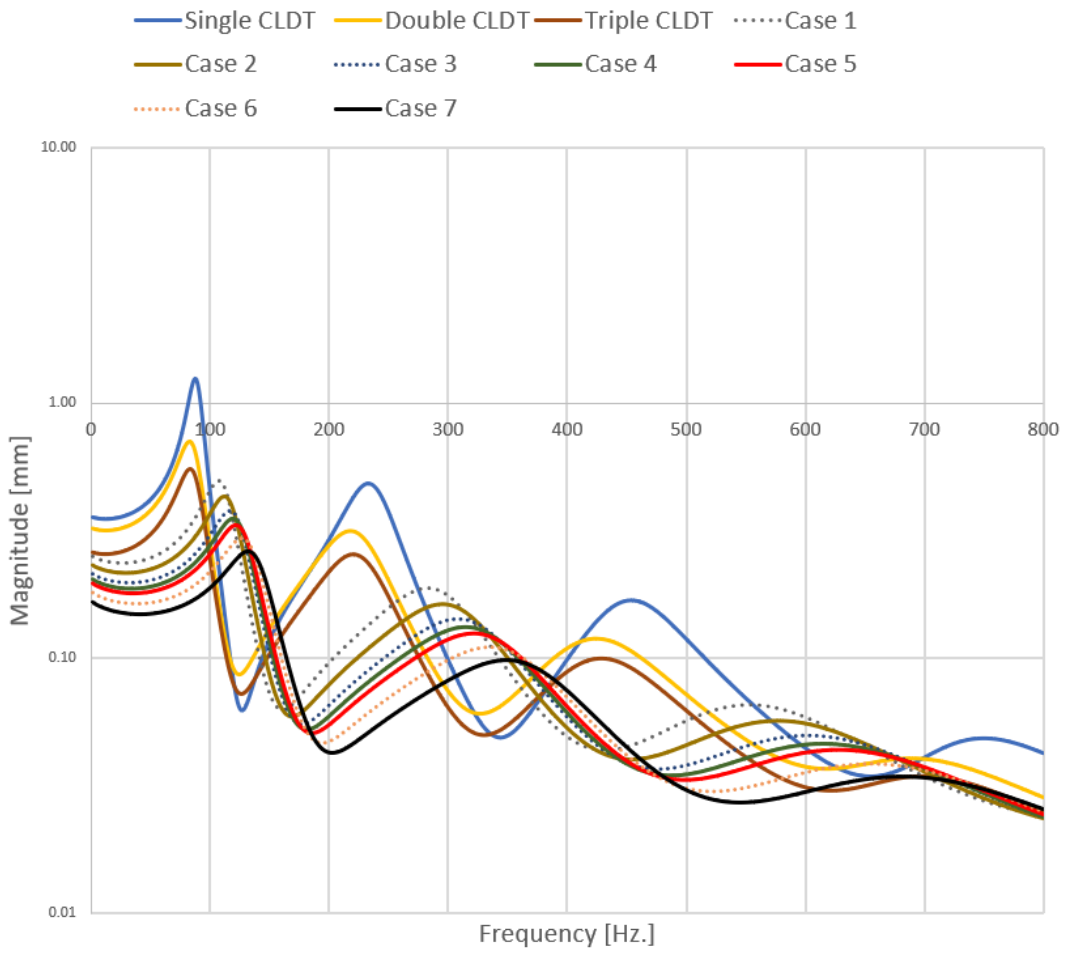

Figure 3.22. The FRF Comparison Plot for the Optimization Cases

CHAPTER 4

THE OPTIMIZATION OF THE NOVEL DESIGN ALTERNATIVES FOR STANDOFF LAYER GEOMETRIES

The results of the reference base, CLDT and CLDT with a uniform standoff layer beam and the novel design alternatives are compared and explained in this section. Several design alternatives are introduced from previous studies of Eyyupoglu [31], Ulubalci [36] and Sun [38]. Also, the design logic used in Ulubalci's thesis is extended to propose novel standoff layer geometries. Moreover, the structural optimization module of the ANSYS is used to optimize the standoff layer geometries in a width direction. The standoff layer geometries are created by removing materials periodically along the beam length in width direction which is called shape optimization throughout this study. After novel standoff layer geometries are found, the finite element model is developed as explained in chapter 3 for the fixed-fixed boundary condition. Therefore, the optimized novel design alternatives are fixed on both ends. The loading is applied between 1/5 and 1/4 of the beam length from the left tip in order to capture the first three mode shapes. The frequency response function results are found by measuring the displacement at the same location. It is also essential to indicate that the total added mass of the novel design alternatives and reference configuration for CLDT with a uniform standoff layer will be similar which is one of the objectives of this study.

4.1 Vibration Characteristics of the Reference CLDT Beam with a Uniform Standoff Layer

The geometric properties, the finite element model, and the boundary conditions of the reference CLDT beam with a uniform standoff layer, which can be named reference PSLDT beam for simplicity, are given in table 4.1 and figure 4.1 respectively.

Table 4.1 The Geometric Properties of the Reference PSLDT Beam

Property	Value	Units	Symbol
Thickness of the Base Layer	1	mm	H_1
Thickness of the Standoff Layer	0.8	mm	H_2
Thickness of the Viscoelastic Layer	0.127	mm	H_3
Thickness of the Constraining Layer	0.254	mm	H_4
Width of the Beam	10	mm	w_b
Length of the Beam	260	mm	L_b

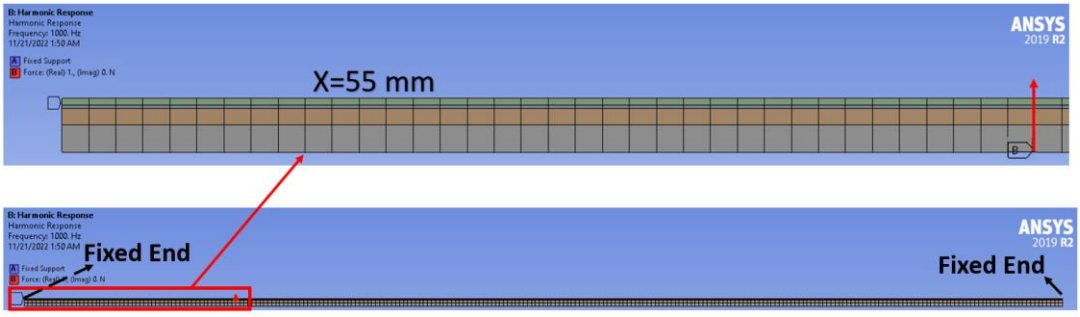

Figure 4.1. The Finite Element Model of the Reference PSLDT Beam

The results and FRF comparison plot are given in table 4.2 and figure 4.2 respectively. Comparing the frequency response function, it can be concluded that adding damping layer and the standoff layer to the structure improves damping performance of the structure as indicated in literature. Moreover, the reference PSLDT beam is superior to double CLDT application since the vibration amplitudes and total vibration response are less with similar total added mass.

Table 4.2 The FEM Results of Reference PSLDT Beam

The Reference PSLDT		FEM (Harmonic)
1st Mode	The Natural Frequency [Hz.]	121.00
	Loss Factor [-]	0.362
2nd Mode	The Natural Frequency [Hz.]	321.00
	Loss Factor [-]	0.367
3rd Mode	The Natural Frequency [Hz.]	623.00
	Loss Factor [-]	0.395

Figure 4.2. The FRF Comparison Plot between Reference Baseline Configurations

4.2 Vibration Characteristics of the PSLDT Beam in Literature [31] (OE)

Eyyupoglu proposed various novel standoff layer geometries using topology optimization with genetic algorithms in his study [31]. Enhanced genetic algorithm solution, namely, case 10 has the best performance among the results. Therefore, the proposed geometry is implemented in this study for comparison purposes. The solution of the topology optimization which demonstrates material distribution is given in figure 4.3.

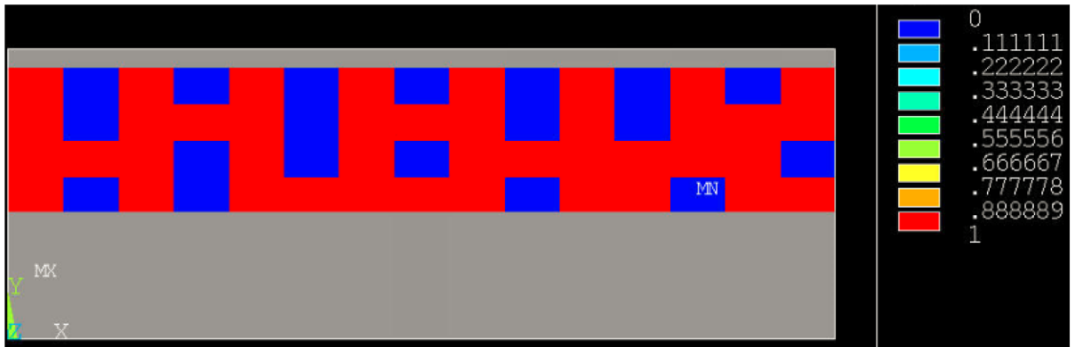

Figure 4.3. Material Distribution of the Novel Standoff Layer Geometry [31]

The proposed standoff layer geometry in his study is 150 mm long and 4 mm thick. In order to apply material distribution to the standoff layer geometry of this study, it is scaled such that the first 13 portion of material distribution along the beam length is doubled continuously so that the beam length is fully covered. Moreover, thickness of the standoff layer geometry is reduced to 0.8 mm since the total added mass percentage is restricted to around sixty percent. Designed standoff layer geometry in full scale and small portion of the proposed optimized PSLDT design are given in figure 4.4.

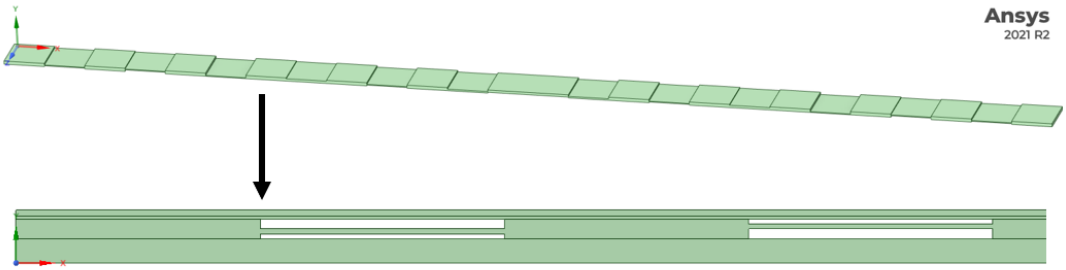

Figure 4.4. Optimized PSLDT Design (OE)

The results and FRF comparison plot are given in table 4.3 and figure 4.5 respectively. Comparing the frequency response function, the vibration amplitudes around resonance frequencies are increased. Also, the loss factor value for the first mode is increased compared to reference PSLDT beam.

Table 4.3 The FEM Results of Optimized PSLDT Design (OE)

Optimized PSLDT (OE)		FEM (Harmonic)
1st Mode	The Natural Frequency [Hz.]	113.00
	Loss Factor [-]	0.378
2nd Mode	The Natural Frequency [Hz.]	299.00
	Loss Factor [-]	0.324
3rd Mode	The Natural Frequency [Hz.]	568.00
	Loss Factor [-]	0.354

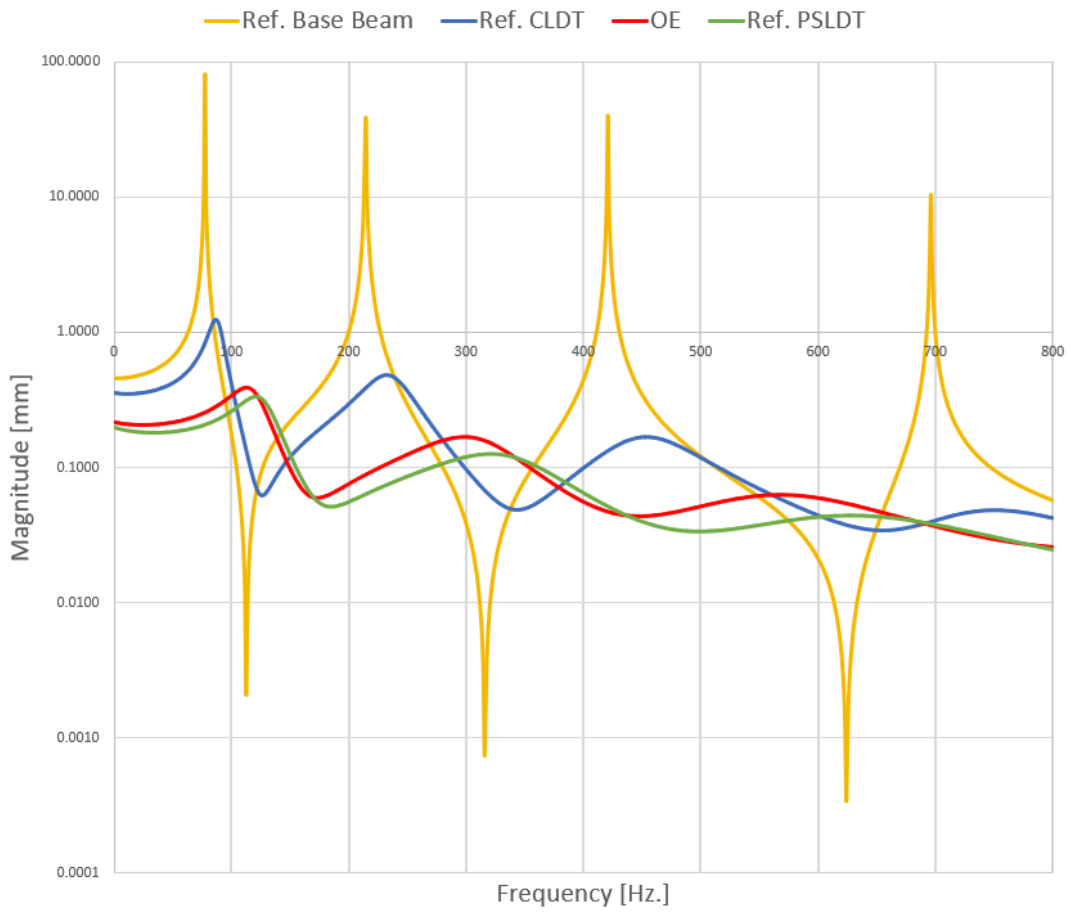

Figure 4.5. The FRF Comparison Plot for the Optimized PSLDT (OE)

4.3 Vibration Characteristics of the PSLDT Beam in Literature [36] (BU)

Ulubalci proposed various standoff layer geometries considering slotted standoff layer geometry can be placed periodically along the plate length and width in his study [36]. Parametric design solution is used to adjust tower height and length to increase neutral axis shift so that damping performance of the structure is also improved. Twice width of tower to slot configuration, namely, “slotted 15 mm 2v1” has the best performance among the parametric design alternatives. Therefore, the proposed geometry is implemented in this study for comparison purposes. The proposed material layout for standoff layer geometry is given in figure 4.6.

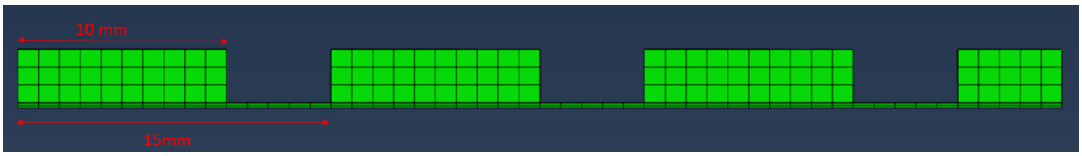

Figure 4.6. Material Layout for the Slotted Standoff Layer Geometry [36]

Tower height is adjusted for slotted design such that removed material is placed top of the 10 mm portion in each 15 mm length so that total mass is maintained same. In order to apply the proposed design to the standoff layer geometry, uniform thickness of 0.8 mm is adjusted and scaled to fully cover beam length. Designed standoff layer geometry in full scale and small portion of the proposed optimized PSLDT design are given in figure 4.7.

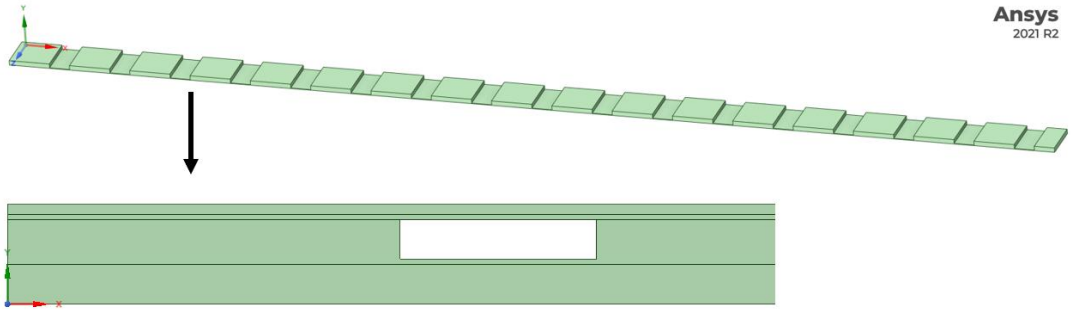

Figure 4.7. Optimized PSLDT Design (BU)

The results and FRF comparison plot are given in table 4.4 and figure 4.8 respectively. Comparing the frequency response function, total vibration response is decreased. Also, the loss factor value for each mode is increased compared to reference PSLDT beam.

Table 4.4 The FEM Results of Optimized PSLDT Design (BU)

Optimized PSLDT (BU)		FEM (Harmonic)
1st Mode	The Natural Frequency [Hz.]	129.00
	Loss Factor [-]	0.577
2nd Mode	The Natural Frequency [Hz.]	341.00
	Loss Factor [-]	0.457
3rd Mode	The Natural Frequency [Hz.]	658.00
	Loss Factor [-]	0.396

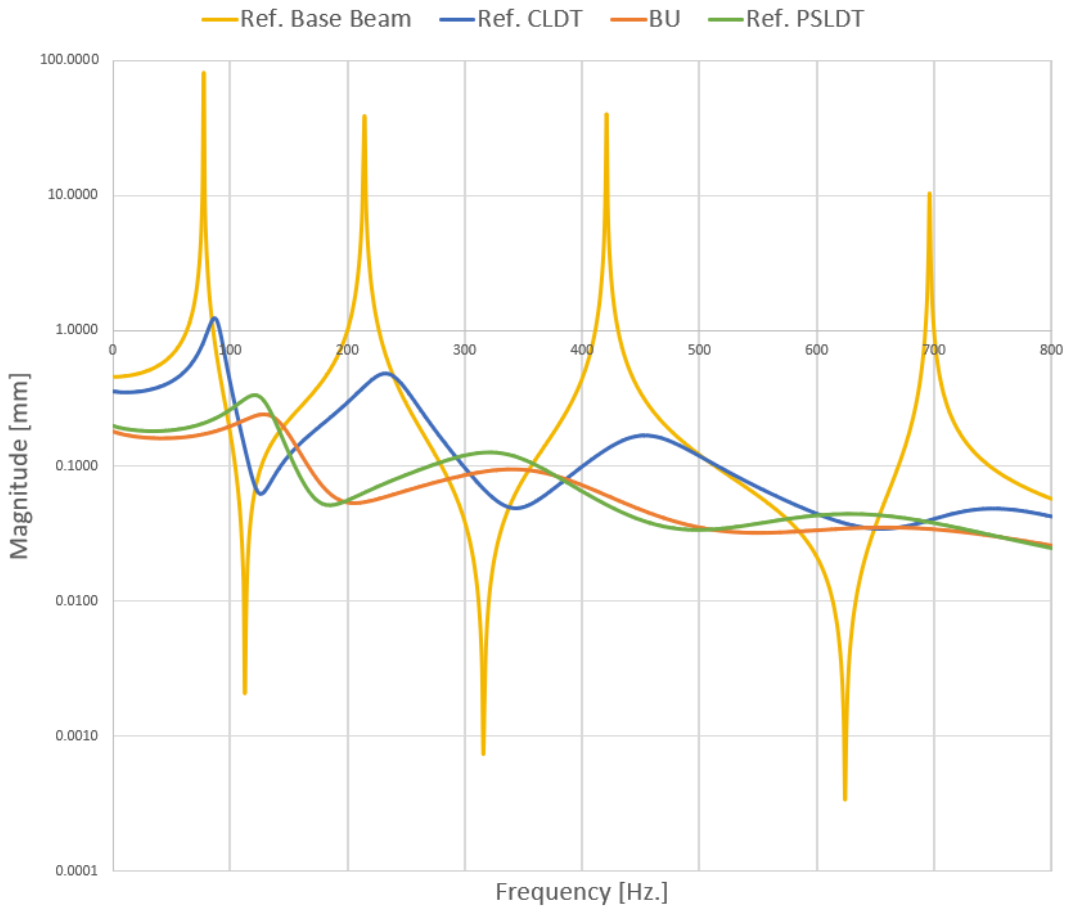

Figure 4.8. The FRF Comparison Plot for the Optimized PSLDT (BU)

4.4 Vibration Characteristics of the PSLDT Beam in Literature [38] (ES)

Sun proposed various novel standoff layer geometries using topology and parametric optimization with optimization algorithms in his study [38]. Multi objective genetic algorithm (MOGA) solution of his study has good performance among the results. The algorithm suggests reduced thickness with material removal from each 10 mm portion along the beam length instead of uniform 10 mm thick standoff layer geometry. The proposed material layout and optimum values for standoff layer geometry are given in figure 4.9.

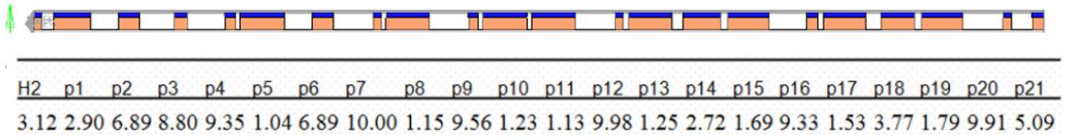

Figure 4.9. Material Layout and Optimum Values for the Slotted Standoff Layer Geometry [38]

The material layout is adjusted to cover fully beam length such that the first 5 portion of the material removal doubled from the right end of the proposed design. Therefore, a total of 26 portion where each portion is 10 mm long is created. The small portion of the proposed optimized PSLDT design is given in figure 4.10.

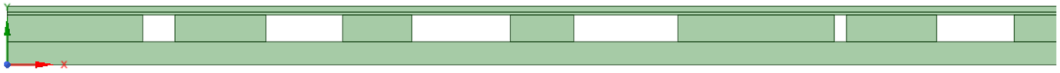

Figure 4.10. Optimized PSLDT Design (ES)

The results and FRF comparison plot are given in table 4.5 and figure 4.11 respectively. Comparing the frequency response function, the vibration amplitudes around resonance frequencies are increased. Also, the loss factor value for the first mode is increased compared to reference PSLDT beam.

Table 4.5 The FEM Results of Optimized PSLDT Design (ES)

Optimized PSLDT (ES)		FEM (Harmonic)
1st Mode	The Natural Frequency [Hz.]	105.00
	Loss Factor [-]	0.416
2nd Mode	The Natural Frequency [Hz.]	277.00
	Loss Factor [-]	0.353
3rd Mode	The Natural Frequency [Hz.]	546.00
	Loss Factor [-]	0.376

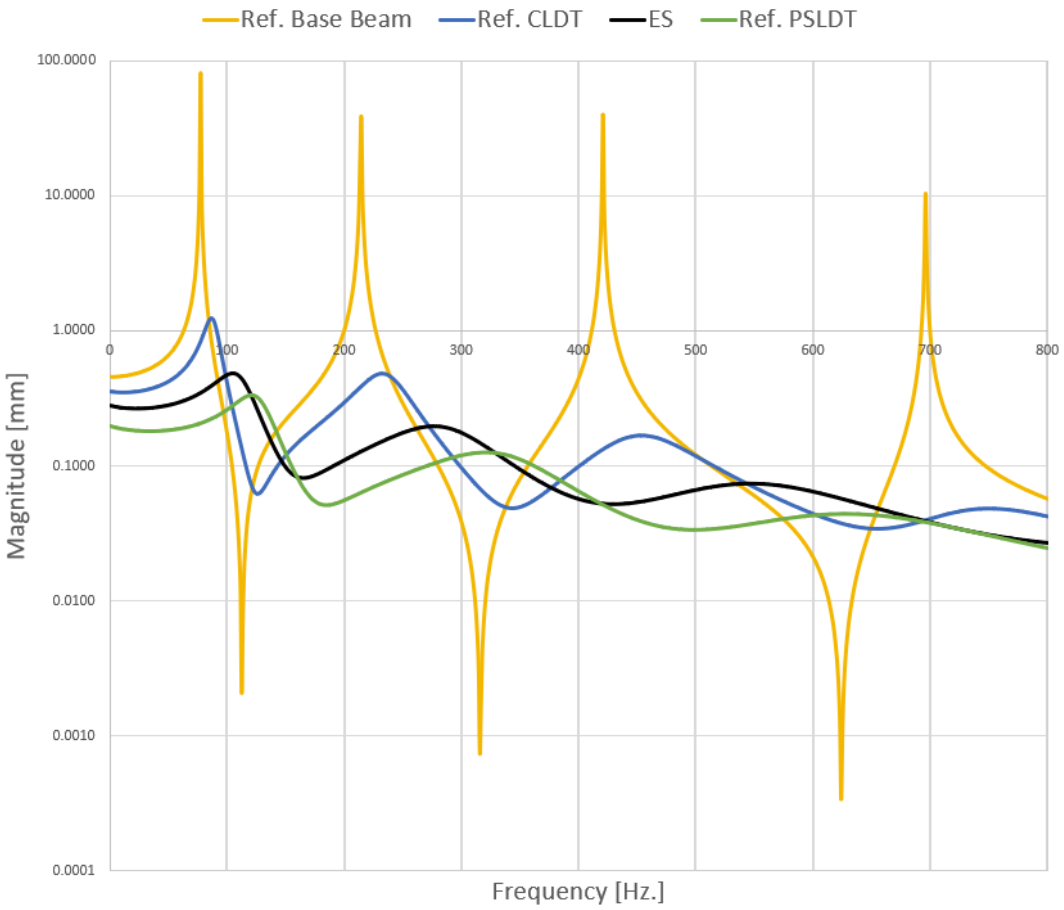

Figure 4.11. The FRF Comparison Plot for the Optimized PSLDT (ES)

4.5 Vibration Characteristics of Novel Design Alternative (ND-1)

Parametric design optimization is used to adjust tower height and length to increase neutral axis shift so that the damping performance of the structure is also improved. In this alternative, equal width of tower to slot configuration in a length of 15 mm portion is used so that the tower height, that is the uniform layer thickness, is adjusted for slotted design such that removed material is placed top of the 7.5 mm portion in each 15 mm length so that total mass is maintained same. In order to apply the proposed design to the standoff layer geometry, uniform thickness of 0.8 mm is adjusted and increased to 1.4 mm. The total of 17 slotted portion is placed periodically along the beam length. Designed standoff layer geometry in full scale and small portion of the proposed novel design alternative are given in figure 4.12.

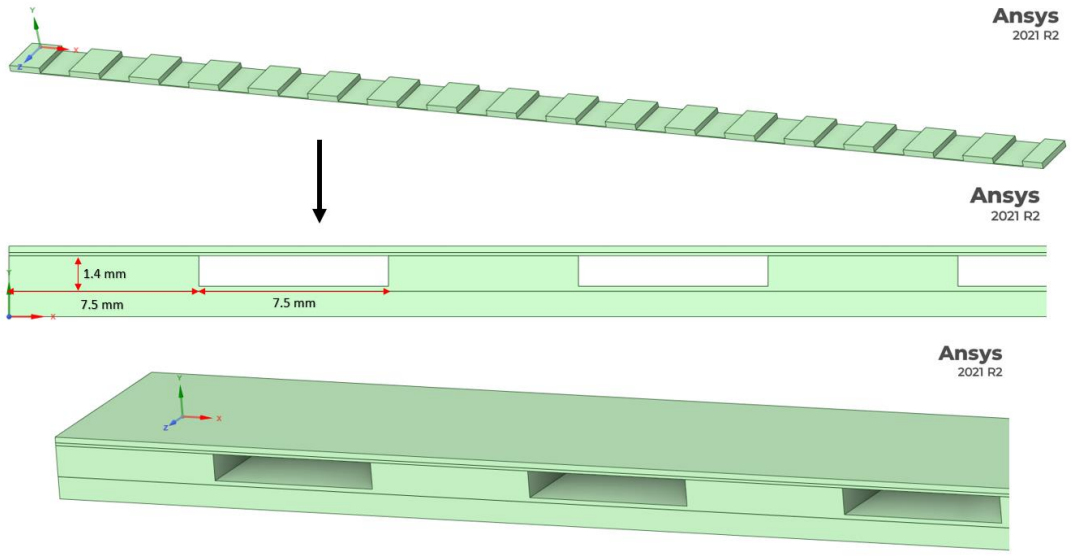

Figure 4.12. Novel Design Alternative (ND-1)

The results and FRF comparison plot are given in table 4.6 and figure 4.13 respectively. Comparing the frequency response function, the total vibration response is decreased. Also, the loss factor value for each mode is decreased compared to reference PSLDT beam.

Table 4.6 The FEM Results of Novel Design Alternative (ND-1)

ND-1		FEM (Harmonic)
1st Mode	The Natural Frequency [Hz.]	130.00
	Loss Factor [-]	0.531
2nd Mode	The Natural Frequency [Hz.]	345.00
	Loss Factor [-]	0.524
3rd Mode	The Natural Frequency [Hz.]	656.00
	Loss Factor [-]	0.400

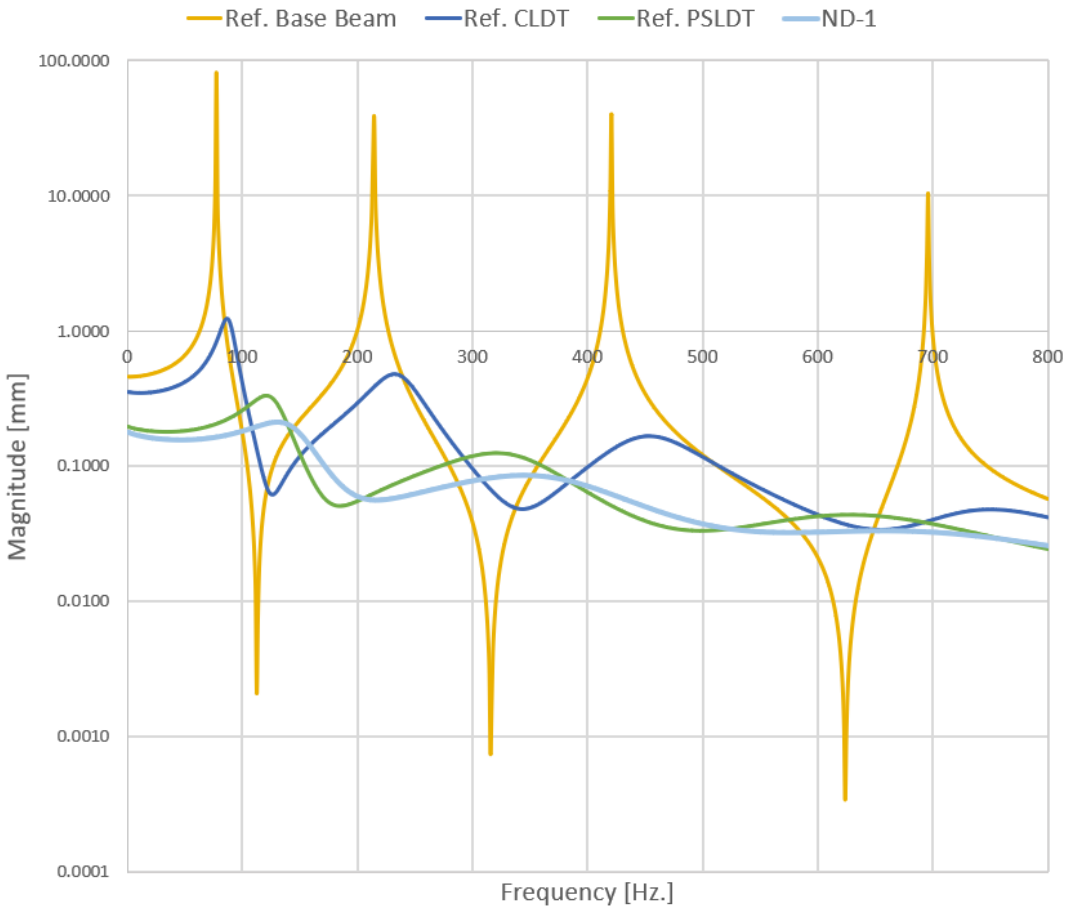

Figure 4.13. The FRF Comparison Plot for Novel Design Alternative (ND-1)

4.6 Vibration Characteristics of Novel Design Alternative (ND-2)

Parametric design optimization is used to adjust tower height and length to increase neutral axis shift so that the damping performance of the structure is also improved. In this alternative, equal width of tower to slot configuration in a length of 20 mm portion is used so that the tower height, that is the uniform layer thickness, is adjusted for slotted design such that removed material is placed top of the 10 mm portion in each 20 mm length so that total mass is maintained same. In order to apply the proposed design to the standoff layer geometry, uniform thickness of 0.8 mm is adjusted and increased to 1.4 mm. Considering boundary condition, 6 slotted portion is placed on both ends. Therefore, a total of 12 slotted portion is used along the beam length. Designed standoff layer geometry in full scale and small portion of the proposed novel design alternative are given in figure 4.14.

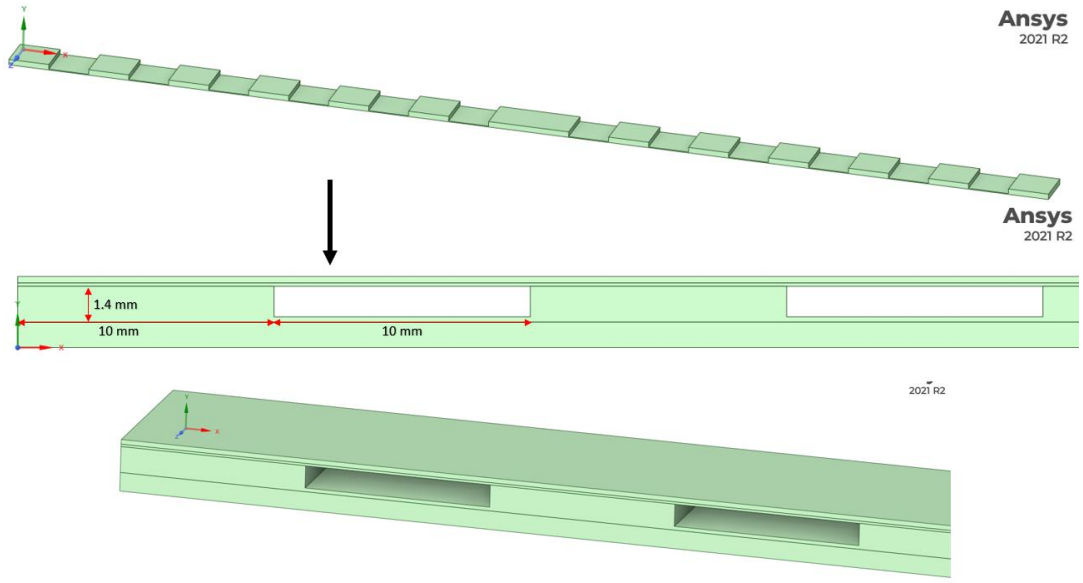

Figure 4.14. Novel Design Alternative (ND-2)

The results and FRF comparison plot are given in table 4.7 and figure 4.15 respectively. Comparing the frequency response function, the total vibration response is decreased. Also, the loss factor value for each mode is decreased compared to reference PSLDT beam.

Table 4.7 The FEM Results of Novel Design Alternative (ND-2)

ND-2		FEM (Harmonic)
1st Mode	The Natural Frequency [Hz.]	129.00
	Loss Factor [-]	0.518
2nd Mode	The Natural Frequency [Hz.]	349.00
	Loss Factor [-]	0.493
3rd Mode	The Natural Frequency [Hz.]	655.00
	Loss Factor [-]	0.392

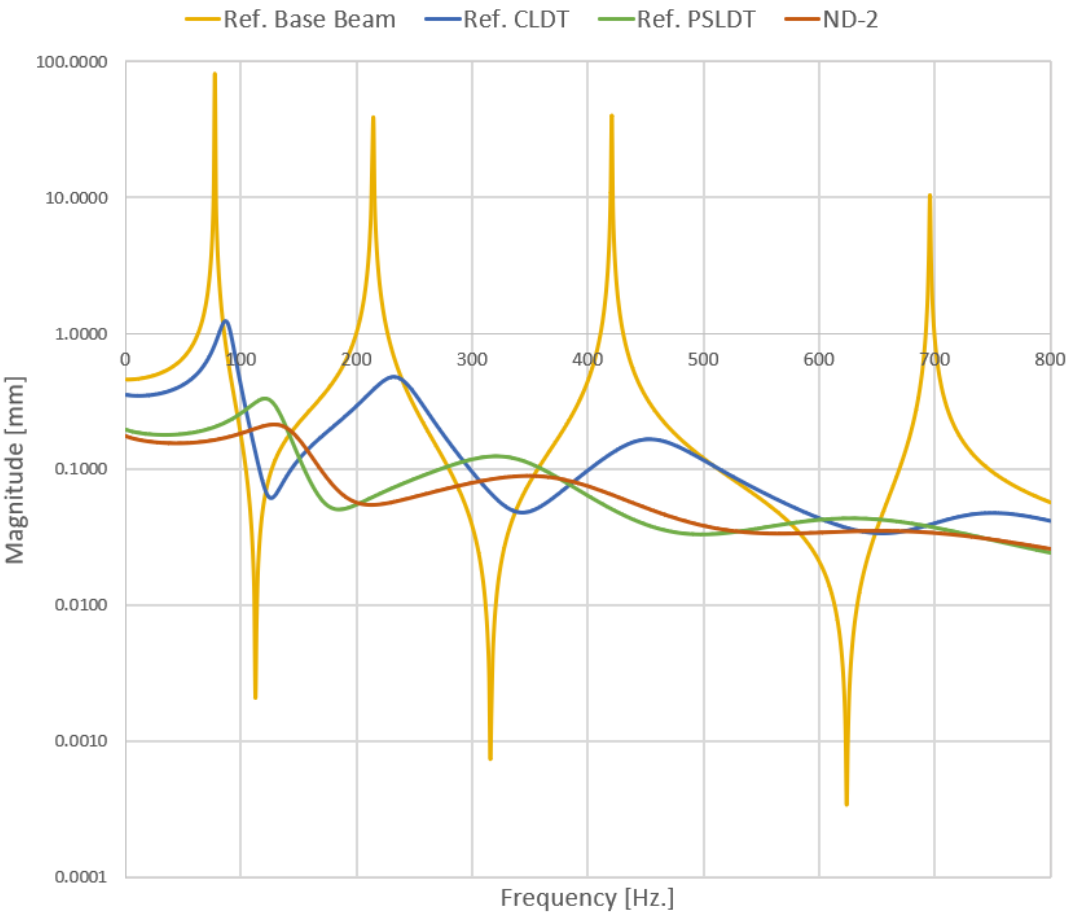

Figure 4.15. The FRF Comparison Plot for Novel Design Alternative (ND-2)

4.7 Vibration Characteristics of Novel Design Alternative (ND-3)

Parametric design optimization is used to adjust tower height and length to increase neutral axis shift so that the damping performance of the structure is also improved. In this alternative, quadruple width of tower to slot configuration in a length of 20 mm portion is used so that the tower height, that is the uniform layer thickness, is adjusted for slotted design such that removed material is placed top of the 16 mm portion in each 20 mm length so that total mass is maintained same. In order to apply the proposed design to the standoff layer geometry, uniform thickness of 0.8 mm is adjusted and increased to 0.96 mm. Considering boundary condition, 6 slotted portion is placed on both ends. Therefore, a total of 12 slotted portion is used along the beam length. Designed standoff layer geometry in full scale and small portion of the proposed novel design alternative are given in figure 4.16.

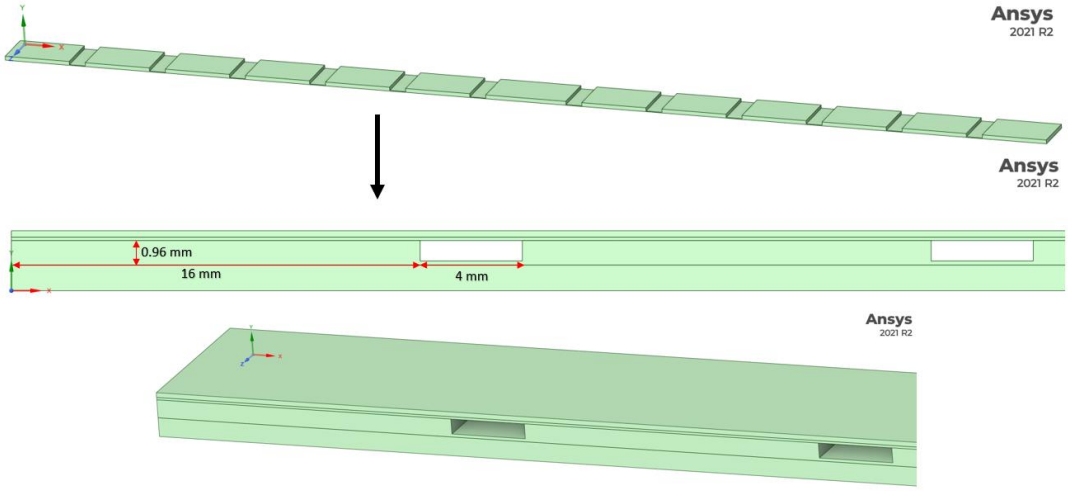

Figure 4.16. Novel Design Alternative (ND-3)

The results and FRF comparison plot are given in table 4.8 and figure 4.17 respectively. Comparing the frequency response function, the total vibration response is decreased. Also, the loss factor value for each mode is decreased compared to reference PSLDT beam.

Table 4.8 The FEM Results of Novel Design Alternative (ND-3)

ND-3		FEM (Harmonic)
1st Mode	The Natural Frequency [Hz.]	125.00
	Loss Factor [-]	0.454
2nd Mode	The Natural Frequency [Hz.]	331.00
	Loss Factor [-]	0.411
3rd Mode	The Natural Frequency [Hz.]	642.00
	Loss Factor [-]	0.328

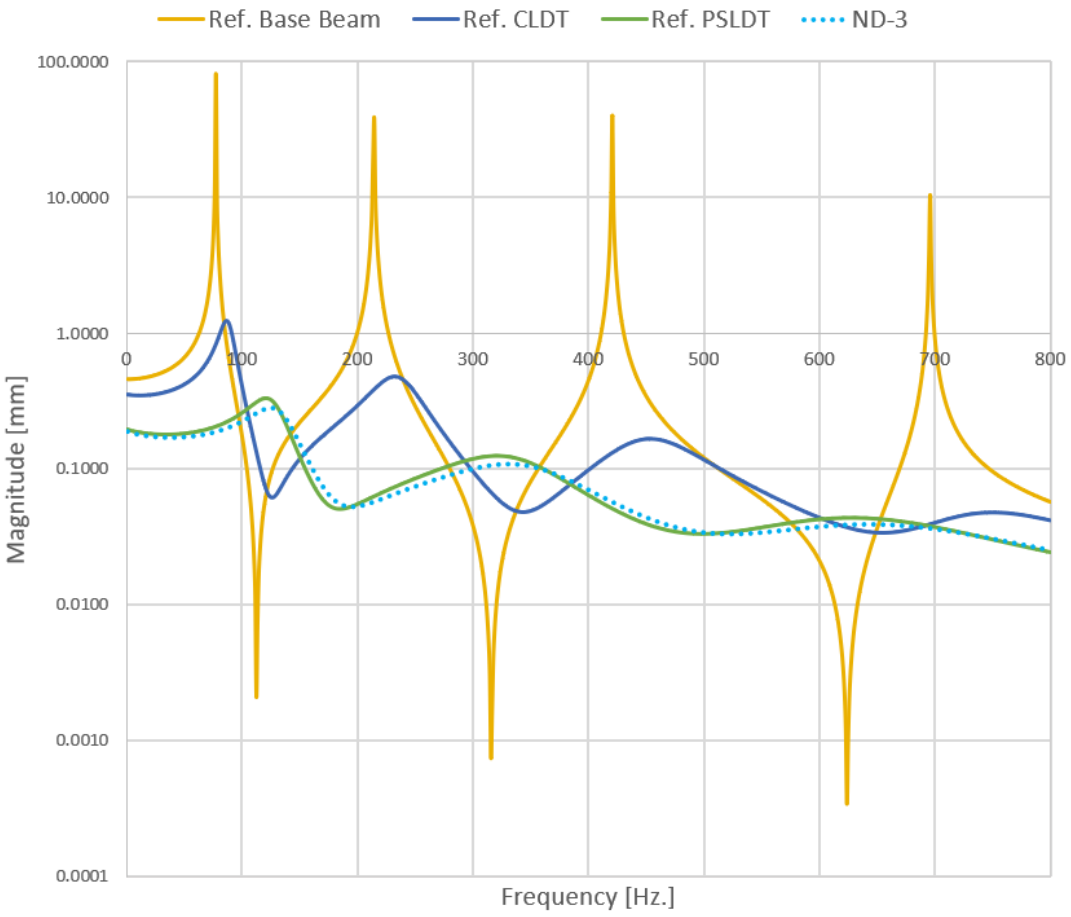

Figure 4.17. The FRF Comparison Plot for Novel Design Alternative (ND-3)

4.8 Vibration Characteristics of Novel Design Alternative (ND-4)

The structural optimization module of the ANSYS is used to find parametrically optimized standoff layer geometry. The thickness is increased to 1.35 mm for an analysis where volume constraint is defined as 60 percent since the total added mass percentage is restricted to around sixty percent so that optimized standoff layer geometry has similar total added mass. Here, the shape optimized small portions are placed periodically along the beam. The results of the shape optimization in full scale and small portion of the proposed novel design alternative are given in figure 4.18.

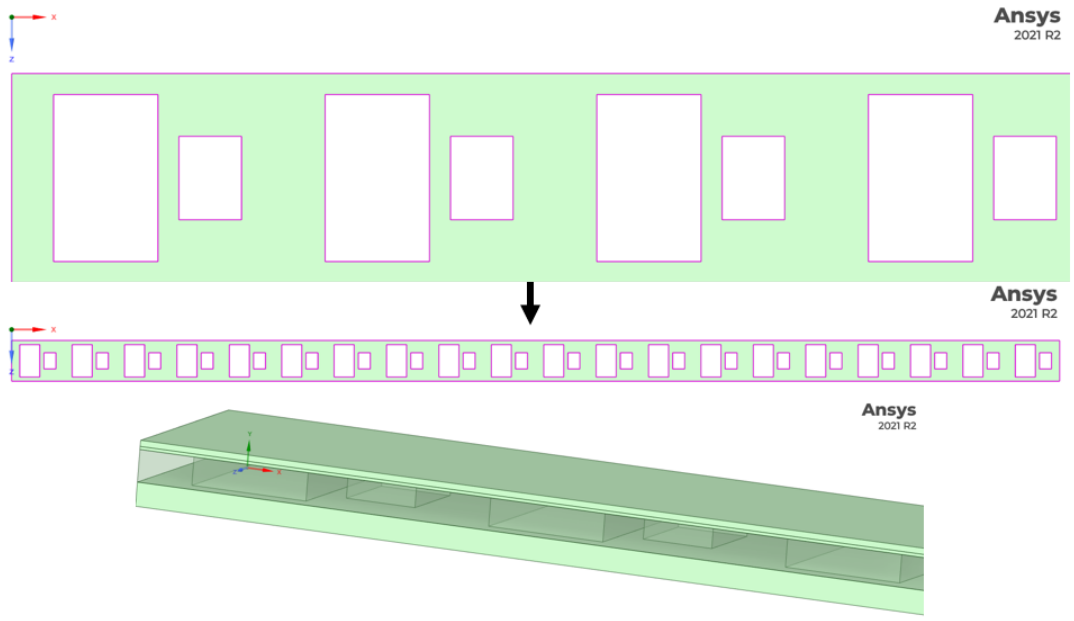

Figure 4.18. Novel Design Alternative (ND-4)

The results and FRF comparison plot are given in table 4.9 and figure 4.19 respectively. Comparing the frequency response function, the total vibration response is decreased. Also, the loss factor value for each mode is decreased compared to reference PSLDT beam.

Table 4.9 The FEM Results of Novel Design Alternative (ND-4)

ND-4		FEM (Harmonic)
1st Mode	The Natural Frequency [Hz.]	190.00
	Loss Factor [-]	0.27
2nd Mode	The Natural Frequency [Hz.]	509.00
	Loss Factor [-]	0.273
3rd Mode	The Natural Frequency [Hz.]	997.00
	Loss Factor [-]	0.25

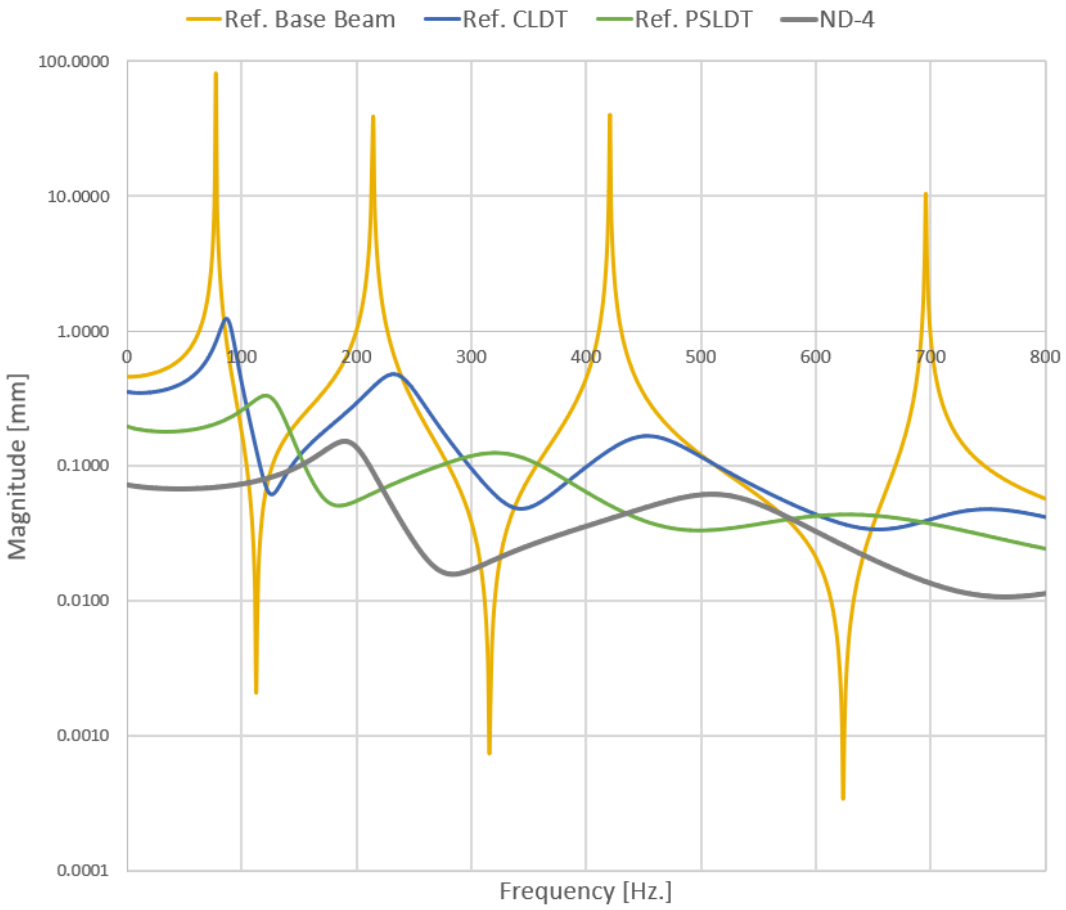

Figure 4.19. The FRF Comparison Plot for Novel Design Alternative (ND-4)

4.9 Vibration Characteristics of Novel Design Alternative (ND-5)

The structural optimization module of the ANSYS is used to find parametrically optimized standoff layer geometry. The thickness is increased to 1.6 mm for an analysis where volume constraint is defined as 50 percent since the total added mass percentage is restricted to around sixty percent so that optimized standoff layer geometry has similar total added mass. Here, the shape optimized small portions are placed periodically along the beam. The results of the shape optimization in full scale and small portion of the proposed novel design alternative are given in figure 4.20.

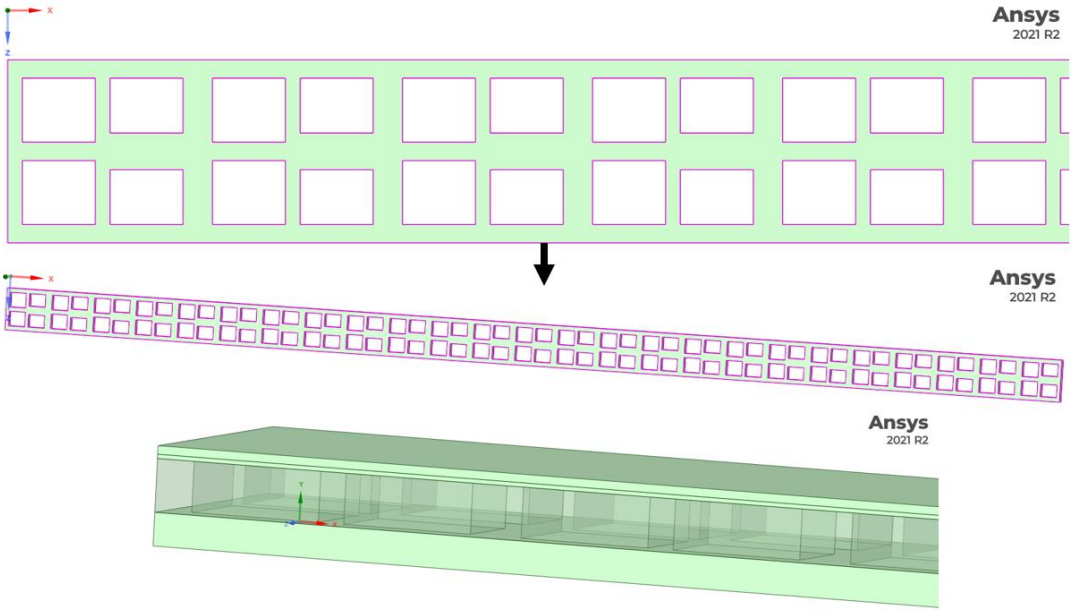

Figure 4.20. Novel Design Alternative (ND-5)

The results and FRF comparison plot are given in table 4.10 and figure 4.21 respectively. Comparing the frequency response function, the total vibration response is decreased. Also, the loss factor value for each mode is decreased compared to reference PSLDT beam.

Table 4.10 The FEM Results of Novel Design Alternative (ND-5)

ND-5		FEM (Harmonic)
1st Mode	The Natural Frequency [Hz.]	205.00
	Loss Factor [-]	0.299
2nd Mode	The Natural Frequency [Hz.]	550.00
	Loss Factor [-]	0.281
3rd Mode	The Natural Frequency [Hz.]	1072.00
	Loss Factor [-]	0.262

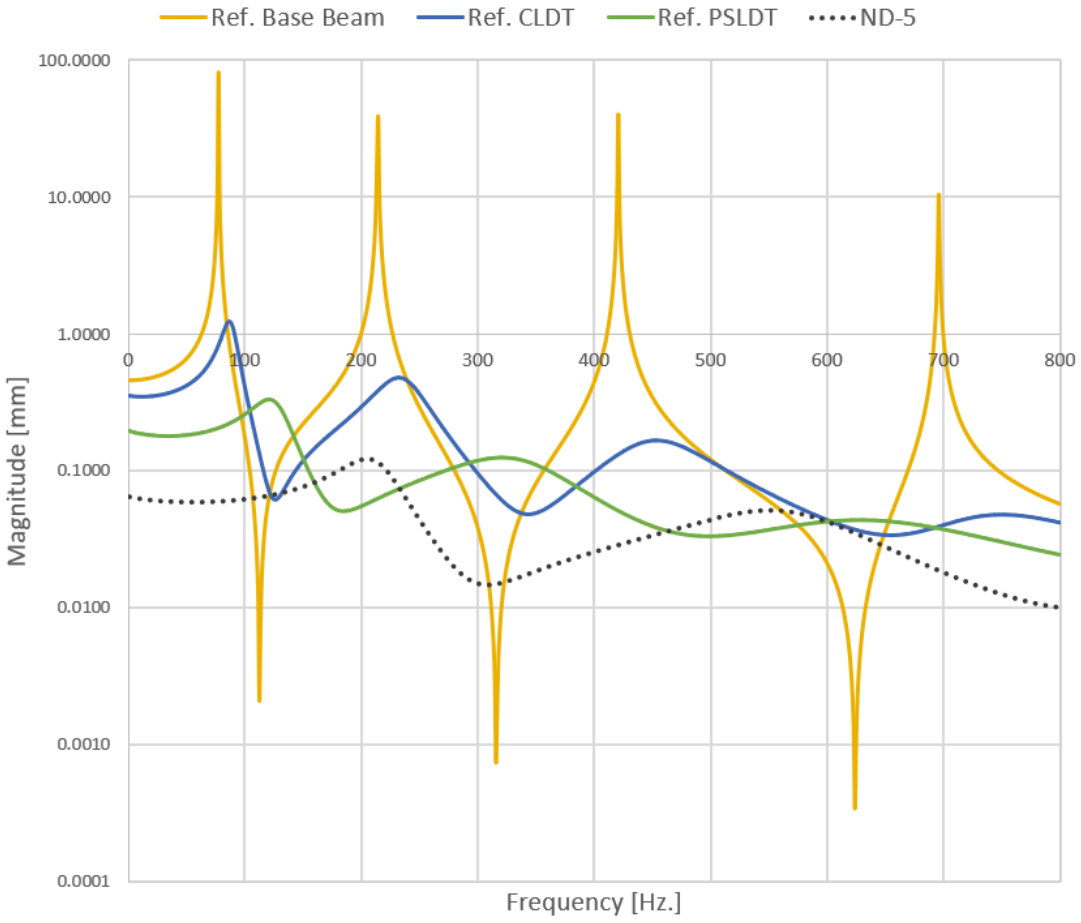

Figure 4.21. The FRF Comparison Plot for Novel Design Alternative (ND-5)

4.10 Vibration Characteristics of the Novel Design Alternative (ND-6)

Essink utilizes metastructure concept in her thesis where the zigzag beam is placed top of the base structure [39]. The material is removed in a width direction which is resembled to her thesis study. The thickness of the standoff layer is increased so that the total added mass percentage is restricted to around sixty percent. Therefore, optimized standoff layer geometry has similar total added mass with other novel design alternatives. The zigzag beam geometry and its geometric properties are given in figure 4.22.

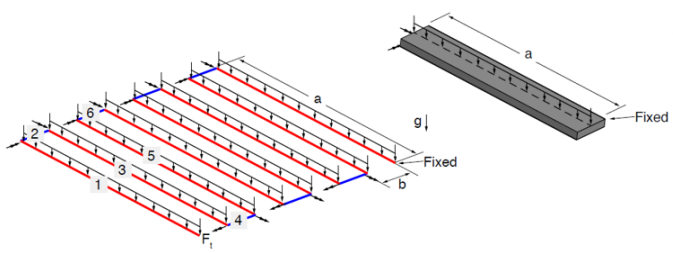

Zigzag Dimension	Symbol	Value	Units
a-Beam Length	a	2.794	cm
a-Beam Width	w_a	5.080	mm
b-Beam Length	b	6.096	mm
b-Beam Width	w_b	4.064	mm
Thickness	h	1.588	mm
Number of a-Beams	N_a	11	-

Figure 4.22. The Zigzag Beam Geometry and its Geometric Properties [39]

Designed standoff layer geometry in full scale and small portion of the proposed novel design alternative are given in figure 4.23.

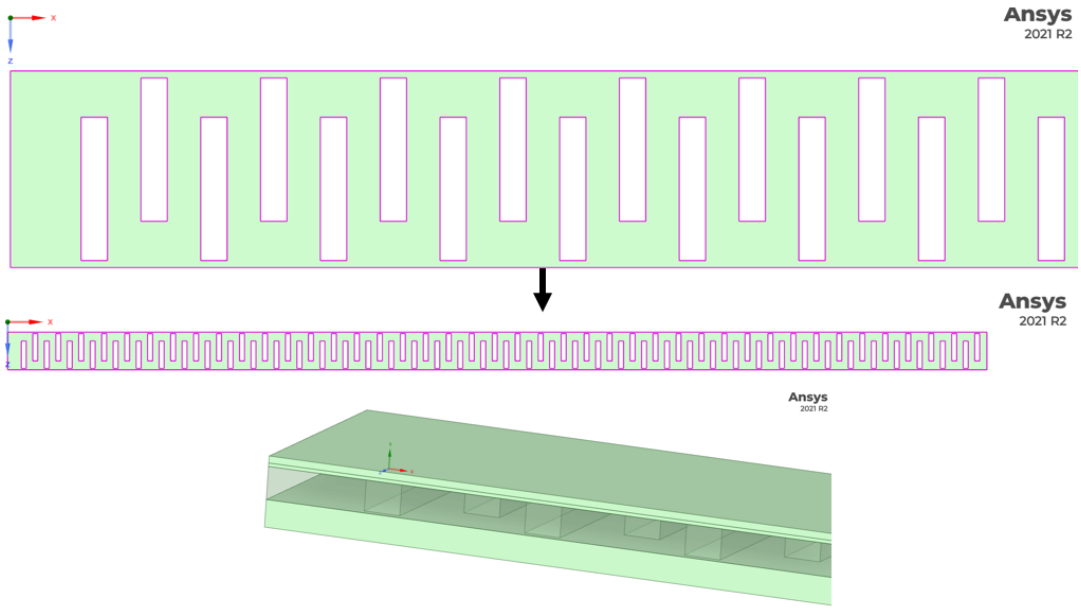

Figure 4.23. Novel Design Alternative (ND-6)

The results and FRF comparison plot are given in table 4.11 and figure 4.24 respectively. Comparing the frequency response function, total vibration response is decreased. Also, the loss factor value for each mode is decreased compared to reference PSLDT beam.

Table 4.11 The FEM Results of Novel Design Alternative (ND-6)

The Reference PSLDT		FEM (Harmonic)
1st Mode	The Natural Frequency [Hz.]	184.00
	Loss Factor [-]	0.236
2nd Mode	The Natural Frequency [Hz.]	494.00
	Loss Factor [-]	0.253
3rd Mode	The Natural Frequency [Hz.]	966.00
	Loss Factor [-]	0.216

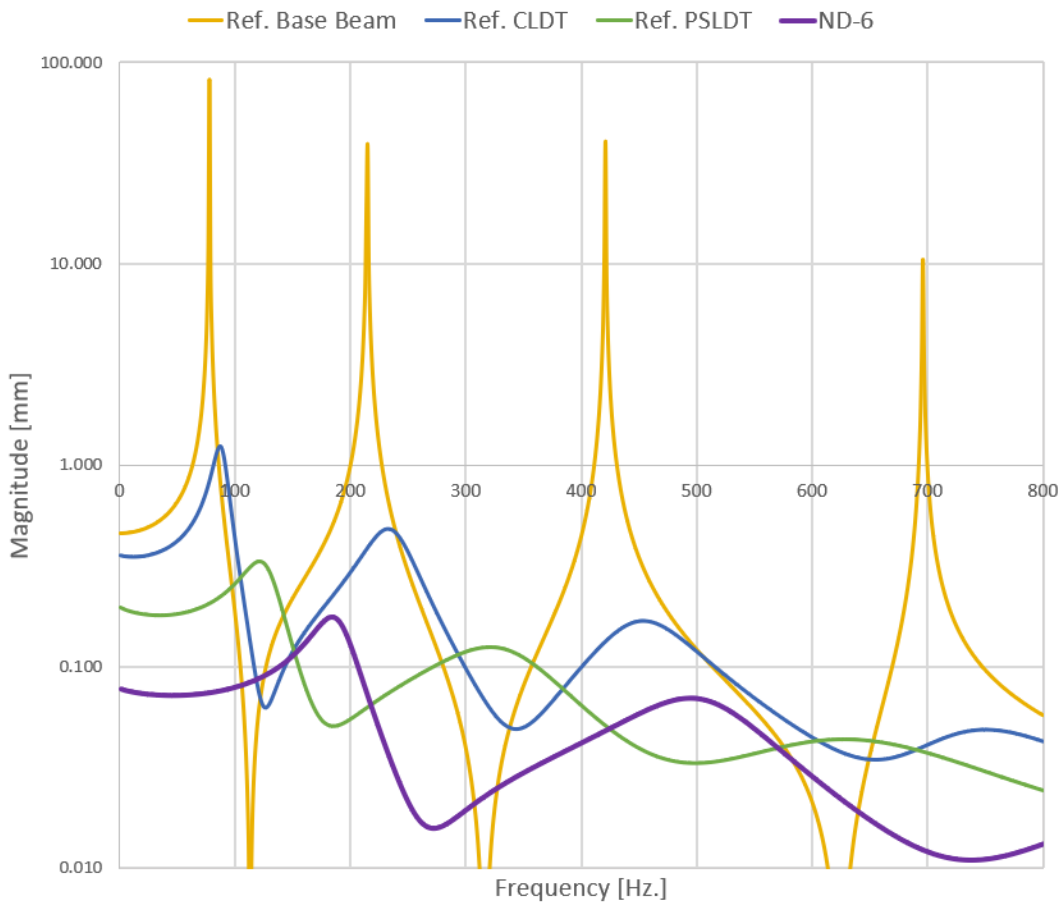

Figure 4.24. The FRF Comparison Plot for Novel Design Alternative (ND-6)

4.11 The Evaluation of the Results

4.11.1 The Broadband Vibration Evaluation

In this section, the reference base, CLDT and CLDT with a uniform standoff layer beam are compared with proposed novel design alternatives. The various standoff layer geometries are developed using literature knowledge and analysis tools. It is crucial to notice that even though the loss factor values are decreased, the total vibration response can still decrease. Therefore, the primary evaluation of these results can be performed using the proposed performance metric, total added mass percentage and loss factor values from a broader perspective. The results and the

FRF comparison between novel design alternatives and reference beams are given in table 4.12 and figure 4.25 respectively.

Table 4.12 Results for Reference Baseline Configurations and Novel Design Alternatives

CASE	Total Mass [g]	Total Added Mass [g]	Added SOL Mass [g]	Added Total Mass [%]	Avg. of First Three Loss Factor	Power Value
Ref. Base	7.02	NA	NA	NA	0.005	10000.07
Ref. CLDT	9.10	2.08	NA	29.63	0.182	54.13
Ref. PSLDT	11.26	4.24	2.16	60.45	0.375	10.22
BU	11.33	4.31	2.23	61.34	0.477	7.57
OE	10.60	3.58	1.50	50.97	0.352	13.97
ES	11.08	4.06	1.98	57.78	0.376	20.37
ND-1	11.29	4.27	2.19	60.89	0.485	6.94
ND-2	11.39	4.37	2.29	62.23	0.467	7.06
ND-3	11.30	4.28	2.20	60.92	0.398	8.78
ND-4	11.29	4.27	2.19	60.83	0.264	2.64
ND-5	11.26	4.24	2.16	60.45	0.281	2.06
ND-6	11.31	4.29	2.21	61.14	0.235	3.09

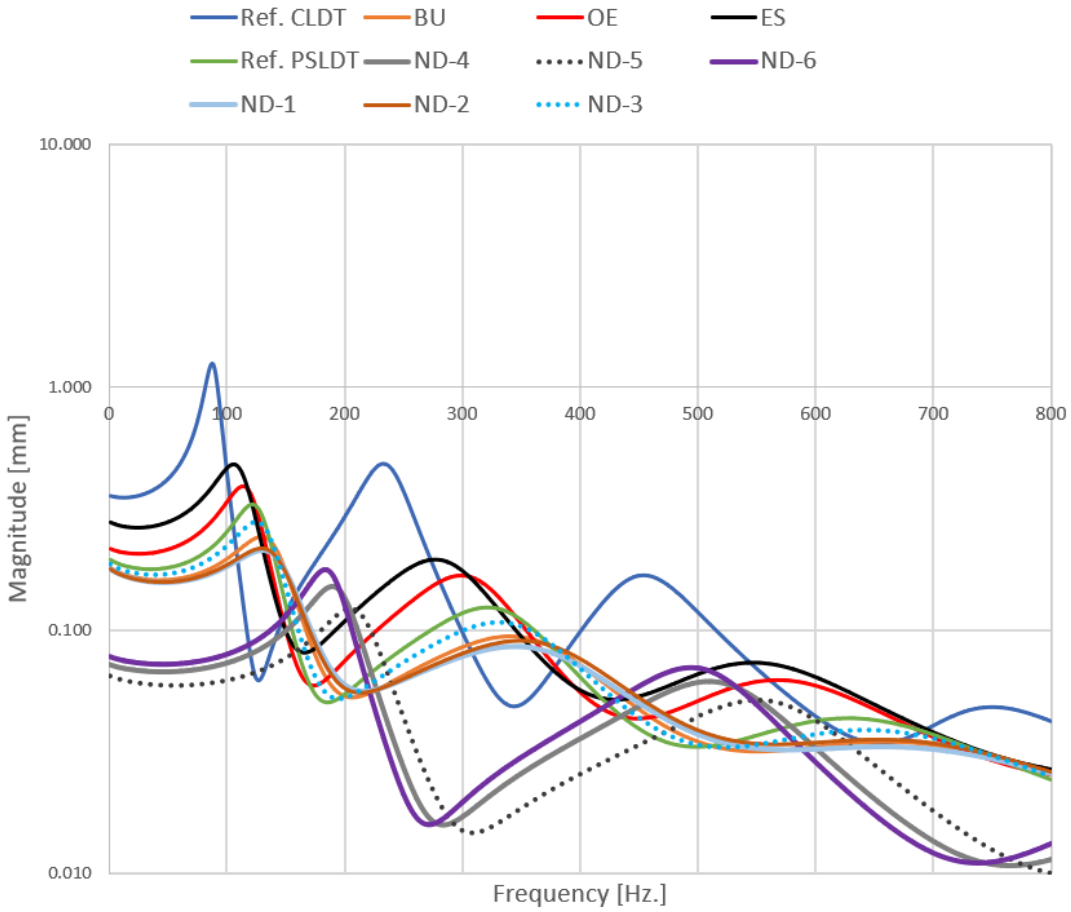

Figure 4.25. The FRF Comparison Plot for Reference Baseline Configurations and Novel Design Alternatives

From these results, the vibration characteristics of the reference PSLDT beam are significantly improved compared to the reference base and CLDT beam considering the loss factor values and the total vibration response. Therefore, novel design alternatives are developed to improve the vibration characteristics of the reference PSLDT beam. The total added mass is restricted to around sixty percent. Thus, the average of the first three loss factors and power value are the only parameters used to compare cases.

Firstly, three different optimized standoff layer geometries in literature are adjusted to use for this study. The result of the optimized PSLDT (BU) showed that both the loss factor values and total vibration response are greatly improved. Although the

loss factor values of the optimized PSLDT (ES) is improved, the total vibration response is also increased. It can be easily noticed since the power value of the optimized PSLDT (ES) is almost doubled compared to the reference PSLDT beam. Moreover, the optimized PSLDT (OE) does not provide any enhancement, so it has insufficient damping performance for the fixed-fixed boundary condition. It can be expected since the proposed material layout is optimized for the cantilever boundary condition.

Secondly, five different novel design alternatives are proposed using the structural optimization module of the ANSYS and parametric optimization. Although the loss factor values for novel design alternatives 4 and 5 are reduced, the total vibration response is significantly improved. The power value for novel design alternatives 4 and 5 is almost reduced to one quarter of the reference PSLDT beam while the power value of other alternatives (ND-1, 2, and 3) is reduced to sixty percent of it. Hence, it is concluded that the proposed novel design alternatives improved damping performance in this frequency range of interest. Also, the material is removed in width direction similarly to the developed zigzag geometry of Essink's thesis study. The novel design alternative is called ND-6. It is shown that the total vibration response is greatly improved while the loss factor values are decreased.

Comparing all of these results, proposed novel design alternatives of ND-1, ND-2, ND-3, ND-4, ND-5 and ND-6 significantly improved the damping performance of the reference PSLDT beam. Although the average loss factor values for ND-1, ND-2 and ND-3 are greater than ND-4, ND-5 and ND-6 the total vibration response of these alternatives does not improve significantly. It can be concluded that novel design alternative 5 (ND-5) gives the best damping performance since it has a lower power value and higher loss factor values than ND-4 and ND-6. The FRF comparison plot for these novel design alternatives is given in figure 4.26.

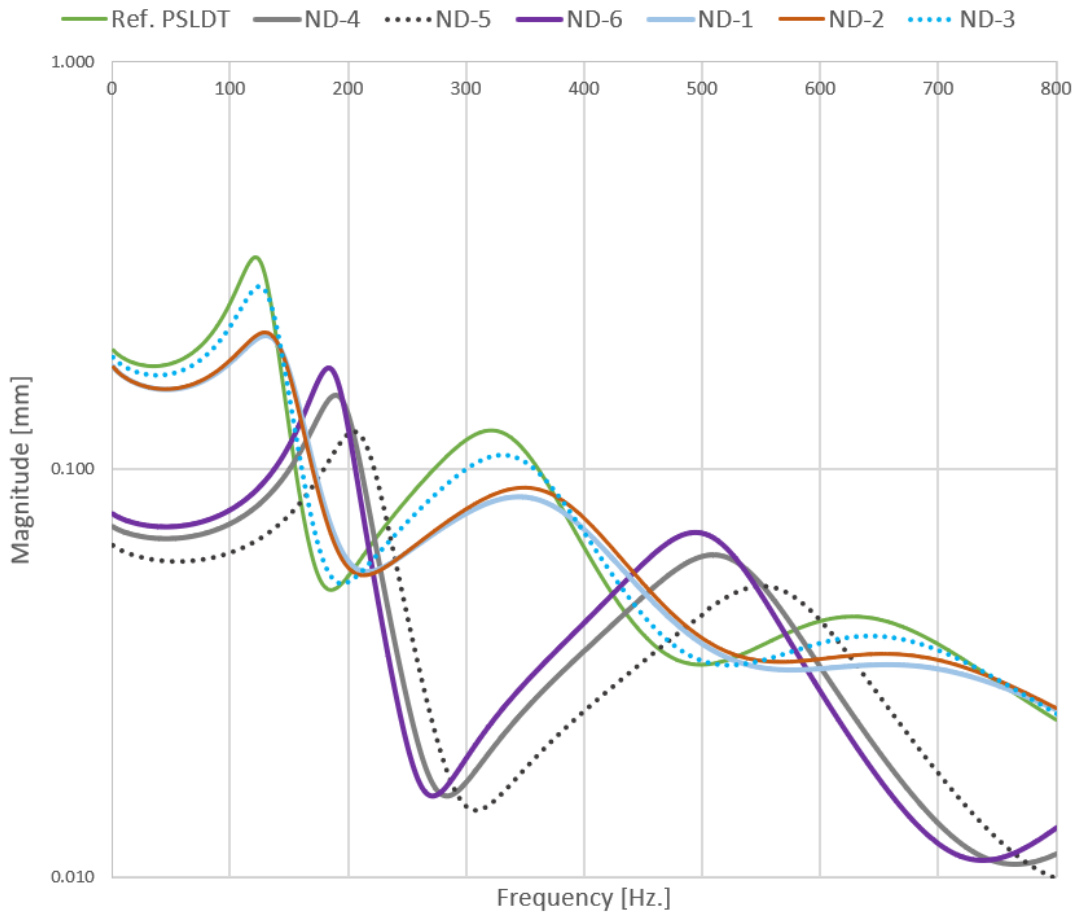

Figure 4.26. The FRF Comparison Plot for Novel Design Alternatives

4.11.2 The Narrowband Vibration Evaluation

In this section, the results of best design alternatives are compared using the defined frequency bands to examine whether the best design alternative is effective around resonance frequencies. For this purpose, the resonance frequencies are chosen to be central frequencies. Therefore, the lower and higher frequency limits are defined below and above 25 Hz. for the first central frequency, 50 Hz. for the second central frequency and 100 Hz. for the third central frequency since the frequency shift occurs between design alternatives. The area under the frequency curve squared function is calculated using the trapezoidal numerical integration method in defined frequency limits. The results are given in table 4.13.

Table 4.13 The Result Comparison for Defined Frequency Bands

CASE	1st Loss Factor	Power Value	2nd Loss Factor	Power Value	3rd Loss Factor	Power Value
Ref. PSLDT	0.362	3.87	0.367	1.29	0.395	0.32
BU	0.577	2.39	0.457	0.80	0.396	0.22
ND-1	0.531	1.98	0.524	0.67	0.400	0.21
ND-2	0.518	2.02	0.493	0.74	0.392	0.23
ND-3	0.454	3.01	0.411	1.02	0.328	0.27
ND-4	0.270	0.88	0.273	0.33	0.250	0.08
ND-5	0.299	0.62	0.281	0.24	0.262	0.06

Moreover, the defined overall frequency range is divided into 16 equal frequency bands in order to compare energy reduction between design alternatives based on the reference CLDT with a uniform standoff layer beam. For this purpose, the power value calculated for the reference baseline configuration is subtracted from the power value calculated for novel design alternatives in each defined frequency bands. The difference between these cases is defined as vibratory reduction in DB scale which is given in equation 64. Hence, it can be used to compare and evaluate damping performance of the novel design alternatives in the defined frequency band. The frequency band reduction comparison is given in figure 4.27.

$$Reduction[dB] = Power\ Value_{Novel\ Design} - Power\ Value_{Ref.Baseline} \quad (64)$$

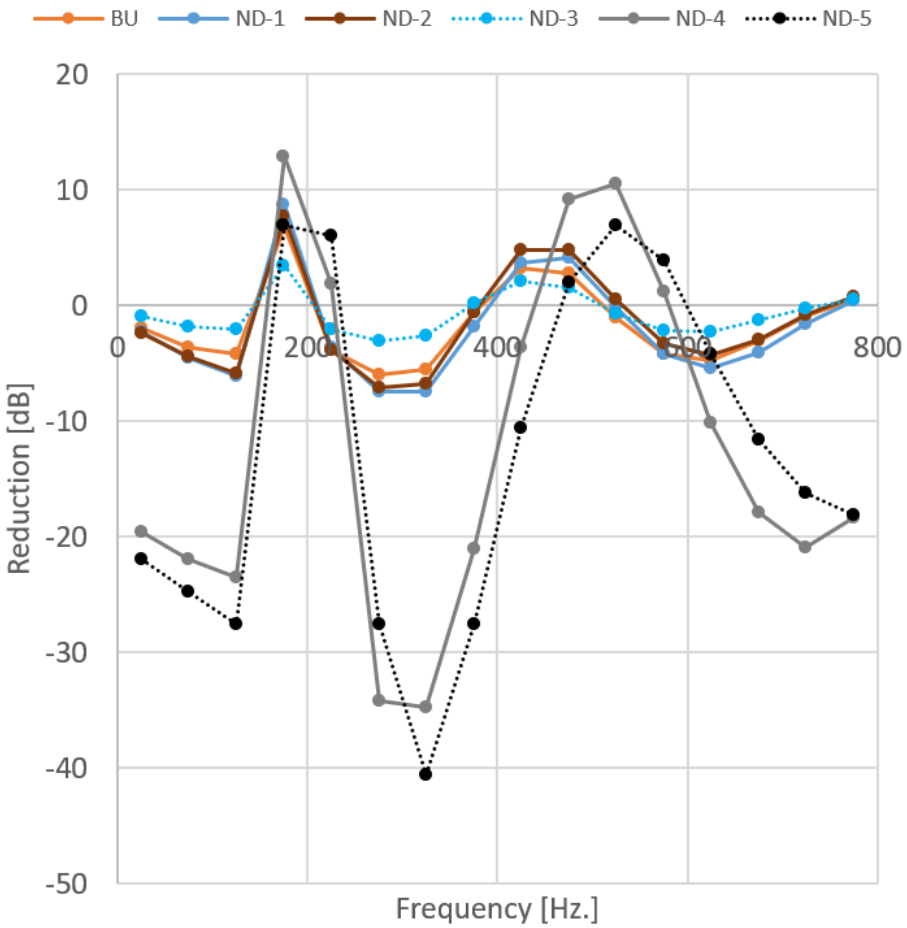

Figure 4.27. The Vibratory Reduction Comparison between Design Alternatives

Comparing all of these results, proposed novel design alternatives of ND-1, ND-2, ND-3, ND-4, ND-5 and BU significantly improved the damping performance of the reference PSLDT beam around resonance frequencies over the defined frequency limits. Although the loss factor values for the first three modes of ND-1, ND-2, ND-3 and BU are greater than ND-4 and ND-5, the vibration response of these alternatives does not improve significantly as ND-4 and ND-5. It can be concluded that novel design alternative 5 (ND-5) gives the best damping performance since it has lower power values for the first three modes over the defined frequency limits and higher loss factor values than ND-4. Moreover, the proposed novel design alternatives of ND-4 and ND-5 have greater vibratory reduction except 5 frequency bands. This is expected result since the frequency shift occurs for these novel design

alternatives compared to ND-1, ND-2 and ND-3 which results in higher vibration amplitudes where these design alternatives does not effective in these frequency bands. As a result, novel design alternative 5 (ND-5) gives the best vibratory reduction since it has bigger reduction values almost all of the frequency bands.

CHAPTER 5

CONCLUSION

The main objective of this study is to develop a novel standoff layer geometry which provides the best damping performance according to design parameters defined using the concept of the surface damping treatment applications. The 3D finite element model is developed to find harmonic analysis results of the proposed design alternatives. The effects of the element types, element order and contact types are investigated to describe dynamic behaviour correctly. It is found that SOLID185 element with linear element order and the shared topology method for contacting layers must be used. The developed finite element model is verified using experimental data in the literature and analytical results. In order to compare the damping performance of the proposed design alternatives, another objective of this study is defined. For this purpose, the performance metric is defined to quantify the damping performance of the structure more precisely. This metric includes the total vibration response, total added mass to the base structure and the average of the loss factor values.

Ulubalci, in his thesis, proposed fuselage geometry to improve the damping performance of plates [36]. The thickness of the base beam is chosen to be 1 mm considering the proposed fuselage geometry and most sheet metals have very low thickness. Therefore, the reference base and CLDT beam geometry are defined accordingly. In order to optimize the thickness of the standoff layer, both the fixed-free and fixed-fixed boundary conditions are considered. The reference CLDT with a uniform standoff layer beam is found using the performance metric defined.

Finally, the results of the reference base, CLDT and CLDT with a uniform standoff layer beam and proposed novel design alternatives are compared and evaluated. The total added mass percentage of the double CLDT beam decided to be a reference value so that it is restricted to around sixty percent for optimized PSLDT designs. 3

design alternatives in previous literature on surface damping treatment application and 6 design alternatives using structural and parametric optimization methods are developed. The structural optimization module of the ANSYS is used for parametric optimization of the standoff layer geometry. From the result comparison, it is shown that the proposed novel design alternatives found using parametric optimization greatly improved the damping performance of the reference CLDT with a uniform standoff layer beam. The power value for the proposed novel design alternatives almost decreased to 25% of the reference CLDT with a uniform standoff layer beam. It can be understood that the proposed novel design alternatives for standoff layer geometries can significantly improve the damping performance. Also, the results of parametric optimization which resembles removing material periodically along the beam in width direction, gives the best damping performance since it has lower power value and higher loss factor values among the best design alternatives.

As a future work, the results of the finite element model for the novel design alternatives can be verified by the experiment. The structural damping values of the base and the standoff layer can be implemented in the finite element model to improve accuracy. The contact between layers was assumed to be rigid. These layers are generally bonded using adhesives. It can be implemented in the finite element model using experimental data. The concept of metamaterials can be further investigated to develop metastructure for a broader frequency range.

REFERENCES

[1] - Veselago, V. G. (1968). The Electrodynamics of Substances with Simultaneously Negative Values ϵ and μ. *Soviet Physics Uspekhi*, *10(4)*, 509–514.

[2] - Liu, Z., Zhang, X., Mao, Y., Zhu, Y. Y., Yang, Z., Chan, C. T., & Sheng, P. (2000). Locally resonant sonic materials. *Science*, *289*(5485), 1734–1736. https://doi.org/10.1126/science.289.5485.1734

[3] - Sun, H., Du, X., & Pai, P. F. (2010). Theory of metamaterial beams for broadband vibration absorption. *Journal of Intelligent Material Systems and Structures*, *21*(11), 1085–1101. https://doi.org/10.1177/1045389X10375637

[4] - Pai, P. F. (2010). Metamaterial-based broadband elastic wave absorber. *Journal of Intelligent Material Systems and Structures*, *21*(5), 517–528. https://doi.org/10.1177/1045389X09359436

[5] - Cveticanin, L., & Mester, G. (2016). Theory of acoustic metamaterials and metamaterial beams: An overview. *Acta Polytechnica Hungarica*, *13*(7), 43–62. https://doi.org/10.12700/aph.13.7.2016.7.3

[6] - Chen, J. S., Sharma, B., & Sun, C. T. (2011). Dynamic behaviour of sandwich structure containing spring-mass resonators. *Composite Structures*, *93*(8), 2120–2125. https://doi.org/10.1016/j.compstruct.2011.02.007

[7] - El-Borgi, S., Fernandes, R., Rajendran, P., Yazbeck, R., Boyd, J. G., & Lagoudas, D. C. (2020). Multiple bandgap formation in a locally resonant linear metamaterial beam: Theory and experiments. *Journal of Sound and Vibration*, *488*, 115647. https://doi.org/10.1016/j.jsv.2020.115647

[8] - Hobeck, J., & Inman, D. J. (2015). 3D Printing of Metastructures for Passive Broadband Vibration Suppression. International Conference on Composite Materials, July. https://doi.org/10.13140/RG.2.1.5003.8489

[9] - Reichl, K. K., & Inman, D. J. (2017). Lumped mass model of a 1D metastructure for vibration suppression with no additional mass. *Journal of Sound and Vibration*, *403*, 75–89. https://doi.org/10.1016/j.jsv.2017.05.026

[10] - Reichl, K. K., & Inman, D. J. (2017). Constant Mass Metastructure with Vibration Absorbers of Linearly Varying Natural Frequencies. *Topics in Modal Analysis & Testing*, *10*, 153–158. https://doi.org/10.1007/978-3-319-54810-4

[11] - Reichl, K. K., & Inman, D. J. (2019). Lumped Mass Model of a 1D Metastructure with Vibration Absorbers with Varying Mass (Vol. 8).

[12] - Bettini, P., Airoldi, A., Sala, G., Landro, L. Di, Ruzzene, M., & Spadoni, A. (2010). Composite chiral structures for morphing airfoils: Numerical analyses and development of a manufacturing process. *Composites Part B: Engineering*, *41*(2), 133–147. https://doi.org/10.1016/j.compositesb.2009.10.005

[13] - Baravelli, E., & Ruzzene, M. (2013). Internally resonating lattices for bandgap generation and low-frequency vibration control. *Journal of Sound and Vibration, 332*(25), 6562–6579. https://doi.org/10.1016/j.jsv.2013.08.014

[14] - Abdeljaber, O., Avci, O., & Inman, D. J. (2016). Genetic algorithm use for internally resonating lattice optimization: Case of a beam-like metastructure. *Conference Proceedings of the Society for Experimental Mechanics Series*, *2*, 289–295. https://doi.org/10.1007/978-3-319-29751-4_29

[15] - Abdeljaber, O., Avci, O., & Inman, D. J. (2016). Optimization of chiral lattice based metastructures for broadband vibration suppression using genetic algorithms. *Journal of Sound and Vibration*, *369*, 50–62. https://doi.org/10.1016/j.jsv.2015.11.048

[16] - Essink, B. C., & Inman, D. J. (2016). Optimized 3D printed chiral lattice for broadband vibration suppression. Conference Proceedings of the Society for Experimental Mechanics Series, 10, 199–203. https://doi.org/10.1007/978-3-319-30249-2_16

[17] - Abdeljaber, O., Avci, O., Kiranyaz, S., & Inman, D. J. (2017). Optimization of linear zigzag insert metastructures for low-frequency vibration attenuation using genetic algorithms. *Mechanical Systems and Signal Processing, 84*, 625–641. https://doi.org/10.1016/j.ymssp.2016.07.011

[18] - Avci, O., Abdeljaber, O., Kiranyaz, S., & Inman, D. (2017). Vibration suppression in metastructures using zigzag inserts optimized by genetic algorithms. Conference *Proceedings of the Society for Experimental Mechanics Series, 9B*(April), 275–283. https://doi.org/10.1007/978-3-319-54735-0_29

[19] - Essink, B. C., Hobeck, J. D., Owen, R. B., & Inman, D. J. (2015). Magnetoelastic energy harvester for structural health monitoring applications. *Active and Passive Smart Structures and Integrated Systems 2015, 9431*, 943123. https://doi.org/10.1117/12.2084580

[20] - Hobeck, J. D., & Inman, D. J. (2015). Magnetoelastic metastructures for passive broadband vibration suppression. *Active and Passive Smart Structures and Integrated Systems 2015, 9431*(2011), 943119. https://doi.org/10.1117/12.2083887

[21] - Hobeck, J. D., & Inman, D. J. (2017). Simultaneous passive broadband vibration suppression and energy harvesting with multifunctional metastructures. A Tribute Conference Honoring Daniel Inman, 10172, 101720K. https://doi.org/10.1117/12.2260093

[22] - Essink, B., & Inman, D. (2016). A comparison of damping and vibration absorption in metastructures. Proceedings of ISMA 2016 - International Conference on Noise and Vibration Engineering and USD2016 - International Conference on Uncertainty in Structural Dynamics, 2025–2030.

[23] - Failla, G., Santoro, R., Burlon, A., & Russillo, A. F. (2020). An exact approach to the dynamics of locally-resonant beams. *Mechanics Research Communications*, *103*, 103460. https://doi.org/10.1016/j.mechrescom.2019.103460

[24] - Ghachi, R. F., Alnahhal, W. I., Abdeljaber, O., Renno, J., Haque, A. B. M. T., Shim, J., & Aref, A. (2020). Optimization of Viscoelastic Metamaterials for Vibration Attenuation Properties. *International Journal of Applied Mechanics*. https://doi.org/10.1142/s1758825120501161

[25] - Liu, M. L., Reichl, K. K., & Inman, D. J. (2018). Complex modulus variation by manipulation of mechanical test method and print direction. Conference Proceedings of the Society for Experimental Mechanics Series, 9, 5–11. https://doi.org/10.1007/978-3-319-62834-9_2

[26] - Whittier, J. S., 1959, "The Effect of Configurational Additions Using Viscoelastic Interfaces on the Damping of a Cantilever Beam," Wright Air Development Center, WADC Technical Report 58-568.

[27] - Yellin, J. M., Shen, I. Y., & Reinhall, P. G. (2005). Experimental and FEA of stand-off layer damping treatments for beams. *Smart Structures and Materials 2005: Damping and Isolation*, 5760, 89–99. https://doi.org/10.1117/12.599879

[28]- Yellin, J. M., Shen, I. Y., Reinhall, P. G., & Huang, P. Y. H. (2000). An analytical and experimental analysis for a one-dimensional passive stand-off layer damping treatment. *Journal of Vibration and Acoustics, Transactions of the ASME*, *122*(4), 440–447. https://doi.org/10.1115/1.1287789

[29] - Chaudry, A. H. (2006). *Passive Stand-off Layer Damping Treatment: Theory and Experiments*. https://doi.org/10.1016/b978-012397720-5.50034-7

[30] - Trindade, M. A. (2007). Optimization of active-passive damping treatments using piezoelectric and viscoelastic materials. *Smart Materials and Structures*, *16(6)*, 2159–2168. https://doi.org/10.1088/0964-1726/16/6/018

[31] - Eyyupoglu, K. O. (2016). *Development of a Novel Surface Damping Treatment*.

[32] - Jones, D. I. G. (2001). *Handbook of Viscoelastic Vibration Damping*. Wiley.

[33] - Baz, A. M. (2019). *Active and Passive Vibration Damping*. Wiley.

[34] - Soovere, J., & Drake, M. L. (1985). *Aerospace Structures Technology Damping Design Guide*. Ohio: Air Force Wright Aeronautical Laboratories.

[35] – ANSYS, Inc. *ANSYS Theory Reference*, 2021.

[36] - Ulubalci, B. (2019). *Development of a Constrained Layer Surface Damping Treatment with Optimized Spacer Geometry for Plates (Issue December)*

[37] - Ozgen, G.O. *Techniques for Vibration Control and Isolation. ME708.*

[38] - Sun, E. (2016). *Design and Analysis of a Radar Antenna Structure with Optimum Dynamic Behaviour* (Issue February).

[39] – Essink, B. C. (2020). *Design and Implementation of Mechanical Metamaterials*. University of Michigan.